TGF-β-induced Pathogenic Changes in Mouse Podocytes

Ranjan Das

The Graduate School

Yonsei University

Department of Medicine

TGF-β-induced Pathogenic Changes in Mouse Podocytes

A Dissertation

Submitted to the Department of Medicine

And the Graduate School of Yonsei University

In partial fulfillment of the Requirements for the degree of

Doctor of Philosophy

Ranjan Das

February, 2014

This certifies that the dissertation of
Ranjan Das is approved

Thesis Supervisor: Kyu-Sang Park

Committee Member: Choon Hee Chung

Committee Member: Byoung Geun Han

Committee Member: Yangsik Jeong

Committee Member: Seung-Kuy Cha

The Graduate School

Yonsei University

February, 2014

ACKNOWLEDGEMENTS

First of all, I would like to express my heartfelt and sincere gratitude to my supervisor, Professor Kyu-Sang Park who provided me an opportunity to undertake this project wok in his laboratory for the degree of PhD. It was his excellent guidance, continuous encouragement and great support that made my work successful. I would also like to express my deepest thanks to my committee members, Professor Choon Hee Chung, Professor Byoung Geun Han, Professor Yangsik Jeong and Professor Seung-Kuy Cha for their teaching, guidance and constructive criticism that had a great impact to accomplish my project. I remain grateful to all my Professors at the Department of Physiology including Professor Kong In Deok and Seong-Woo Jeong for unsparingly sharing their knowledge and for their concern over my studies during my stay in Korea. A special note of thanks to Professor Seung-Kuy Cha for his guidance and for proofreading this dissertation. I would also like to thank all my colleagues, especially from the Departments of Physiology, for their continuous assistance and support in my studies for the last four years.

This thesis would have not been possible without support from my family. I am indebted to my parents and my uncle who always encouraged me to take the challenge and supported me whenever needed.

January, 2014

Ranjan Das

CONTENTS

IV. RESULTS

LIST OF FIGURES

LIST OF TABLES

ABBREVIATIONS

α-SMA - α-smooth muscle actin

ACE - Angiotensin converting enzyme

AGE - Advanced glycation end products

Alk - Activin receptor-like kinase

AMPK - AMP-activated protein kinase

ANG II - Angiotensin II

AT1R - Angiotensin type 1 receptor

BMP - Bone morphogenesis proteins

CD2AP - CD2-associated protein

CDK - Cyclin dependent kinase

CKD - Chronic kidney disease

CM-H_2DCFDA - 5-(and-6)-chloromethyl-2',7'-dichlorodihydrofluorescein diacetate, acetyl ester

Cox2 – Cyclooxygenase-2

CYP4A - Cytochrome P450 4A

DAPI - 4',6'-diamidino-2-phenylindole

DPI - Diphenyleneiodonium

DUOX - Dual oxidase

DUOXA - DUOX activator

EMT - Epithelial mesenchymal transition

ER - Endoplasmic reticulum

ERK1/2 – Extracellular signal-regulated kinases1/2

FAD - Flavin adenine dinucleotide

FBS – Fetal bovine serum

FPE - Foot process effacement

FSGS - Focal segmental glomerulosclerosis

GBM - Glomerular basement membrane

GPx - Glutathione peroxidase

Hcys – Homocysteine

HETE - Hydroxyeicosatetraenoic acids

Id1 - Inhibition-of-differentiation

JC-1 - 5,5’,6,6’-tetrachloro-1,19,3,39-tetraethylbenzimidazolyl-carbocyanine iodide

JNK - c-Jun N-terminal kinase

KRB - Krebs-Ringer bicarbonate

MAPK - Mitogen-activated protein kinase

MCD - Minimal change disease

mitoCFP - Mitochondria-targeted cyan fluorescence protein

MKK3 - Mitogen-activated protein kinase kinase 3

MKK4 - Mitogen-activated protein kinase kinase 4

MMP - Matrix metalloproteinase

MPTP - Mitochondrial permeability transition pore

MR - Mineralocorticoid receptor

mTOR - Mammalian target of rapamycin

NAC - N-acetylcysteine

NADPH - Reduced form of nicotinamide adenine dinucleotide phosphate

Neph - Nephrin-like protein

Nox - NADPH oxidase

NOXA - NOX activator

NOXO - NOX organizer

PAI-1 - Plasminogen activator inhibitor-1

PAN - Puromycin aminonucleoside nephrosis

PCR – Polymerase chain reaction

PI3K - Phosphatidylinositol 3-kinase

PIP-complex - PINCH1-integrin linked kinase and α-parvin complex

PKC-α – Protein kinase C-α

Poldip2 - Polymerase δ-interacting protein 2

PVDF - Polyvinylidene difluoride membrane

PRR - Prorenin receptor

PUMA - p53-upregulated-modulator-of-apoptosis

RAAS - Renin-angiotensin-aldosterone system

RLU - Relative light units

ROS - Reactive oxygen species

RT-PCR – Reverse transcriptase polymerase chain reaction

Sgk1 - Serum and glucocorticoid-regulated kinase 1

siRNA - Small interfering RNA

TAK - TGF-β-activated kinase 1

TdT - Terminal deoxynucleotidyl transferase

TGF-β - Transforming growth factor β

TGF-βR - TGF-β receptor

TRPC - Transient receptor potential channel

Tsc1 - Tuberous sclerosis-1

TUNEL - Terminal deoxynucleotidyl transferase dUTP nick end labeling

VEGF - Vascular endothelial growth factor

ZO-1 - Zonula occludens

z-VAD - Z-VAD (OMe)-FMK

ABSTRACT

TGF-β-induced Pathogenic Changes in Mouse Podocytes

Ranjan Das
Dept. of Medicine
The Graduate School
Yonsei University

Injury to podocytes leads to the onset of chronic renal diseases characterized by proteinuria. Elevated TGF-β in kidney tissue is associated with podocyte damage that ultimately results in apoptosis and detachment. Proapoptotic mechanism of TGF-β in immortalized mouse podocytes was investigated. Exogenous TGF-β1-induced podocyte apoptosis through caspase-3 activation which was related to elevated reactive oxygen species (ROS) levels generated by selective upregulation of Nox4. In mouse podocytes, Nox4 was predominantly localized to mitochondria and Nox4 upregulation by TGF-β1 markedly depolarized the mitochondrial membrane potential. TGF-β1-induced ROS production and caspase activation was mitigated by an antioxidant, Nox inhibitor DPI, or siRNA for Nox4. A TGF-β receptor I blocker, SB431542, completely reversed the changes triggered by TGF-β1. Knock-down of either Smad2 or Smad3 attenuated increase of Nox4 expression, ROS generation, loss of mitochondrial membrane potential and caspase-3 activation by TGF-β1. TGF-β1 also phosphorylated mTOR and

downstream target p70S6K. Rapamycin, an inhibitor of mTOR complex I, prevented TGF-β1-induced ROS generation, total Nox activity, mitochondrial membrane potential depolarization and caspase activation indicating the role of mTOR activation in TGF-β1-induced podocyte apoptosis. In addition, rapid phosphorylation of ERK1/2 by TGF-β1 was observed. Pharmacological inhibition of ERK1/2 protected from TGF-β1-induced mTOR and p70S6K phosphorylation, enhanced Nox activity, loss of mitochondrial membrane potential, and casapase-3 activation. Taken together, these data suggest that TGF-β1-induced oxidative stress and podocyte apoptosis are mediated by TGF-β receptor-Smad2/3-mitochondrial Nox4 axis and/or activation of ERK1/2-mTORC1 cascade also co-operates to enhanced Nox activity which may contribute to the development and progression of proteinuric glomerular diseases such as diabetic nephropathy.

Keywords: Podocyte, Transforming growth factor-β, Apoptosis, NADPH oxidase 4, Mitochondria, mTOR, ERK1/2.

I. INTRODUCTON

Kidney plays many essential roles in vertebrate animals such as urine formation through glomerular filtration, regulation of electrolytes, maintenance of acid-base balance, and regulation of blood pressure. Urine is produced in the Bowman space through filtration of approximately 20% of plasma volume present in the blood. Though blood is enriched with albumin and other protein components, urine contains very low concentration of proteins. This ultrafiltration is achieved by three components in the kidney, i.e. fenestrated endothelium together with its glycocalyx, glomerular basement membrane (GBM), and the slit diaphragm formed by special type of epithelial cells known as podocytes[35]. Nowadays it is well established that diabetic and non-diabetic glomerular diseases lead to chronic and end-stage renal diseases. In kidney glomerulus, mesangial cells, endothelial cells, parietal epithelial cells and podocytes are major targets in different types of nephrotic and non-nephrotic syndromes. Injuries to podocytes are mainly associated with proteinuria, with or without nephritic syndrome[100]. Podocytes are postmitotic cells which do not proliferate anymore throughout our life after its maturation during embryonic stage. No evidence suggests the replacement of lost podocytes by replication and glomerular diseases dramatically accelerate the loss of podocytes. During the last two decades, efforts have taken to address different types and mechanisms of podocyte injury. Many pathogenic factors inducing high glucose, transforming growth factor β (TGF-β), angiotensin II (ANG II), etc have been identified which have been proved to be involved in podocyte apoptosis, epithelial mesenchymal transition (EMT), fibrosis, hypertrophy, etc. TGF-β1 is upregulated in glomerular diseases and experimental and human nephropathy[79, 128]. Elevated expressions of TGF-β1 and TGF-β receptors are

the hallmark of virtually all human and experimental chronic kidney diseases[8]. In addition, broad range of products of metabolism including glucose, advanced glycation end products (AGE), reactive oxygen species (ROS), and free fatty acids can induce TGF-β secretion[133] which may further deteriorate renal function through podocyte damage.

1.1. Structure of podocytes

Podocytes are terminally differentiated cells present on the glomerular basement membrane and possesses a quiescent phenotype[99]. These cells are originally derived from embryonic mesenchymal cells[84]. Podocytes are highly specialized cells with distinct anatomical features. It has a large cell body at the center of the cell where reside the nucleus, endoplasmic reticulum (ER), mitochondria, golgi apparatus. Primary processes are produced from the main cell body and the end of which forms the characteristic foot processes. Foot processes are attached to GBM mainly through integrins and dystroglycans. Thus podocytes are anchored to the glomerular tuft. Foot processes of the neighboring podocytes interdigitate to form slit diaphragm which plays the important role in filtration.

Podocytes are polarized cells - apical domain faces towards the urinary space in the Bowman's space, and the basal domain is attached to the GBM and the junctional cell membrane domain is composed of proteins associated with slit diaphragm formation[48]. The unique structure of podocytes is due to rich actin cytoskeleton serving as the backbone of podocytes and regulating dramatic change of podocyte shapes[72]. Microfilaments are the main cytoskeletal component of the foot process, containing a dense network of F-actin and myosin. One of most important slit diaphragm proteins is nephrin. Nephrin interacts with podocin[93, 97] and CD2-associated protein (CD2AP)[104].

Other important slit diaphragm proteins are densin, zonula occludens (ZO-1), nephrin-like protein 2 (Neph-2) and nephrin-like protein 3 (Neph-3). The apical domain is negatively charged due to the presence of proteins podocalyxin and podoplanin. Negative charges of these proteins do not allow the passage of albumin which is also negatively charged and keep separating adjacent podocytes. Integrins α3β1 and α,β-dystroglycans anchor podocytes to the matrix proteins of GBM on the basal domain[32].

1.2. Functions of podocytes

Podocytes play an important role to maintain proper renal function. It counteracts the intraglomerular pressure, thus maintenance of the glomerular capillary loop shape. Podocytes act as a size barrier to plasma protein. The negative charge of podocalyxin in apical surface limits the leakage of negatively charged proteins. Podocytes produce and secrete vascular endothelial growth factor (VEGF) which is an important requirement for glomerular endothelial cell activity. Podocytes also produce collagen and fibronectin which are main component of GBM.

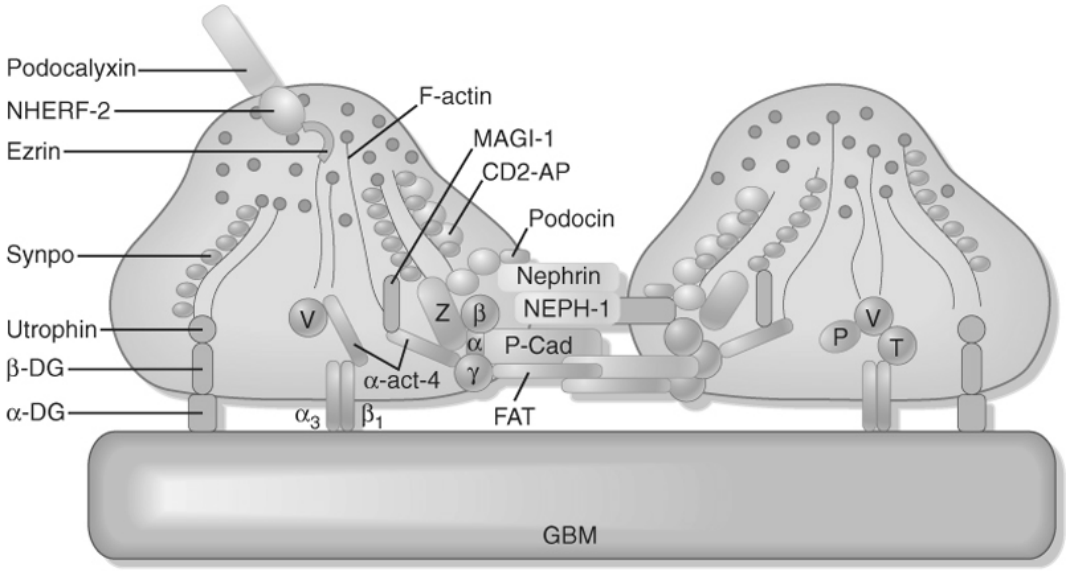

Fig. 1. Structure of podocytes.

α-act4, α-actinin-4; α3β1, α3β1 integrin; α-DG, α-dystroglycan; β-DG, β-dystroglycan; NHERF2, Na^+/H^+ exchanger regulatory factor 2; P, paxillin; P-cad, P-cadherin; Synpo, synaptopodin; T, talin; V, vinculin. Adopted from Mundel and Shankland, 2002[19].

1.3. Diseases of podocytes

In clinical point of view, predominant causes of nephrotic range proteinuria as a result of podocyte damage or malfunction include diabetic nephropathy, focal segmental glomerulosclerosis (FSGS), minimal change disease, membranoproliferative glomerulonephritis and amyloid nephropathy. Podocyte diseases can also be classified into congenital, hereditary, and acquired (immune and non-immune) based on the origin of disease[100]. Congenital nephritic syndrome of Finnish type is a classical example of congenital podocyte disorder caused by abnormalities in structural proteins in slit diaphragm (e.g. nephrin)[49, 113]. Membranous nephropathy is also resulted from congenital defects[22, 92]. Mutations in podocin[11], α-actinin[47], and TRPC6[121] are the hereditary cause of podocyte damage. Minimal change and membranous nephropathy are acquired diseases. Minimal change disease is immune-mediated and likely due to abnormalities in T cell, though the mechanism is not well understood. A causative antibody responsible for idiopathic membranous nephropathy in man remains unknown. Human immunodeficiency virus (HIV) associated nephropathy and diabetic nephropathy are non-immune causes of acquired podocyte damage. HIV associated nephropathy is resulted from HIV viral infection[124]. Diabetic nephropathy is mainly caused by metabolic disorders. Large number of evidences shows that tension and stress resulted in increased glomerular pressure cause podocyte injury[27, 80].

1.4. Mediators of podocyte injuries

The major culprits of podocyte injuries are TGF-β1, ANG II, high glucose, prostaglandins, excess mechanical stretch, VEGF, advanced glycation end products, reactive oxygen species etc[100]. TGF-β1 mediates podocyte apoptosis, EMT and

accelerates GBM thickening by matrix protein synthesis[42, 64, 94]. ANG II accounts for podocyte apoptosis, hypertrophy and synthesis of TGF-β and VEGF[24, 100]. Mechanical stretch increases accumulation of ANG II resulting in reduction of nephrin expression in human podocytes and also causes podocyte detachment, apoptosis, and hypertrophy[23, 71, 87]. Endoplasmic reticulum stress is induced by prostaglandins and saturated free fatty acid[55, 109]. VEGF mediates over production of collagen IVα3 and TGF-β level in mouse podocytes[17].

1.5. Responses to injuries by podocytes

Accumulating evidences suggest that podocytes respond to different noxious stimulus in different ways including apoptosis, foot process effacement (FPE), hypertrophy, detachment from GBM, etc. Recently, podocyte proliferation has been reported as a response to injury in collapsing FSGS.

Recent clinical findings suggest that glomerular podocyte numbers are reduced in membranous nephropathy, diabetic nephropathy, classic FSGS and amyloid aging[100] resulting in proteinuria and glomerulosclerosis. Proteinuria occurs due to lack of charge and size selectivity in areas of podocyte loss. In excellent reviews, Lamley and coworkers explain the mechanism of glomerulosclerosis resulted from reduction in podocyte number[59, 62, 80]. In short, loss of podocytes produces ‘bare and denuded GBM’. As podocytes maintain capillary loop shape by opposing the outward pressure raised by blood flow, the denuded GBM is bulged out and contact to parietal epithelial cells and Bowman’s capsule, the process denoted as first ‘committed step’ for formation of FSGS. Apoptosis and detachment of viable podocytes are considered as two major mechanisms responsible for reduction in glomerular podocyte number.

1.5.1. Podocyte apoptosis

Emerging literatures reflect that programmed cell death or apoptosis is the critical factor for reduction of podocyte number. For the first time in 2001, Schiffer *et al.* reported pro-apoptotic role of TGF-β1 in podocyte apoptosis[94]. Using albumin/TGF-β1 transgenic mice (TG) mice (characterized by progressive renal failure due to glomerular sclerosis by high expression of TGF-β1), they showed that TUNEL positive apoptotic nuclei of podocytes increased compared to wild type mice and 2 week old TG mice showed significantly higher rate of apoptosis compared to 5 week old TG mice. In this experiment, they also observed podocyte apoptosis occurred earlier than other glomerular cells. Kim *et al.* showed podocyte apoptosis in puromycin aminonucleoside nephrosis (PAN) model of podocyte injury in which glomerulosclerosis was detected following a 20% reduction in podocyte number[54]. Accumulating clinical observations indicate protective role of angiotensin-converting enzyme inhibitors and ANG II receptor blockers over proteinuria irrespective of their role in lowering blood pressure identifying deleterious effect of ANG II in reduction of podocyte number. ANG II mediated podocyte apoptosis occurs through AT1 receptor activation and pharmacological inhibition of AT1 receptor significantly recovers stress-tension induced podocyte apoptosis[24, 27]. Simultaneously, it was also found that ANG II induced podocyte apoptosis was blocked by pre-treatment with TGF-β1 antibody, indicating the role of TGF-β1 in angiotensin II mediated podocyte apoptosis. Role of hyperglycemia in podocyte apoptosis has been described in both in vitro cultured cells as well as in vivo rat and mouse model of diabetic nephropathy[29, 30].

1.5.2. Podocyte detachment from GBM

Podocytes are normally 'floating cells' in the urinary space with their basal side

attached to GBM with help of integrins and dystroglycans. The presence of viable podocytes and podocyte specific proteins in the urine from patients with proteinuric renal diseases, but not in healthy subjects and non-podocyte glomerular diseases, raises the concept of podocyte detachment before apoptosis[38, 74, 86, 115]. Studies by Pichler showed that high glucose treatment can potentially detach cultured podocytes[100]. The mechanisms of podocyte detachment are not well established and it is considered that loss of anchoring proteins integrins and dystroglycans can accelerate podocyte detachment.

1.5.3. Podocyte hypertrophy

Podocyte hypertrophy is an adaptive response to stress and an attempt to cover the denuded GBM owing to detachment or apoptosis of neighboring cell to reduce proteinuria. It is believed that this phenomenon appears as podocytes are incapable of proliferation. Clinical studies have already demonstrated podocyte hypertrophy in diabetic nephropathy and FSGS[5]. In mechanistic studies, high glucose and angiotensin II are proven to mediate hypertrophy *in vitro*[127]. Experiments shows that increased expression of specific cyclin dependent kinase (CDK) inhibitors (p21 and p27) are responsible for podocyte hypertrophy[39].

1.5.4. Foot process effacement

Foot process effacement (FPE) is referred to stereotypical changes due to fusion, retraction or simplification of foot processes. Scanning electron microscopy revealed that FPE consists of gradual simplification of interdigitating foot processes giving rise to flat and elongated podocytes. The process does not involve fusion of neighboring podocytes,

rather due to retraction, widening, and shortening of foot processes of each podocytes. As a result, frequency of filtration slits is reduced resulting in the appearance of a continuous cytoplasmic sheet covering the GBM[100].

Studies have shown that FPE is not a passive process, rather an energy dependent active process which involves rearrangement of podocyte cytoskeleton[100]. FPE is known to occur owing to abnormal expression of actin-associated proteins and slit diaphragm proteins, changes in podocyte-GBM interaction, changes in apical membrane proteins, etc. α-actinin-4 is an actin filament cross linking proteins and its expression is increased in experimental proteinuric disease[105]. Its mutations also cause proteinuria and effacement in human[47]. Mutations in slit diaphragm protein nephrin encoded by gene NPHS1 result in proteinuria[112]. Podocin which binds to nephrin is encoded by gene NPHS2 and mutation of this gene in human[11] or podocin-null mice develop proteinuria[93]. Null-mutation of multi-adapter protein CD2AP in mice develops massive proteinuria and haplo-insufficiency in human leads to glomerular diseases[51]. Integrin α3β1 is the abundant integrin in podocytes and binds to collagen, fibronectin, laminin and entactin/nidogen in GBM. Knock out study with integrin β1-null mice or blocking integrin β1 with specific antibody reveals its importance against foot process effacement[57]. Integrin linked kinase is also an important cell signaling molecule and its abnormality leads to FPE and proteinuria[58]. Another GBM binding protein is dystroglycan which exists as hetero-dimer of α and β-dystroglycan. α-dystroglycan has a polyanionic binding site for laminin. In minimal change disease, dystroglycan level is reduced. Redistribution of dystroglycan in clustered manner is observed in FSGS. Kerjaschki and co-workers observed that reactive oxygen species and protamine sulfate directly splits dystroglycan–GBM interaction leading to podocyte effacement[56]. Reduction of apical membrane protein

podocalyxin and podoplanin also result in EPF. Reduced expression of podocalyxin is reported by high glucose treatment and in streptozotocin-induced diabetic nephropathy model in rat[28]. Podoplanin reduction is observed in PAN nephrosis model[70].

1.6. TGF-β signaling pathways

TGF-β is an multifunctional cytokine regulating proliferation, apoptosis, differentiation, embryogenesis, etc in species ranging from flies and worms to mammals[83]. TGF-β family consists of 30 known family members including three different isoforms of TGF-β (TGF-β1, TGF-β2 and TGF-β3), activins and bone morphogenesis proteins (BMPs). TGF-β ligand binds to TGF-β receptor II (TGF-βRII) and brings together type II and type I receptors (serine/threonine kinases) on the cell surface. This induces receptor II to phosphorylate the receptor I kinase domain allowing propagation of signals from cell membrane to nucleus.

Two distinct signaling pathways are known to be activated by TGF-β1. Smad proteins mediate the canonical TGF-β signaling, while mitogen-activated protein kinase (MAPK) and phosphatidylinositol 3-kinase (PI3K) signaling cascades are activated in non-canonical pathway. There are eight different Smad proteins constituting three functional classes: receptor regulated Smad (R-Smad: Smad1,2,3,5 and 8), co-mediator Smad (Co-Smad: Smad4), and inhibitory Smad (I-Smad: Smad6 and Smad7). R-Smads are directly phosphorylated by TGF-βRI kinases, undergo homotrimerization, form heteromeric complexes with Co-Smad (Smad4) and translocated to the nucleus where they regulate the transcription of target genes. Smad signaling is negatively regulated by I-Smad either by competing with R-Smad for receptor/Co-Smad or targeting the receptors for degradation.

In non-canonical pathways, TGF-β receptors directly phosphorylate or interact with non-Smad proteins, thereby initiating parallel signaling that cooperates with the Smad pathway[102, 130]. TGF-β-activated kinase 1 (TAK1) activation by TGF-βRI leads to activation of mitogen-activated protein kinase kinase 3 (MKK3) or mitogen-activated protein kinase kinase 4 (MKK4) which are upstream regulators of p38 MAPK and JNK, respectively[77, 85]. Activation of Extracellular signal-regulated kinases 1/2 (ERK1/2) MAPK is reported by TGF-β[78]. TGF-β also activates AKT signaling through PI3K which is known to be the survival signal for podocytes. The adaptor molecule CD2AP bridges between PI3K regulatory subunit (p85) and TGF-βRs[125]. Several studies have reported that tight balance between anti-apoptotic and proapoptotic signaling by direct activation of MAPK pathways and PI3K/AKT is important for podocyte survival[100].

1.7. Roles of TGF-β in podocyte pathophysiology

1.7.1. Apoptosis

Pro-apoptotic effect of TGF-β on mouse glomerular epithelial cells was first reported by Schiffer and co-workers in 2001[94]. They showed that TGF-β1 is a strong inducer of caspase-3 via p38 MAPK which mediates translocation of Bax, one of the Bcl family members, to mitochondria where oligomerization of Bax releases cytochrome c from mitochondria and eventually activation of executioner caspase (caspase-3) to mediate podocyte cell death. In the same time, they observed that TGF-β1 rapidly accelerates expression of Smad7, a negative regulator of Smad signaling, which inhibits nuclear translocation of NF-κB, a survival factor for podocytes, resulting in caspase independent apoptosis. The same group reported that Smad7 is significantly upregulated in injured

podocytes of FSGS and MCD (minimal change disease) patients[95]. Interestingly they found that TGF-β1 stimulation increases expression of only Smad7, and not that of Smad6 in podocytes. Wu *et al.* showed that pro-apoptotic effect of TGF-β1 is concentration dependent as high dose of TGF-β1 (>4ng/ml) induces apoptosis whereas lesser dose favors differentiation as shown by synaptopodin expression[122]. Recent studies showed that cytoplasmic-extracellular matrix interaction is critical for podocyte survival. TGF-β1 treatment inhibited PINCH1-integrin linked kinase and α-parvin complex (PIP-complex) integrity by dissociating α-parvin from the complex resulting in activation of p38 MAPK and caspase-mediated podocyte apoptosis[46]. Activation of Notch pathway also causes podocyte apoptosis. High expression of intracellular domain of Notch1 is reported in diabetic nephropathy and FSGS[75, 76]. Moreover, they observed that Notch1 ligand Jagged1, which leads to cleavage and activation of Notch1, is a direct transcriptional target of TGF-β1 in podocytes. Notch1-induced apoptosis, which is mediated by activation of p53 and caspase-3, is independent of p38 MAPK and Smad3 activation. It has been also reported that TGF-β1 mediates Ca^{2+} overload through ERK1/2-NF-κB pathway and Fyn-dependent TRPC6 phosphorylation, which activates proapoptotic signaling in podocytes[129]. Activation of protein kinase C-α (PKC-α)-p38 MAPK pathway by TGF-β1 has also been reported to activate podocyte apoptosis[110].

1.7.2. Epithelial mesenchymal transitions

In response to injury, podocytes resort to adaptive changes like hypertrophy, dedifferentiation, and detachment from GBM or apoptosis depending on duration and severity of injury. If the injury persists, podocytes undergo EMT to escape from apoptosis resulting in loss of highly specialized podocyte phenotype. Li and co-workers (2008)

showed that podocytes undergo EMT in presence of TGF-β1[64]. TGF-β1 stimulates expression of key transcription factor, Snail which is implicated in EMT. *In vivo* results showed that nephrin and ZO-1 are reduced, whereas expressions of mesenchymal markers (matrix metalloproteinase-9 (MMP-9), desmin) are increased in animal model of diabetic nephropathy[64]. Wang *et al.* showed that TGF-β1 induces Wnt1 expression and β-catenin activation in podocytes[116]. β-catenin activation leads to EMT and albuminuria by augmenting the expression of MMP-9, MMP-7, desmin, plasminogen activator inhibitor-1 (PAI-1) both *in vivo* and *in vitro*.

1.8. NADPH oxidases and ROS generation

NADPH oxidases (Nox) are a class of enzymes which produces reactive oxygen species using NADPH. The prototype Nox is Nox2, also known as gp91phox, and was discovered first time in phagocytes. Nox family consists of seven members – Nox1, Nox2, Nox3, Nox4, Nox5, dual oxidase 1 (DUOX1) and dual oxidase 2 (DUOX2) consisting the catalytic core of the enzyme complex. All Nox enzymes require their membrane bound and/or regulatory subunits to execute functions. Cytosolic organizing subunits for Nox enzymes are p40phox, p47phox and NOX organizer 1 (NOXO1). NOX activator 1 (NOXA1), p67phox and small GTPases (Rac1 and Rac2) are cytosolic activators and the membrane bound stabilization partners are p22phox, DUOX activator 1 (DUOXA1) and DUOX activator 2 (DUOXA2)[26]. Recent studies also show that polymerase δ-interacting protein 2 (Poldip2) regulates Nox4 activity and generates ROS to remodel cytoskeleton arrangement[67].

1.9. Role of NADPH oxidases in podocyte injuries

1.9.1. NADPH oxidases and podocyte apoptosis

In diabetic nephropathy, increased expression of NADPH oxidases leads to proteinuria and podocyte apoptosis. In OVE26 type 1 diabetic mice model, Nox1 and Nox4 protein expressions are elevated in glomerulus resulting in podocyte apoptosis, albuminuria and loss of podocyte foot processes[29, 30]. Prolong exposure to high glucose is accounted for oxidative stress through Nox4 in cultured mouse podocytes and increased ROS by Nox4 mediates podocyte apoptosis[29]. Report also suggests that hyperglycemia-induced oxidative damage is mediated by inactivation of AMP-activated protein kinase (AMPK) which negatively regulates Nox4 upregulation in podocytes. In this signaling cascade, p53 and p53-upregulated-modulator-of-apoptosis (PUMA) are downstream players of Nox4-induced apoptotic cell death in podocytes[30]. It is also reported that a tight oxidant-antioxidant balance is important to maintain the normal podocyte metabolism which is impaired by high glucose concentration through overproduction of ROS[88]. Hyperglycemia-induced ROS is generated through Nox4 upregulation and reduction of the activity of key antioxidant enzymes glutathione peroxidase (GPx) and catalase[88]. A recent study also describes the significance of mammalian target of rapamycin (mTOR) activation in podocyte loss and proteinuria[31]. In cultured mouse podocytes and OVE26 type 1 diabetic mouse model, high glucose stimulates Nox4 upregulation through activation of mTOR signaling cascades[31].

1.9.2. Activation of renin-angiotensin-aldosterone system (RAAS) through NADPH oxidases

Renin-angiotensin-aldosterone system regulates blood pressure and water balance in the body. Podocytes express functional components of RAAS including neprilysin, aminopeptidase A, angiotensin converting enzyme (ACE), prorenin receptor (PRR), renin, and mineralocorticoid receptor (MR), indicating presence of a local RAAS in the glomerulus[103, 114]. Accumulating evidence indicates that Nox is associated with RAAS-induced podocyte injury and filtration dysfunction. Experiment with transgenic rat models [TGR(mRen2)27 and Ren2] over-expressing renin gene, exhibit elevated RAAS activity, ANG II levels, and oxidative stress[13, 120]. Hsu *et al.* showed that angiotensin type 1 receptor (AT1R) over- expression in podocytes increases ROS-mediated reorganization of podocyte cytoskeleton[40]. Whaley and co-workers examined components of RAAS and NADPH oxidase systems in Ren2 rats. In kidney cortical tissues from Ren2 rats show elevation of ANG II, AT1R, and total Nox activity subunits (NOX2, p67phox, p47phox, and Rac1) expression, ROS production, podocyte effacement, and loss of the slit-pore diaphragm integrity in comparison with that of age-matched Sprague-Dawley rats[117]. The same group also reported that rennin inhibition, AT1R blockade, and MR antagonism can attenuate elevated Nox activity and subunit expression, followed by restoring podocyte slit diaphragm protein nephrin and ultrastructural changes in Ren2 rats[118, 119]. Fujita and colleagues first time reported the existence of MR in podocytes *in vivo* and *in vitro* and discovered the role of aldosterone in podocyte damage[73]. In aldosterone-induced podocyte injury model, augmentation of p67phox, Rac1, NOX2, p47phox, p22phox gene expressions, ROS overproduction, decreased nephrin and podocin expressions and enhanced expression of aldosterone effector kinase, serum and glucocorticoid-regulated

kinase 1 (Sgk1), have been observed[103]. These observations indicate the pathophysiologic roles of Nox enzymes in RAAS-mediated podocyte damage.

1.9.3. Nox-derived ROS and EMT

Hallmark of podocyte EMT is marked reduction of epithelial markers P-cadherin and ZO-1 and high increase of mesenchymal markers like fibronectin and α-smooth muscle actin (α-SMA). Evidences show that ROS generated by NADPH oxidases mediates EMT to podocytes. Nox1[65], Nox2[25], Nox4[10] and Rac1b[61] mediates EMT in various types of epithelial cells, indicating that Nox-derived ROS promotes activation of EMT program. In hyperhomocystemia, homocysteine (Hcys)-induced EMT of podocytes is mediated by enhanced superoxide production, which was substantially suppressed by inhibition of Nox enzymes. Mice lacking NOX2 ($gp91^{-/-}$) are resistant to Hcys-induced podocyte EMT[131]. Recent studies by Li *et al.* showed that growth hormone can protect podocytes from Hcys-induced EMT via upregulation of NADPH oxidase[63].

II. PURPOSES

Chronic kidney diseases (CKD) are one of major causes of increased mortality around the world. It is characterized by extensive damage of functional kidney tissues and the survival of affected individuals relies on life-long treatments with dialysis or renal allograft transplantation. The main causes of CKD are diabetes, hypertension and aging. TGF-β and its downstream signaling pathways play a central role in activation of kidney pathogenesis in human patients and experimental animal models[8]. One of the first target cells for proteinuric CKD is glomerular epithelial cells, also known as podocytes. These are terminally differentiated, actin-rich epithelial cells present on the glomerular basement membrane and critical for glomerular filtration process. Enhanced TGF-β signaling induces apoptosis, EMT, and fibrosis in podocytes[4, 64, 94]. TGF-β superfamily consists of secreted peptides exhibiting pleiotropic functions in cell proliferation, differentiation, immune response, apoptosis and matrix remodeling, depending on physiological context. Increased level of TGF-β in diabetic nephropathy is known to be associated with podocyte damage ultimately resulting in apoptosis and detachment[9]. Increased ROS is responsible for podocyte apoptosis in diabetic nephropathy[29, 30]. However, the sources of ROS and pathways to damage podocytes are largely unknown. The specific aims of this study were i) investigation of pathogenic changes by TGF-β, ii) identification of signaling pathways downstream of TGF-β, and iii) molecular mechanism of TGF-β1-induced injuries in mouse podocytes. Identification of causative signaling molecules in TGF-β1-induced podocyte damages could be prospective candidates for therapeutic and preventive targets in diabetic nephropathy and other type of CKD.

III. MATERIALS AND METHODS

3.1. Cell culture

An immortalized mouse podocyte cell line, mouse podocyte clone-5 (MPC-5), was a kind gift from Prof. Peter Mundel (Harvard Medical School, Charlestown, MA, USA), and this line was cultured as described previously[29]. Dishes coated with rat tail type I collagen were used to grow cells as a monolayer. Cells were cultured in low glucose Dulbecco's Modified Eagles Medium (catalog no. 11885-084, Gibco, Carlsbad, CA, USA) supplemented with 5% fetal bovine serum (FBS), 100 U/ml penicillin and 100 μg/ml streptomycin at two different temperatures that either promoted proliferation or differentiation. At 33°C, cells are allowed to proliferate (permissive condition) in the presence of 20 U/ml mouse recombinant interferon-γ. In order to induce differentiation (non-permissive condition), the podocytes were thermo-shifted to 37°C in the absence of interferon-γ for 14 days. Before application of TGF-β1, cells were maintained in a serum-deprived condition (0.25% FBS) for 24hr.

3.2. Chemicals

N-acetylcysteine (NAC) (catalog no. A9165), diphenyleneiodonium (DPI) (catalog no. D2926), SB431542 (catalog no. S4317), rapamycin (catalog no. R8781), lucigenin (catalog no. M8010), NADPH (catalog no. N5130), and 4',6'-diamidino-2-phenylindole (DAPI) (catalog no. D9542) were purchased from Sigma (St. Louis, MO, USA). Mouse recombinant interferon-γ (catalog no. 485-MI) and recombinant human TGF-β1 (catalog no. 240-B) were purchased from R & D Systems (Minneapolis, MN, USA). 5-(and-6)-

chloromethyl-2',7'-dichlorodihydrofluorescein diacetate, acetyl ester (CM-H_2DCFDA) (catalog no. C6827), 5,5',6,6'-tetrachloro-1,19,3,39-tetraethylbenzimidazolyl-carbocyanine iodide (JC-1) (catalog no. T3168) were purchased from Molecular Probes (Grand Island, NY, USA). U0126 (catalog no. 9903) was purchased from Cell Signaling Technology (Danvers, MA, USA). Rat tail type I collagen (catalog no. A10483-01) was purchased from Life Technologies Corporation (Grand Island, NY, USA). SB202190 (catalog no. 559388) was purchased from Millipore Corporation (Billerica, MA, USA). Protease inhibitor cocktail (catalog no. 11836153001) was purchased from Roche Diagnostics (GmbH, Mannheim, Germany).

3.3. Preparation of TGF-β1

TGF-β1 was prepared as manufacturer's instruction. Purified recombinant TGF-β1 is an extremely hydrophobic protein that adheres strongly to the surfaces of the container. It is reconstituted as follows to ensure maximum recovery.

At first, 0.01 g fatty acid free BSA was dissolved into 10 ml of double distilled H_2O (1 mg/ml) by heating at 37°C to reduce foaming. BSA solution was divided into two haves each containing 5 ml. 20 µl of 1 N HCl was added to 5 ml BSA solution to prepare 1 mg/ml BSA containing 4 mM HCl. Next, 100 µl from that solution (HCl containing BSA) was mixed with solid TGF-β1 powder (TGF-β1 of 2 µg/vial). 900 µl BSA solution (no HCl) was added to reconstitute 1 ml solution of TGF-β1 (final conc. = 2 µg/ml). TGFβ1, thus prepared, was aliquot into several tubes (50 µl/tube) and stored at -80°C for 6 months. All the solutions were filtered through 0.2 µm syringe filter inside a laminar flow clean bench.

3.4. Immunocytochemistry

Experiments were performed with differentiating podocytes on 18 mm coverslips for 14 days at 37°C without interferon-γ. Cells were washed twice with phosphate-buffered saline (PBS) and fixed with 4% paraformaldehyde in PBS for 15 min at 37°C. Next, cells were permeabilized with 0.25% Triton X-100 in PBS for 5 min and blocked with 1% BSA in PBS for 30 min. Incubation with specific antibodies for Nox4 (5 µg/ml), mitochondrial Cox I (5 µg/ml), and synaptopodin (1:100 dilution) was performed overnight at 4°C followed by incubation with secondary antibody, Alexa fluor 594 goat anti-rabbit IgG (1:200 dilution) for 1 hr at room temperature in a dark room. The cells were washed and counterstained with 1 µg/ml DAPI for 5 min and mounted on a glass slide. Fluorescence images were obtained using a confocal laser scanning microscope (TCS SPE, Leica Microsystems GmbH, Wetzlar, Germany).

3.5. cDNA preparation

Total RNA was isolated from cultured podocytes using the RNeasy kit (catalog no. 74134, Qiagen GmbH, Hilden, Germany). First strand cDNA was synthesized from 1 µg of total RNA with a reverse transcription kit (Applied Bioscience, Foster City, CA, USA) in a reaction volume of 20 µl. The reaction mixture contains 2 µl of 10x PCR buffer (final conc. = 1 x), 4 µl of 25 mM $MgCl_2$ (final conc. = 5 mM), 2 µl of 40 mM dNTPs mixture (final conc. = 1 mM), 1 µl of oligo $d(T)_{16}$ (final conc. = 2.5 µM), 1 µl of RNase inhibitor (final conc. = 1 U/µl), 1 µl of reverse transcriptase enzyme (final conc. = 2.5 U/µl) and 9 µl of RNA (1 µg). PCR program used for cDNA synthesis was 42°C for 1 hr, 94°C for 10 min and 4°C for infinity.

3.6. Quantitative real-time polymerase chain reaction

Quantitative polymerase chain reaction or real-time PCR is the technique to amplify and simultaneously quantify the gene of our interest. The procedure follows the general principle of polymerase chain reaction with detection of amplified product in “real time” using a specific DNA intercalating fluorescence dye such as SYBR green.

Real-time PCR was performed to measure the mRNA levels of candidate genes using sequence-specific primers (Table 1). β-actin was used as the reference control. For the analysis of each gene expression, experiments were conducted in triplicate in a real time PCR system (7900HT, Applied Bioscience) using SYBR Green PCR Master Mix (catalog no. 204143, Qiagen). Data was analyzed following $2^{-\Delta\Delta C}{}_{T}$ method[66].

The PCR reaction was performed with 10 µl total reaction volume containing 5 µl of 2x SYBR green PCR master mix (final conc. = 1 x), 1 µl of 10 µM forward primer (final conc. = 1 µM), 1 µl of 10 µM reverse primer (final conc. = 1 µM), 1 µl of template cDNA (50 ng/µl) (final conc. = 5 ng/µl) and 2 µl of DNase-RNase free H_2O. PCR was started with two holding temperatures at 50°C for 2 min and 95°C for 15 min as per manufacture’s instruction. In each PCR experiment, 40 cycles were considered including denaturation at 95°C for 15 s, annealing at 58°C for 30 s and extension at 72°C for 30 s. Data was collected after each PCR cycle.

3.7. Detection of condensed and apoptotic nuclei

Podocyte apoptosis were detected by nuclear staining using DAPI. Apoptotic cells display features like cell shrinkage, membrane blebbing, chromatin condensation and nuclear fragmentation resulting from activation of endogenous nuclease(s) which cleaves

DNA into oligonucleosomal fragments. This leads to appearance of dense and crescent-shaped chromatin aggregates. DAPI is a minor groove binder intercalating the A-T regions of DNA helices. Once it enters into cell and binds to DNA, the blue fluorescence will be easily visualized by fluorescent microscopy. During apoptosis, the ability of permeability for DAPI is improved and the apoptotic cells will produce higher fluorescence. Normal cells stains uniformly with a blue, round nucleus and its margin is clear. On the other hand, for apoptotic cells, the margin of nucleus is abnormal and the condensed chromosome is easily detectable.

Podocytes were grown on collagen coated coverslips and maintained for 14 days in non-permissive condition. Before fixation, media was discarded and cells were carefully washed for three times with PBS. The cells were fixed using 4% paraformaldehyde in PBS for 15 min at 37°C followed by washing with PBS for three times (5 min each). Cells were stained with DAPI (1 µg/ml, 5 min) for nuclear staining. Excess stain was washed out by PBS for three times. Cells on coverslips were mounted on a glass slide with the help of Vectashield mounting solution (Vector Laboratories Inc., Burlingame, CA, USA) and sealed the edge of the coverslips to protect it from air. Condensed and apoptotic nuclei were counted under an epifluorescence microscope (excitation at 358 nm and emission at 461 nm).

3.8. TUNEL assay

Terminal deoxynucleotidyl transferase dUTP nick end labeling (TUNEL) assay is performed to identify fragmented DNA due to induction of apoptosis. The principle of this assay is to label the fragmented DNA enzymatically by terminal deoxynucleotidyl transferase (TdT) at 3'-OH terminal with nucleotide triphosphates (dUTPs). TdT catalyzes

a template independent addition of nucleotide triphosphates to the 3'-OH ends of double-stranded or single-stranded DNA. DNA fragments which have been labeled with the digoxigenin nucleotide are then allowed to bind an anti-digoxigenin antibody that is conjugated to fluorescein. The cells are counter stained at the same time with a suitable dye, DAPI that specifically binds to nucleus. Apoptosis is confirmed by colocalization of fluorescein and DAPI using confocal microscopy.

To perform TUNEL assay, podocytes were seeded on 4-chambered glass slide (catalog no. 354114, BD Falcon, Bedford, MA, USA) and allowed to differentiate for 14 days. Cells were treated with 0.25% FBS containing media before application of TGF-β1 and inhibitors. TUNEL was performed using ApopTag Fluorescein In Situ Apoptosis Detection Kit (catalog no. S7110, Millipore Corporation, Billerica, MA, USA) according to manufacturer's instruction with minor modification. First, the cells were fixed with 4% paraformaldehyde in PBS for 15 min followed by permeabilization with 0.25% Triton X-100 at room temperature. Cells were washed thoroughly thrice with PBS and equilibrium buffer (ready to use) was applied for 30 s. Next, cells were treated with TdT enzyme (reaction buffer: TdT enzyme= 7:3) with 25 µl/chamber for overnight at 4°C in a humidified chamber. Reaction was stopped using stop/wash buffer (buffer: H_2O= 1:34) for 10 min inside a coupling jar with slow agitation for 15 s at the beginning. Anti-digoxigenin conjugate (fluorescein incorporated) (blocking solution: anti-digoxigenin conjugate= 34:31) was applied for 3 hr at room temperature inside a humidified chamber. Cells were washed thrice with PBS to remove excess stains and counter stained with DAPI. Cells on the glass-slide were mounted on a coverslip using Vectashield mounting solution and sealed the edge of the coverslip to protect it from air. DAPI (excitation at 358 nm and emission at 461 nm) and fluorescein (excitation at 494 nm and emission at 521 nm) were

colocalized by confocal microscopy to identify the apoptotic cells.

3.9. Western blots

To extract total protein from cultured podocytes, cells were washed with ice cold PBS and lysed with cold RIPA buffer (catalog no. NCI9900KR, Thermo Scientific, Rockford, IL, USA) containing protease inhibitor cocktail. The lysates were centrifuged at 13,000 rpm for 15 min at 4°C and supernatants were collected and used for Western blotting. Protein concentration was determined using BCA protein assay kit (catalog no. 23227, Thermo Scientific) and equal amount of proteins were loaded for SDS PAGE and then transferred to polyvinylidene difluoride membrane (PVDF) (catalog no. IPVH00010, Millipore Corporation). The membrane was blocked with 6% skim milk followed by primary antibody incubation at 4°C overnight. Primary antibodies for Nox4 (1 µg/ml), cleaved caspase-3 (1:1000 dilution), total and phospho p38 MAPK (1:2000 and 1:1000 dilution, respectively), mitochondrial complex I (1:2000 dilution), total and phospho Smad2 (1:1000 dilution for each), and total and phospho Smad3 (1:1000 dilution for each) were prepared with 0.1% Tris-buffered saline and Tween 20 (TBST) containing 5% BSA. β-actin (1:5000 dilution) was used as a loading control. Horseradish peroxidase (HRP)-conjugated secondary antibody against either mouse or rabbit IgG (catalog no. 31450 and 31460, respectively) was incubated for 1hr at room temperature. The bands were visualized with a UVP Biospectrum-600 imaging system using Luminata Forte enhanced chemiluminescence (ECL) solution (catalog no. WBLUF0100, Millipore Corporation). Information about primary and secondary antibodies was given in Table 2 and Table 3, respectively.

3.10. Isolation of mitochondria

Mitochondria from mouse podocytes were isolated using a commercial mitochondria isolation kit (catalog no. ab110171, Abcam, Cambridge, UK) according to manufacturer's instruction with minor modification.

The principle of mitochondria isolation is to rupture the cell using homogenizer and remove debris and extremely large cellular organelles at low speed centrifugation followed by centrifugation at a higher speed to precipitate down mitochondrial pellet.

Podocytes were grown on 100 mm dish containing 75,000cells/dish and allowed to differentiate for 14 days at 37°C. For isolation of mitochondria from a single group, cells were collected from 4 dishes and processed further.

Cells were centrifuged to collect pellet and was resuspended with 200 µl of reagent A. After 10 min incubation on ice, cells were homogenized using a Dounce homogenizer with 120 stokes (pestle B), followed by centrifugation at 1000 g for 10 min at 4°C. Supernatant (No. #1) was saved and pellet was resuspended with 200 µl of reagent B. Similar steps were followed to homogenize and centrifuge the pellet and supernatant (No. #2) was collected. Next, supernatants (No. #1 and #2) were combined and centrifuged at 12,000 g for 15 min. The pellet were collected as isolated mitochondria and resuspended into reagent C, supplemented with protease inhibitors and stored at -80°C for future experiments. The supernatant was collected as cytosolic fraction and frozen at -80°C.

3.11. Measurement of reactive oxygen species

In podocyte, cytosolic ROS generation was measured using CM-H_2DCFDA. The diacetate form, CM-H2DCFDA is passively diffuse into the cells where non-specific

cellular esterases cleave off the lipophilic groups and thereby producing a charged compound that is trapped inside the cell. CM-H_2DCFDA which is a non-fluorescence compound is oxidized in presence of ROS and converted to CM-H_2DCF, which is highly fluorescent. The wavelengths for the measurement of DCF fluorescence are ~492/495 nm for excitation and ~517/527 nm for emission.

Podocytes were differentiated on collagen coated coverslips for 14 days at 37°C. To check ROS generation, CM-H2DCF was diluted to 5 µM working concentration with same culture media and cells were incubated with that solution for 20 min at 37°C. After 20 min, excess dye was washed out using Krebs-Ringer bicarbonate (KRB) solution (135 mM NaCl, 3.6 mM KCl, 2 mM $NaHCO_3$, 0.5 mM NaH_2PO_4, 0.5 mM $MgSO_4$, 1.5 mM $CaCl_2$, 10 mM HEPES, pH 7.4) containing 5.5 mM glucose. Fluorescence intensity was measured by confocal microscopy (IX81, Olympus, Tokyo, Japan) with a confocal spinning disk (CSU10, Yokogawa Electric Corporation, Tokyo, Japan), and intensity was analyzed using MetaMorph 6.1 software (Molecular Devices, Sunnyvale, CA, USA).

3.12. Detection of mitochondrial membrane potential

Mitochondrial membrane potential ($\Delta\Psi_m$) of podocyte was measured using the lipophilic cationic dye 5,5',6,6'-tetrachloro-1,19,3,39-tetraethylbenzimidazolyl-carbocyanine iodide (JC-1) (Molecular Probes)**.** JC-1 monomers enter into mitochondria based on mitochondrial membrane potential and form J-aggregates inside the mitochondria transmitting red fluorescence (excitation/emission maxima: 585/590 nm) while the rest of the monomer outside mitochondria transmit green fluorescence (excitation/emission maxima: 514/529 nm). The ratio of red/green fluorescence was used as an indicator of mitochondrial membrane potential.

For this experiment, cells were grown on 96 well flat clear bottom black polystyrene TC-treated microplates (catalog no. 3603, Corning Inc., Corning, NY, USA). Cells were washed twice with warm PBS before loading with JC-1 (300 nM) for 40 min and the fluorescence was read by a fluorescence micro-plate reader (Flexstation II, Molecular Devices, Sunnyvale, California, USA) as described previously[82].

3.13. Nox activity measurement

Total Nox activity was measured as described previously[29] with minor modification. Podocytes were washed twice with warm PBS and scraped from the dishes with PBS containing protease inhibitor following centrifugation at 2000 rpm for 3 min at 4°C. Cell pellets were dissolved in lysis buffer (20 mM KH_2PO_4, 1 mM EGTA, protease inhibitor cocktail, pH 7.0). The cell suspensions were homogenized with 100 strokes in a Dounce homogenizer and the homogenates (50 µg) were added to 50 mM phosphate buffer (pH 7.0) including 1 mM EGTA, 150 mM sucrose, 5 µM lucigenin and 100 µM NADPH. To check the mitochondrial Nox activity, 30 µg mitochondria (equivalent to mitochondrial protein) was considered. The reaction generated photon particles that were detected by a luminometer (Synergy 2, BioTek Instruments, Winooski, VT, USA) every 20 s for 10 min continuously and this was expressed as relative light units (RLU). The blank buffer reading was subtracted from each test reading and superoxide generation was expressed as RLU/min/µg protein.

3.14. siRNA transfection

Small interfering RNA (siRNA) is a class of double-stranded RNA molecules, 20-25 base pairs in length. It mediates post-transcriptional gene silencing by interfering with the

expression of specific genes with its complementary nucleotide sequence.

To knockdown Nox4, Smad2 and Smad3, SiGENOME Smartpool siRNA duplexes (mixture of 4 different siRNA targeting 4 different regions of one mRNA) were purchased from Dharmacon (Thermo Fisher Scientific Inc., Lafayette, CO, USA). siRNAs for Smad7 and non-targeting sequences (siControl) were synthesized from Bioneer Inc. (Daejeon, Korea), the sequences were already reported in the publication[37, 89]. The sequences for siRNAs are given in Table 4. Transfection of siRNA oligo was carried out using DharmaFECT-1 siRNA transfection reagent (catalog no. T-2001-03, Thermo Scientific).

Podocytes were cultured in 6-well 35 mm collagen coated dishes and allowed for differentiation for 14 days. Transfection was carried out according to manufacturer's protocol with minor variation. For a single 35 mm dish, total transfection volume was 2 ml including 7 µl Dharmafect-1 and siRNA, diluted in opti-MEM media (catalog no. 31985-070, Gibco). In separate tubes, siRNA and Dharmafect-1 were diluted with opti-MEM to the final volume of 200 µl to each tube and kept in room temperature. After 5 min, contents of those two tubes were combined and pipette out gently to mix and kept for 20 min at room temperature. This step allows formation of siRNA-transfection reagent complex which delivers siRNA into the cell. Antibiotic-free opti-MEM (1.6 ml) was added to the cell grown in 35 mm dish so that the final volume reached to 2 ml. After 20 min, siRNA-transfection reagent complex were added drop-wise on the cells with slow swirling to spread properly.

Knockdown of genes were assessed at 48 hr by determining mRNA levels using quantitative PCR. For assessing protein levels, Western blotting was performed at 72 hr after siRNA transfection. Functional assays for siRNA mediated gene silencing were performed at 72 hr for mRNA level and 96 hr for protein level after siRNA treatment.

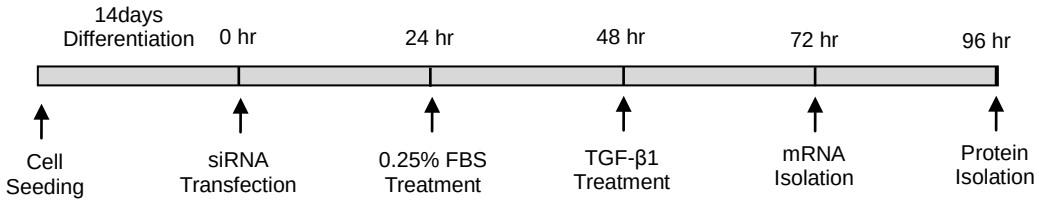

Fig. 2. Schematic representation of siRNA transfection in mouse podocytes.

Podocytes were seeded on either 6-well dishes or coverslips and maintained for 14 days at 37°C before siRNA experiments. Gene silencing steps were conducted using opti-MEM medium (without FBS and penicillin) which was replaced with DMEM low glucose media (containing 0.25% and 0.25% penicillin) after 24 hr followed by TGF-β1 stimulation at 48 hr from the start of siRNA treatment. To check the effect of siRNA, mRNAs and proteins were isolated at 72 hr and 96 hr, respectively.

3.15. Infection of adenovirus and transfection of plasmids

Doxycycline-inducible adenovirus encoding mitochondria-targeted cyan fluorescence protein (mitoCFP) was constructed using the Adeno-X Tet-On expression system (Clontech Laboratories Inc., Mountain View, CA, USA). Adenovirus encoding mitoCFP were applied together with adenovirus expressing the reverse tetracycline-transactivator for 90~120 min at 37°C as described[82] and used after 48 hr for experiments. D1ER plasmid was transfected into podocytes using FuGENE HD transfection reagent (catalog no. E231A, Promega, Madison, WI, USA) according to the manufacturer's instruction. Experiments were conducted 48 hr after transfection. Fluorescence images for mitoCFP and D1ER (excitation/emission: 440/490 nm) were obtained using a confocal laser scanning microscope (TCS SPE, Leica Microsystems GmbH, Wetzlar, Germany).

3.16. Statistical analysis

Experimental values are presented as mean ± SEM. N is the number of independent experiments. Statistical comparisons between two groups of data were analyzed by two-tailed unpaired Student's *t*-test. Multiple comparisons were determined using one-way ANOVA followed by post-hoc test (Tukey's multiple comparison test) and $p<0.05$ was considered significant.

Table 1. List of primer sequences used for PCR.

Primer Name	GeneBank Accession No.	Sequence	Size (bp)
β-actin	NM_007393.3	F-5' AAGAGCTATGAGCTGCCTGA 3'	
		R-5' CACAGGATTCCATACCCAAG 3'	106
Synaptopodin	NM_177340.2	F-5' AAGGGTCTGACCTCATTGGA 3'	
		R-5' GCAAAACCAAGGGCTACAAC 3'	109
Nox1	NM_172203.1	F-5' TCACGAGTGGGATGACCATA 3'	
		R-5' GCAAGGATCCACTTCCAAGA 3'	84
Nox2	NM_007807.4	F-5' AAAGGTGGTCATCACCAAGG 3'	
		R-5' TCCCACCTCCATCTTGAATC 3'	88
Nox4	NM_015760.4	F-5' CCACAGACCTGGATTTGGAT 3'	
		R-5' TGGTGACAGGTTTGTTGCTC 3'	91
p22Phox	NM_007806.3	F-5' GCCATTGCCAGTGTGATCTA 3'	
		R-5' TAGGTGGTTGCTTGATGGTG 3'	115
CYP4A	NM_177406.3	F-5' AATGAGCTGAAGGTGGCTGT 3'	
		R-5' CAAGTGGATCCCATTCTTGG 3'	120
Smad2	NM_001252481.1	F-5' AGACCCATCAAACTCGGAGA 3'	
		R-5' AGCAAACACTTCCCCACCTA 3'	133
Smad3	NM_016769.4	F-5' TTCACTGACCCCTCCAACTC 3'	
		R-5' CGATGTAGTAGAGCCGCACA 3'	121

Continued

Primer Name	GeneBank Accession No.	Sequence	Size (bp)
Smad7	NM_001042660.1	F-5’ CAACCCCCATCACCTTAGTC 3’ R-5’ CGGAGGAAGGTACAGCATCT 3’	119
MMP-9	NM_013599.2	F-5’ AGACGACATAGACGGCATCC 3’ R-5’ GTGGTTCAGTTGTGGTGGTG 3’	86
MMP-2	NM_008610.2	F-5’ GCCAAGGTGGAAATCAGAGA 3’ R-5’ GTTGAAGGAAACGAGCGAAG 3’	105
Fibronectin 1	NM_010233.2	F-5’ AACCGGAATTACACCGACTG 3’ R-5’ TGATCGGCATCGTAGTTCTG 3’	86
α-SMA	NM_007392	F-5’ CATCAGGGAGTAATGGTTGGA 3’ R-5’ GGTGATGATGCCGTGTTCTAT 3’	114
Collagen IVα3	NM_007734.2	F-5’ GCAACGGATCTAAGGGTGAA 3’ R-5’ TCCTTTCAAGCCATCAGGAC 3’	89
Collagen IVα5	NM_009360.4	F-5’ CACGGGGAACAGTTCATATC 3’ R-5’ ATGGTACTGAAGCGACGAAG 3’	118
Integrin α3	NM_001163434.1	F-5’ ATGCCTACCCAGTCCTCAA 3’ R-5’ TTGCTGTCGCACTTGTTG 3’	97
Integrin β1	X77952.1	F-5’ GTCAGCAACGCATATCTGGA 3’ R-5’ ACATTCCTCCAGCCAATCAG 3’	100

Continued

Primer Name	GeneBank Accession No.	Sequence	Size (bp)
Dystroglycan	NM_010017.3	F-5’ GCCCAACACTGACAATTCCT 3’ R-5’ ACTCGTGGCTTCTTTGTGGT 3’	82
Utrophin	NM_011682.4	F-5’ GTTTGAGGTGCTTCCTCAGC 3’ R-5’ CCAGCACTGCACTCTGGATA 3’	119
Cox2	AK138996.1	F-5’ CTCAATGAGTACCGCAAACG 3’ R-5’ CTGCAGCCATTTCCTTCTCT 3’	82
Caveolin-1	NM_007616.3	F-5’ CCGCTTGTTGTCTACGATCT 3’ R-5’ GATGTGCAGGAAGGAGAGAA 3’	82
Caveolin-2	NM_016900.3	F-5’ ATCTGCAGCCATGCTCTCTT 3’ R-5’ ACAGGATACCCGCAATGAAG 3’	100
TGF-βRII	NM_009371.3	F-5’ GTGGGAACGGCAAGATACAT 3’ R-5’ ATCCGTCTGCTTGAACGACT 3’	84
Alk-1	NM_009612.2	F-5’ TGACCTCAAGAGTCGCAATG 3’ R-5’ GTTGTTGCCGATATCCAGGT 3’	115
Alk-5	NM_009370.2	F-5’ TCGACGCTGTTCTATTGGTG 3’ R-5’ CAACCGATGGATCAGAAGGT 3’	80
id-1	NM_010495	F-5’ AGGGGATCTCTGGGAAAGAC 3’ R-5’ AGAGGGTGAGGCTCTGTTGA 3’	94

Continued

Primer Name	GeneBank Accession No.	Sequence	Size (bp)
PAI-1	NM_008871	F-5’ AGTCTTTCCGACCAAGAGCA 3’	
		R-5’ ACAAAGGCTGTGGAGGAAGA 3’	104
TGF-β1	NM_011577.1	F-5’ CGGCAGCTGTACATTGACTT 3’	
		R-5’ CAGACAGAAGTTGGCATGGT 3’	84
Poldip2	NM_026389.3	F-5’ AGGTTCCCATTCAACACGAG 3’	
		R-5’ GTTTCTCGAGCCACAAAAGG 3’	82

F, forward primer

R, reverse primer

bp, base pairs

Table 2. List of primary antibodies.

Antibody Name	Catalog no.	Manufacturer	Host Species
β-actin	ab6276	Abcam	Mouse
Nox4	ab60940	Abcam	Rabbit
Nephrin	ab58968	Abcam	Rabbit
Paxillin (N-term)	1500-1	Epitomics	Rabbit
Cox I	459600	Invitrogen	Mouse
Mitochondrial complex I	459100	Invitrogen	Mouse
Synaptopodin	03-65194	American Research	Mouse
Cleaved caspase-3	9661	Cell Signaling Technology	Rabbit
Smad2 (phospho)	3108	Cell Signaling Technology	Rabbit
Smad2 (Total)	5339	Cell Signaling Technology	Rabbit
Smad3 (phospho)	9520	Cell Signaling Technology	Rabbit
Smad3 (Total)	9523	Cell Signaling Technology	Rabbit
p38 MAPK (phospho)	4092	Cell Signaling Technology	Rabbit
p38 MAPK (Total)	8690	Cell Signaling Technology	Rabbit
mTOR (phospho)	2971	Cell Signaling Technology	Rabbit
mTOR (total)	2972	Cell Signaling Technology	Rabbit
p70S6K (phospho)	2904	Cell Signaling Technology	Rabbit
p70S6K (total)	2902	Cell Signaling Technology	Rabbit
ERK1/2 (phospho)	9101	Cell Signaling Technology	Rabbit
ERK1/2 (total)	9102	Cell Signaling Technology	Rabbit
Vimentin	5741	Cell Signaling Technology	Rabbit

Table 3. List of secondary antibodies.

Antibody Name	Catalog no.	Manufacturer	Host
Anti-mouse HRP	31450	Thermo Scientific	Rabbit
Anti-Rabbit HRP	31460	Thermo Scientific	Goat
Anti-Rabbit Alexa Flour 594	A31631	Molecular Probes	Goat
Anti-Rabbit Alexa Flour 488	A31627	Molecular Probes	Goat
Anti-Mouse Alexa Flour 594	A31632	Molecular Probes	Goat

Table 4. List of siRNA sequences.

Name of siRNA	Sequence	Working Concentration
siNon-Targeting	5’-GAG GCT GTG TTG CTG TGA A-3	50nM/100nM
siNox4		
Dharmacon (D-058509)	5’-UCA CAU GUG GUG UAA CUA U-3’	
(Combination of 4 siRNAs)	5’-AGA CCU GGC CAG UAU AUU A-3’	50nM
	5’-UAC CCU AAG UUA UAC AUU G-3’	
	5’-GAU GGG AUU CAG AAG AUA A-3’	
siSmad2		
Dharmacon (D-040707)	5’-GAA CAA ACC AGG UCU CUU G-3’	
(Combination of 4 siRNAs)	5’-CAA CAG GCC UUU ACA GCU U-3’	50nM
	5’-GGA AAG GGU UGC CAC AUG U-3’	
	5’-GAC AAA GUA UUA ACU CAG A-3’	
siSmaad3		
Dharmacon (D-040706)	5’-GCA CAG CCA CCA UGA AUU A-3’	
(Combination of 4 siRNAs)	5’-GGA AUU UGC UGC CCU CCU A-3’	50nM
	5’-UAA CUU CCC UGC UGG CAU U-3’	
	5’-GAG UUU GCC UUC AAC AUG A-3’	
siSmad7	5’-CCUACGCCACCAAUUUCGU-3’	100nM

IV. RESULTS

4.1. Characterization of mouse podocytes in culture

Immortalized mouse podocyte cell line was a kind gift from Prof. Mundel. Before the start of experiment, the cell line was checked for proper differentiation and podocyte specific marker expression. In standard culture condition, podocytes appeared cobblestone phenotype on collagen coated dish at 33°C (Fig. 3A). After thermoshifting to 37°C, clear structural changes in podocytes were apparent from day 2-3. Increased cytoplasm to nuclear ratio, compared to proliferative cells at permissive condition, was obvious at day 5 (Fig. 3B). Cells were fully differentiated at day 13 or 14 having arborized morphology bearing highly branched processes (Fig. 3C). Podocyte differentiation at molecular level was also evaluated. The specific marker for podocyte differentiation is synaptopodin[101]. Synaptopodin expression was demonstrated by immunostaining, RT-PCR and real-time PCR. Synaptopodin expression and its organization were evaluated by immunocytochemistry using a synaptopodin specific monoclonal antibody. Podocytes at 37°C, but not at 33°C, showed a distinct synaptopodin staining pattern (Fig. 4A-B). Synaptopodin mRNA expression was amplified in 14 days old podocytes at 37°C by RT PCR (Fig. 4C) while synaptopodin mRNA was not detected from podocytes at 33°C. To demonstrate the differentiation of podocytes at 37°C, synaptopodin mRNAs at day 1, 3, 7 and 14 from podocytes were analyzed. Real-time PCR showed gradual increase of synaptopodin mRNA level from day 1 to day 14 (Fig. 4D). Next we demonstrated the expression of nephrin which is a crucial protein for podocyte function[101]. Cultured podocytes expressed nephrin both at 33°C and 37°C culture condition (Fig. 5A-B) but

their organization was completely different at those two temperatures. In undifferentiated podocytes at 33°C, nephrin was stained scattered around inside the cytoplasm, on the other hand at 37°C podocytes, nephrin was well organized and detected on plasma membrane near the junction of two neighboring cells which might resemble slit diaphragm like structural organization *in vitro*[101]. Nephrin expression was also confirmed by Western blotting and its expression was detected in podocytes cultured in both permissive and non-permissive condition (Fig. 5C). Next, organization of actin filament and distribution of intermediate filament protein vimentin were examined. In cobblestones, actin fibers were localized to the cortical area, whereas actin stress-fiber like bundles appeared and extended across the cell in arborized podocytes (Fig. 6A-B). Focal adhesions were detected by paxillin staining. Random distribution of paxillin in cobblestoned cells was changed and was predominantly localized to the tips of the stress fiber (Fib. 6B, enlarged in inset) into arborized cells. Distribution of stress fibers was also shown in a confluent population of differentiated cells (Fig 6C) in which distinct actin fiber bundles were clearly visible (Fig. 6D). Vimentin staining revealed the morphological conversion of vimentin network in differentiated podocytes which was completely absent in undifferentiated cells (Fig 7A-D).

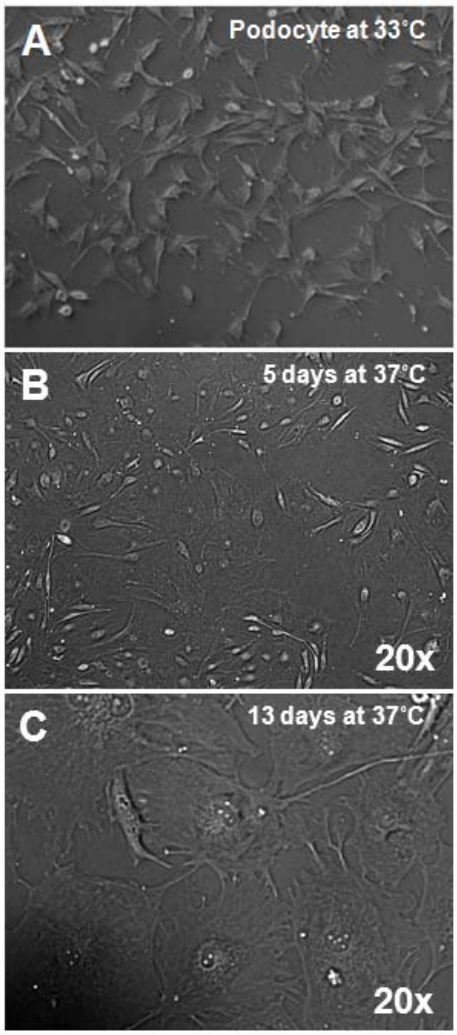

Fig. 3. Changes of podocyte morphology at different culture conditions.

A, Podocytes showed cobblestone phenotype at 33°C on collagen coated dishes in the presence of INF-γ (20 U/ml). *B,* Podocytes began to convert into arborized cells at 37°C in day 5 and some of those cells were died during culture. *C,* Fully differentiated podocytes after 13 days of thermoshift with well-developed processes. (Magnification, x20).

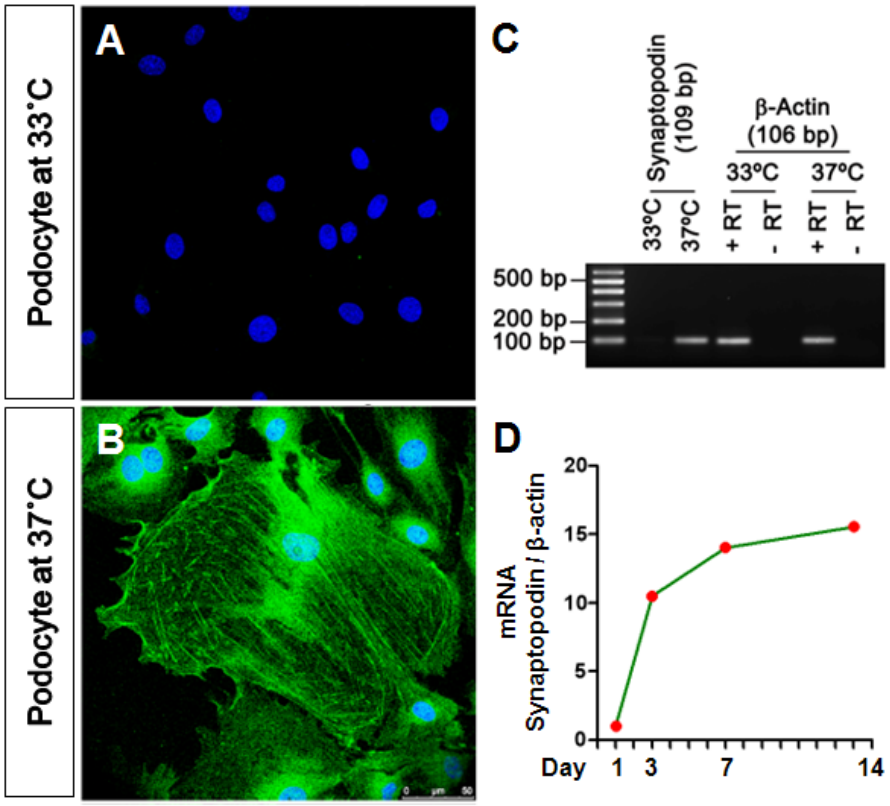

Fig. 4: Expression of synaptopodin, a specific marker for podocyte differentiation.

Synaptopodin expression indicated differentiation of podocytes in culture. *A,* Absence of differentiation marker synaptopodin in undifferentiated cell at 33°C. *B,* Synaptopodin distribution was shown in green with nuclear DAPI staining in fully differentiated podocytes at 37°C. *C,* Semi-quantitative PCR showed amplification of PCR product isolated from cells at 37°C, but not from cells grown at 33°C. β-actin was amplified as in internal control to demonstrate absence of genomic DNA contamination in cDNA. *D,* Real-time PCR analysis showed increase of synaptopodin expression between day 1 and day 14, characteristic of podocyte differentiation.

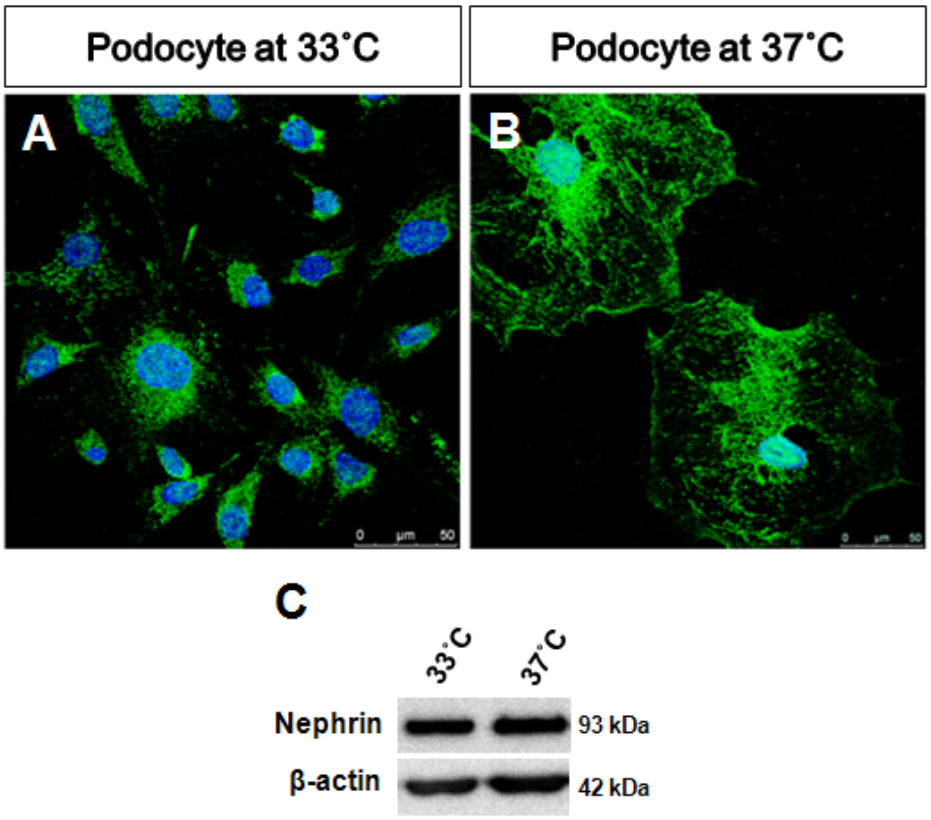

Fig. 5. Expression and distribution of nephrin in mouse podocytes.

Expression of podocyte specific marker, nephrin, was checked in podocytes. *A,* Immunostaining revealed scattered distribution of nephrin in the cytoplasm of undifferentiated podocytes at 33°C. *B,* Re-organization of nephrin on the cell membrane in podocytes at 37°C. *C,* Nephrin was expressed in podocytes in both the culture conditions (33°C and 37°C) shown by Western blotting.

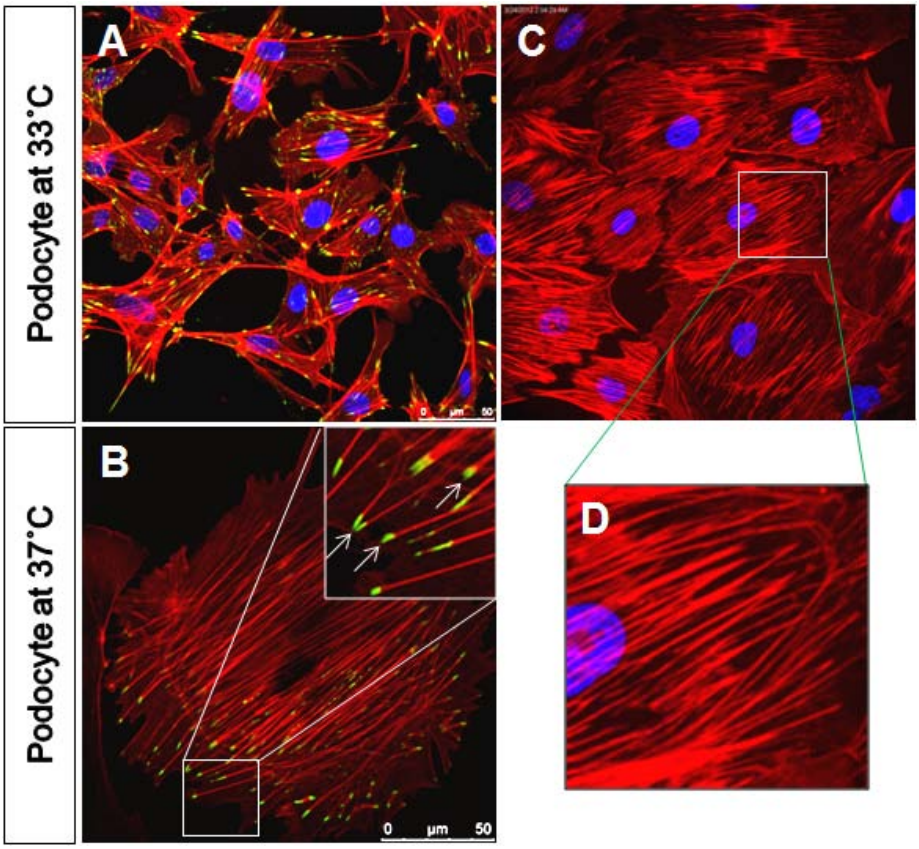

Fig. 6. Organization of actin cytoskeleton in mouse podocytes.

Mouse podocytes were grown on collagen coated coverslips for 14 days. *A,* Actin filaments (red) were predominantly localized to the cortical region with random paxillin staining (green) in undifferentiated podocytes. *B-C,* Well organized stress fiber bundles extended into processes of podocytes. Paxillin was present at the tip of stress fibers (*B*, inset). *D,* Enlargement of a portion of figure *C*.

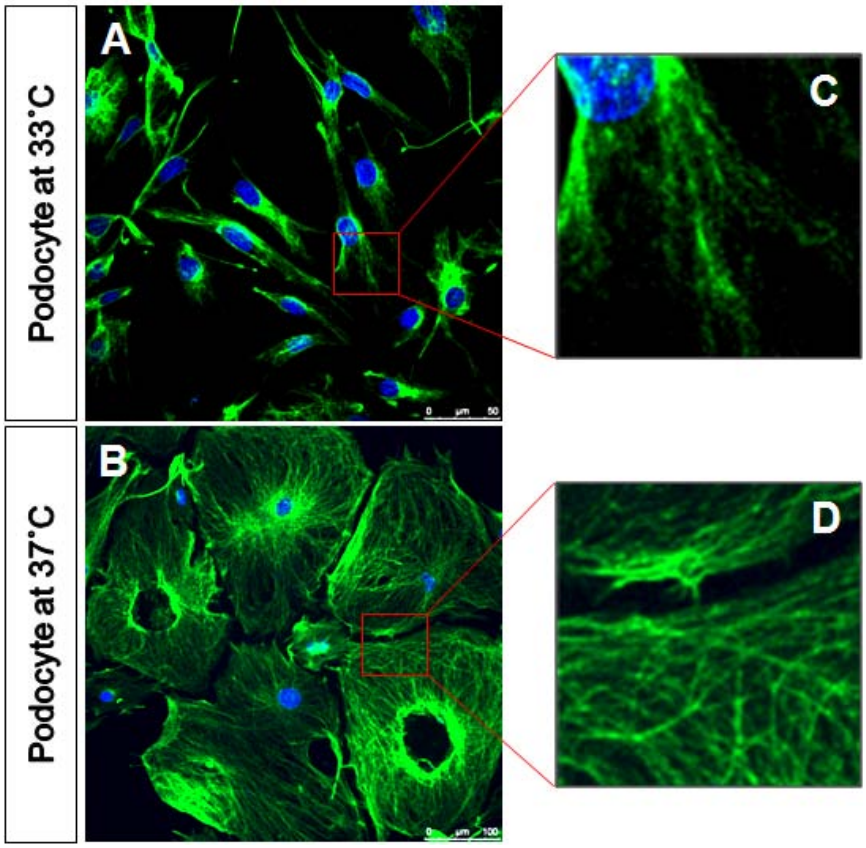

Fig. 7. Organization of intermediate filament protein vimentin in mouse podocytes. Vimentin distribution was observed in differentiated mouse podocytes by immunocytochemistry. *A,* Diffused cytosolic staining of vimentin (green) was apparent in proliferating podocytes cultured in permissive condition. *B,* Fibrillar vimentin network (green) was obvious in differentiated podocytes. *C-D,* Representing enlargement parts of figures *A* and *B*, respectively. Nuclei were stained with DAPI (blue).

4.2. Analysis of gene expressions in control and TGF-β1-treated mouse podocytes

To identify the pathogenic changes by TGF-β1, mRNA expressions were measured by real-time PCR for 20 different genes after TGF-β1 treatment for different time-point and along with TGF-βRI inhibitor, SB431542 (SB). EMT related genes MMP-9 (133.55 ± 0.14 at 6 hr, 244.96 ± 0.25 at 12hr, 133.17 ± 0.06 at 24 hr, 258.03 ± 0.18 at 48 hr, 0.56 ± 0.28 at 12 hr with SB, Fig. 8A), MMP-2 (5.52 ± 0.15 at 6 hr, 4.45 ± 0.23 at 12 hr, 3.83 ± 0.08 at 24 hr, 339 ± 0.17 at 48 hr, 0.63 ± 0.26 at 6 hr with SB, Fig. 8B), Fibronectin (2.45 ± 0.19 at 6 hr, 3.92 ± 0.21 at 12 hr, 4.71 ± 0.20 at 24 hr, 7.36 ± 0.31 at 48 hr, 2.01 ± 0.24 at 48 hr with SB, Fig. 8C) and α-SMA (2.99 ± 0.14 at 6 hr, 2.53 ± 0.22 at 12 hr, 2..35 ± 0.12 at 24 hr, 1.98 ± 0.18 at 48 hr, 0.68 ± 0.09 at 6 hr with SB, Fig. 8D) were increased by TGF-β1. mRNA level of fibrosis marker collagen IVα3 (9.62 ± 0.14 at 6 hr, 36.34 ± 0.24 at 12 hr, 38.60 ± 0.09 at 24 hr, 11.00 ± 0.17 at 48 hr, 0.19 ± 0.02 at 24 hr with SB, Fig. 8E) was increased, whereas collagen IVα5 (0.53 ± 0.15 at 6 hr, 0.49 ± 0.18 at 12 hr, 0.42 ± 0.23 at 24 hr, 0.57 ± 0.27 at 48 hr, 0.83 ± 0.22 at 24 hr with SB, Fig. 8F) were slightly reduced by TGF-β1. Nox4 (0.46 ± 0.25 at 6 hr, 1.62 ± 1.11 at 12 hr, 5.66 ± 0.33 at 24 hr, 9.45 ± 3.51 at 48 hr, 1.01 ± 0.06 at 24 hr with SB, Fig. 9A) mRNA level was also increased with time period. Inflammatory gene cyclooxygenase-2 (Cox2) (24.68 ± 0.34 at 6 hr, 19.43 ± 0.29 at 12 hr, 12.00 ± 0.25 at 24 hr, 10.30 ± 0.30 at 48 hr, 1.38 ± 0.45 at 6 hr with SB, Fig. 9B) expression was highly increased at 6 hr and slowly reduced over time. Though caveolin-1 (1.37 ± 0.13 at 6 hr, 0.46 ± 0.23 at 12 hr, 0.28 ± 0.05 at 24 hr, 0.81 ± 0.16 at 48 hr, 0.86 ± 0.25 at 24 hr with SB, Fig. 9C) expression was greatly reduced at 24 hr. Caveolin-2 (0.72 ± 0.14 at 6 hr, 0.97 ± 0.22 at 12 hr, 0.66 ± 0.10 at 24 hr, 2.10 ± 0.16 at 48 hr, 0.77 ± 0.25 at 24 hr with SB, Fig. 9D) expression was not greatly changed by TGF-β1 treatment.

Podocyte GBM interacting proteins integrin α3 (0.49 ± 0.22 at 6 hr, 0.93 ± 0.21 at 12 hr, 0.84 ± 0.13 at 24 hr, 1.25 ± 0.47 at 48 hr, 1.15 ± 0.22 at 6 hr with SB, Fig. 10A) and integrin β1 (0.45 ± 0.15 at 6 hr, 1.12 ± 0.08 at 12 hr, 1.16 ± 0.02 at 24 hr, 1.25 ± 0.47 at 48 hr, 0.75 ± 0.24 at 6 hr with SB, Fig. 10B) were reduced by TGF-β1 at 6 hr, but their expressions were reached to basal level at 12 hr and maintained till 48 hr. Another GBM anchoring protein dystroglycan (1.03 ± 0.14 at 6 hr, 0.55 ± 0.21 at 12 hr, 0.39 ± 0.07 at 24 hr, 0.78 ± 0.16 at 48 hr, 0.65 ± 0.25 at 24 hr with SB, Fig. 10C) was significantly reduced at 24 hr of TGF-β1 treatment. Utrophin (0.35 ± 0.14 at 6 hr, 1.39 ± 0.22 at 12 hr, 1.01 ± 0.12 at 24 hr, 1.08 ± 0.18 at 48 hr, 0.98 ± 0.63 at 24 hr with SB, Fig. 10D), another component of dystrophin-associated glycoprotein complex, was greatly reduced at 6 hr, but regained its expression to basal level at 12 hr to 48 hr. Time-dependent expression of TGF-β, TGF-β receptors and their downstream target molecules were also analyzed after TGF-β1 stimulation. Expression of TGF-βRII (0.23 ± 0.04 at 6 hr, 0.48 ± 0.28 at 12 hr, 0.37 ± 0.11 at 24 hr, 0.20 ± 0.02 at 48 hr, 0.97 ± 0.58 at 48 hr with SB, Fig. 11A) was reduced from early time point to 48 hr. Activin receptor-like kinase-1 (Alk-1) (7.59 ± 0.16 at 6 hr, 40.79 ± 0.35 at 12 hr, 56.49 ± 0.26 at 24 hr, 23.59 ± 0.18 at 48 hr, 0.37 ± 0.30 at 24 hr with SB, Fig. 11B) expression was greatly elevated with its peak at 24 hr. Alk-5 (1.66 ± 0.40 at 6 hr, 2.98 ± 0.29 at 12 hr, 2.47 ± 0.17 at 24 hr, 1.02 ± 0.0.57 at 48 hr, 1.09 ± 0.25 at 12 hr with SB, Fig. 11C) expression was slightly increased at 12 hr, but reduced to basal level at 48 hr. Expression of inhibition-of-differentiation (id-1) (5.40 ± 0.11 at 6 hr, 2.74 ± 0.14 at 12hr, 1.65 ± 0.21 at 24 hr, 1.61 ± 0.0.16 at 48 hr, 1.33 ± 0.07 at 1 hr with SB, Fig. 11D) reached at peak at 1 hr and sharply returned to base between 6 to 12 hr. PAI-1 (49.85 ± 0.14 at 6 hr, 25.51 ± 0.23 at 12 hr, 18.47 ± 0.05 at 24hr, 39.46 ± 0.0.16 at 48 hr, 1.04 ± 0.30 at 6 hr with SB, Fig. 11E) expression was highly increased by TGF-β1

treatment and remained elevated till 48 hr. The mRNA level of TGF-β1 (4.49 ± 2.06 at 6 hr, 4.42 ± 1.20 at 12 hr, 3.67 ± 1.59 at 24 hr, 2.16 ± 0.72 at 48 hr, 1.13 ± 0.37 at 12 hr with SB, Fig. 11F) was slightly increased by TGF-β1 stimulation from 6 to 24 hr. Interesting to notice that expressional changes of all the genes was effectively inhibited by addition of SB, a TGF-βRI inhibitor.

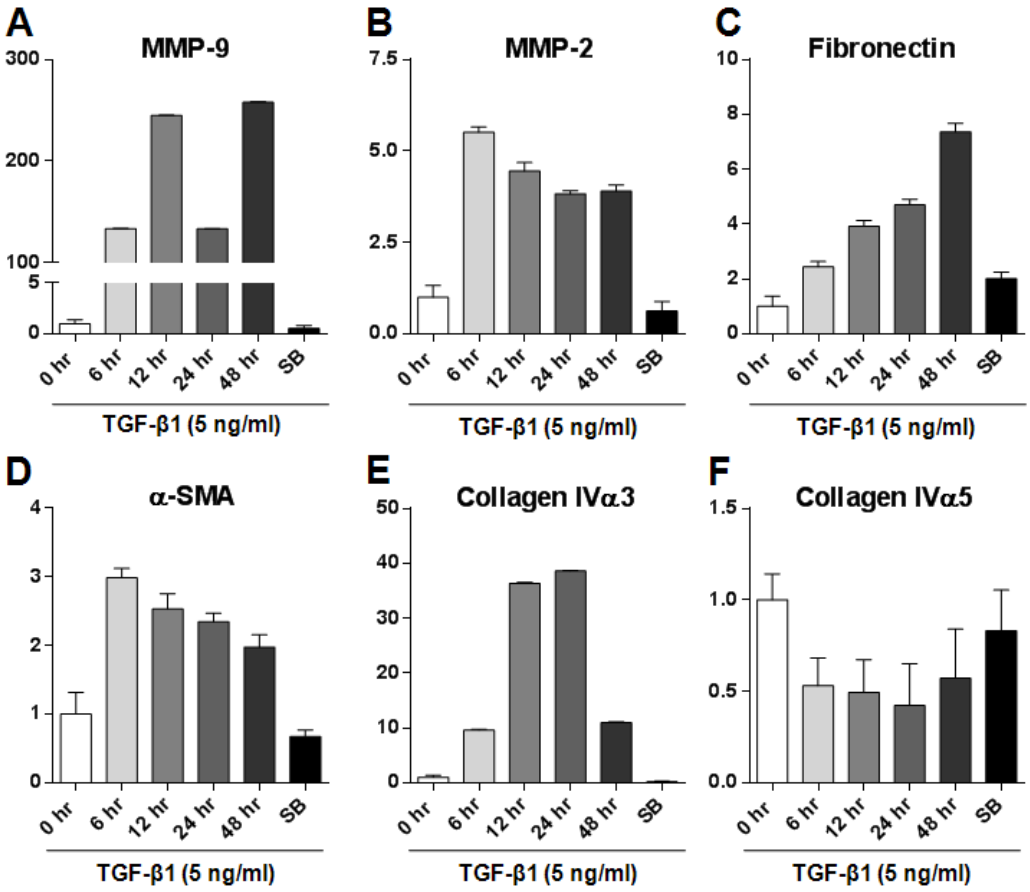

Fig. 8. Alternation of mRNA levels of EMT and fibrosis related genes by TGF-β1 treatment in mouse podocytes.

Podocytes were treated with TGF-β1 (5 ng/ml) for different time point (0-48 hr) and in combination with TGF-βRI inhibitor SB431542 (SB) (10 μM). *A-F*, Real-time PCR was performed to check the mRNA expression of matrix metalloproteinase-9 (MMP-9), MMP-2, Fibronectin, α-smooth muscle actin (α-SMA), Collagen IVα3 and Collagen IVα5. Data are presented as mean ± SEM.

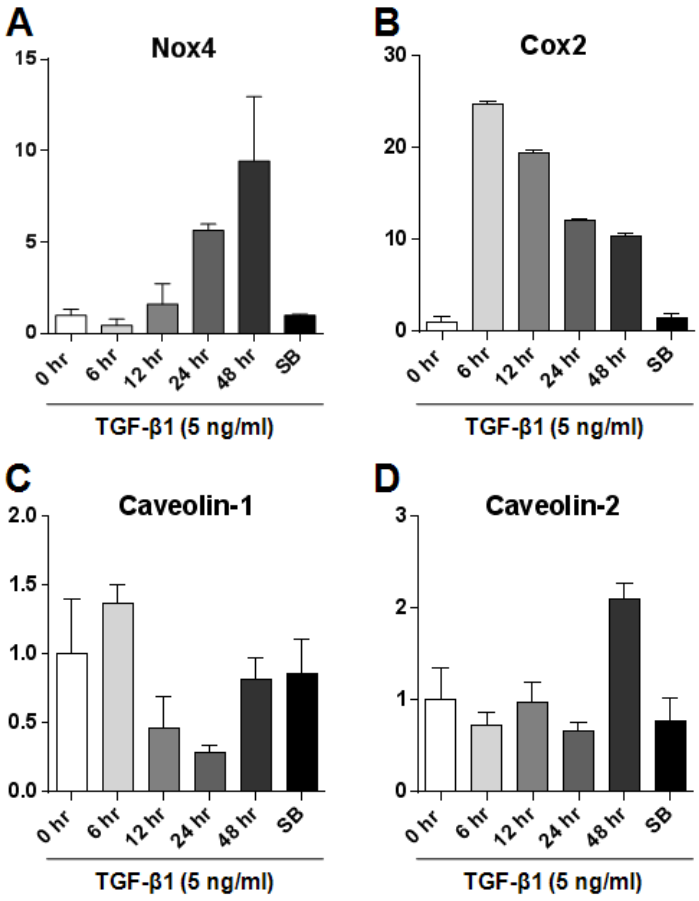

Fig. 9. TGF-β1-induced alteration of mRNA level of pathogenesis related genes in mouse podocytes.

Podocytes were treated with TGF-β1 (5 ng/ml) for different time point (0-48 hr) and in combination with TGF-βRI inhibitor SB431542 (SB) (10 μM). *A-D,* Real-time PCR was performed to check the mRNA expression of Nox4, Cox2, Caveolin-1, and Caveolin-2. Data are presented as mean ± SEM.

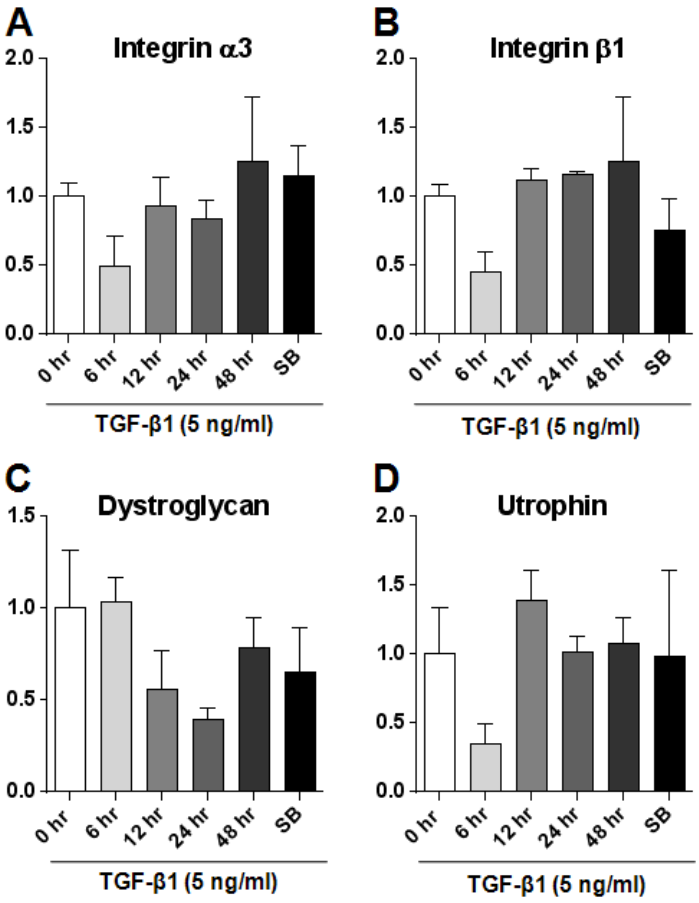

Fig. 10. qPCR analysis of genes required for podocyte adhesion to GBM after TGF-β1 treatment.

Podocytes were treated with TGF-β1 (5 ng/ml) for different time point (0-48 hr) and in combination with TGF-βRI inhibitor SB431542 (SB) (10 μM). *A-D,* Real-time PCR was performed to check the mRNA expression of Integrin α3, Integrin β1, Dystroglycan and Utrophin. Data are presented as mean ± SEM.

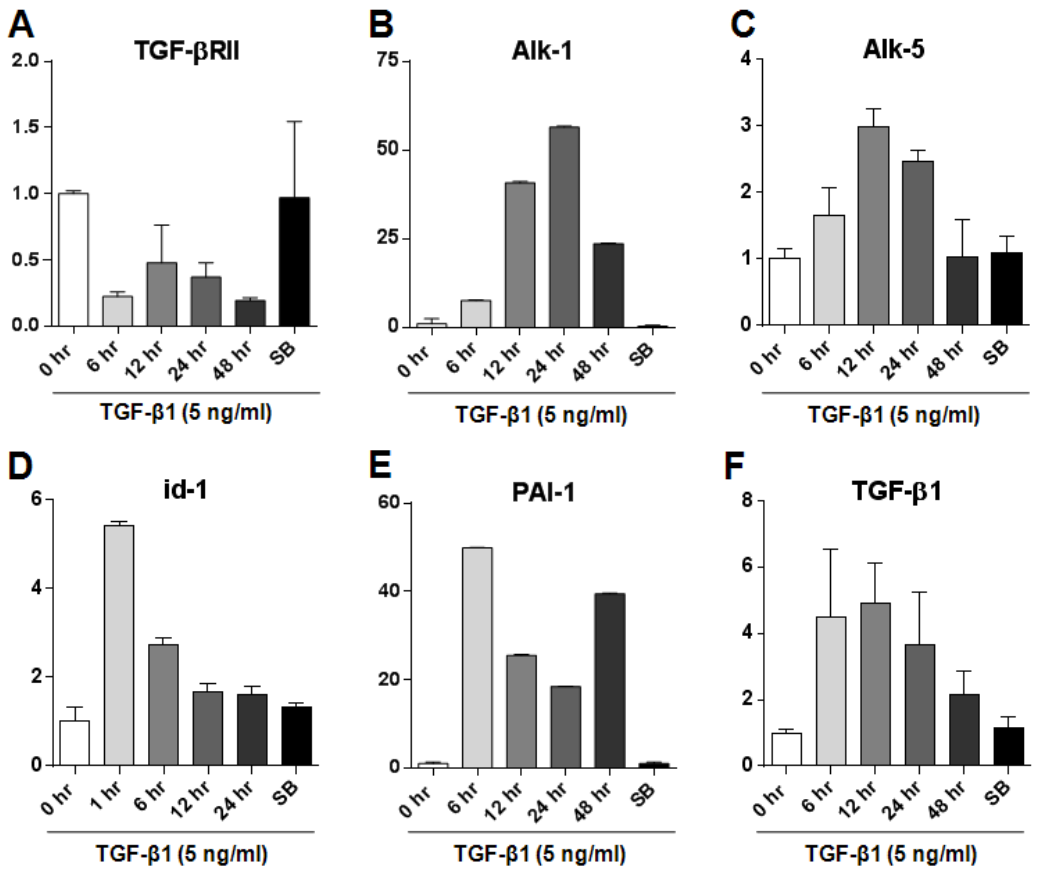

Fig. 11. mRNA analysis of TGF-β1, its receptors and downstream signaling molecules after TGF-β1 stimulation.

Podocytes were treated with TGF-β1 (5 ng/ml) for different time point (0-48 hr) and in combination with TGF-βRI inhibitor SB431542 (SB) (10 μM). *A-F,* Real-time PCR was performed to check the mRNA expression of TGF-βRII, activin receptor-like kinase-1 (Alk-1), Alk-5, inhibition-of-differentiation (id-1), plasminogen activator inhibitor 1 (PAI-1) and TGF-β1. Data are presented as mean ± SEM.

4.3. TGF-β1 induced podocyte apoptosis

Using differentiated podocytes, a dose-dependent experiment with different concentration of TGF-β1 was performed. Apoptotic cells were estimated using nuclear staining with DAPI, Western blotting for cleaved caspase-3, and TUNEL assay. Compared to the control group, TGF-β1 stimulation greatly increased the proportion of condensed and fragmented nuclei (Fig. 12A-C) and TUNEL positive nuclei (Fig. 13B-C) indicated by the white arrows. Counting apoptotic nuclei by DAPI staining showed that 5 ng/ml of TGF-β1 induced the maximum apoptotic response (18.1 ± 0.9%, N=5) compared to 10 ng/ml of TGF-β1 (15.5 ± 0.7%, N=6) in our culture condition (Fig. 12D). TGF-β1 also increased activation of caspase-3 maximally at 5 ng/ml (Fig. 13A). Thus, all the subsequent experiments were carried out using 5 ng/ml TGF-β1, unless otherwise mentioned. To check whether cleaved caspase-3 activation induced podocyte cell death by TGF-β1 treatment, we performed TUNEL assay in presence of pan-caspase inhibitor Z-VAD (OMe)-FMK (z-VAD) (Millipore). Z-VAD (OMe)-FMK (25 μM) was treated 1 hr before TGF-β1 treatment and reduced podocyte cell death by 65.15% (Fig. 13D, N=3, $p<0.05$).

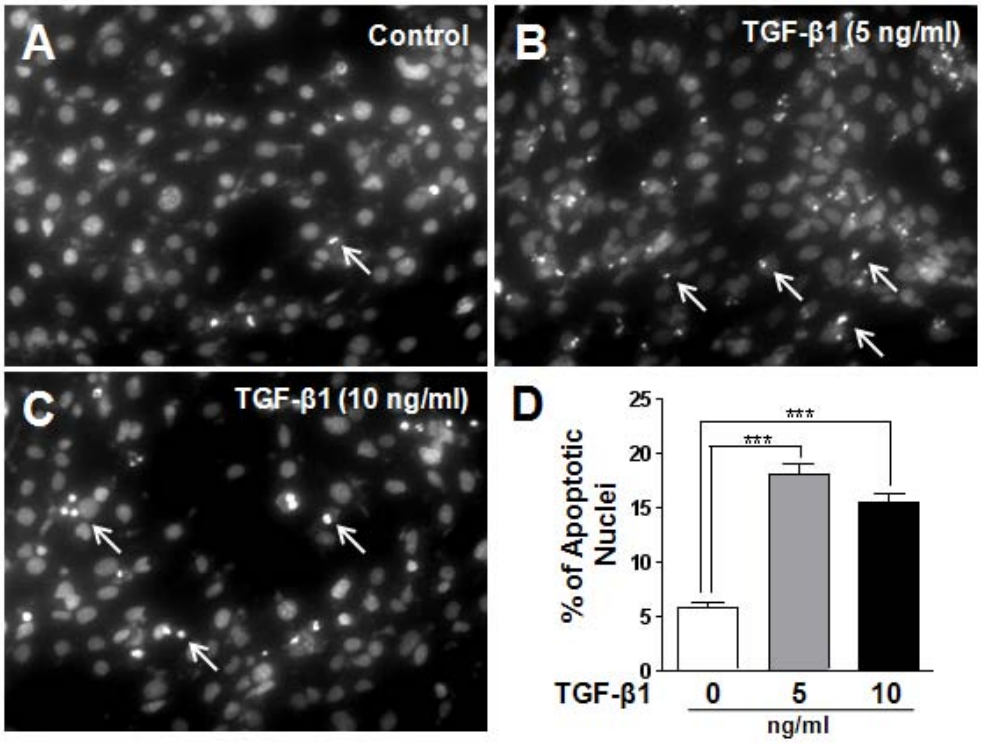

Fig. 12. Effect of different concentrations of TGF-β1 on podocyte apoptosis.

Podocytes were seeded on 18 mm coverslips and differentiated for 14 days. Cells were treated with different doses of TGF-β1 for 72 hr and apoptosis was detected by the presence of fragmented and condensed nuclei (indicated by white arrow) stained with DAPI. *A-C*, No treatment, 5 ng/ml TGF-β1 and 10 ng/ml TGF-β1. *D,* Summary of *A-C*. Values are the mean ± SEM and *** denotes as $p<0.001$.

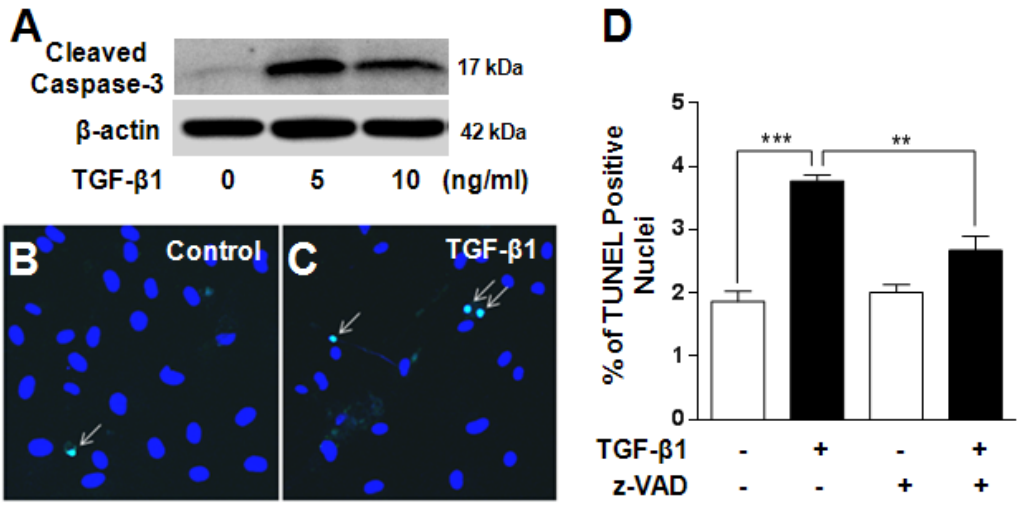

Fig. 13. TGF-β1 activated caspase-3 and increased TUNEL positive nuclei in cultured mouse podocytes.

Mouse podocytes were differentiated for 14 days and deprived with 0.25% FBS before TGF-β1 treatment. *A*, Representative Western blots of cleaved caspase-3 with different concentrations of TGF-β1. *B-C,* Representative images of TUNEL positive nuclei in control and TGF-β1-treated group indicated by white arrows. *D,* Quantification of podocyte apoptosis by TUNEL assay in presence or absence of TGF-β1 (5 ng/ml) and pan-caspase inhibitor z-VAD (25 μM). All the values are the mean ± SEM and **, *** denotes $p<0.01$, and $p<0.001$, respectively.

4.4. TGF-β1-induced reactive oxygen species mediated podocyte apoptosis

To investigate the mechanism of podocyte apoptosis, reactive oxygen species (ROS) generation was measured by DCF as a ROS indicator. TGF-β1 treatment for 24 hr significantly increased DCF fluorescent intensity compared to untreated group and pre-incubation with an antioxidant, NAC, scavenged TGF-β1-mediated ROS generation by 60.7% ($N=3$, $p<0.05$) (Fig. 14A-E). NAC also ameliorated mitochondrial depolarization mediated by TGF-β1 (37.7% recovery, $N=3$, $p<0.01$, Fig. 15A), caspase-3 activation as demonstrated by Western blotting analysis (Fig. 15B) and reduced TUNEL positive nuclei (67.78% reduction of Δ increase, $N=3$, $p<0.05$, Fig. 15C).

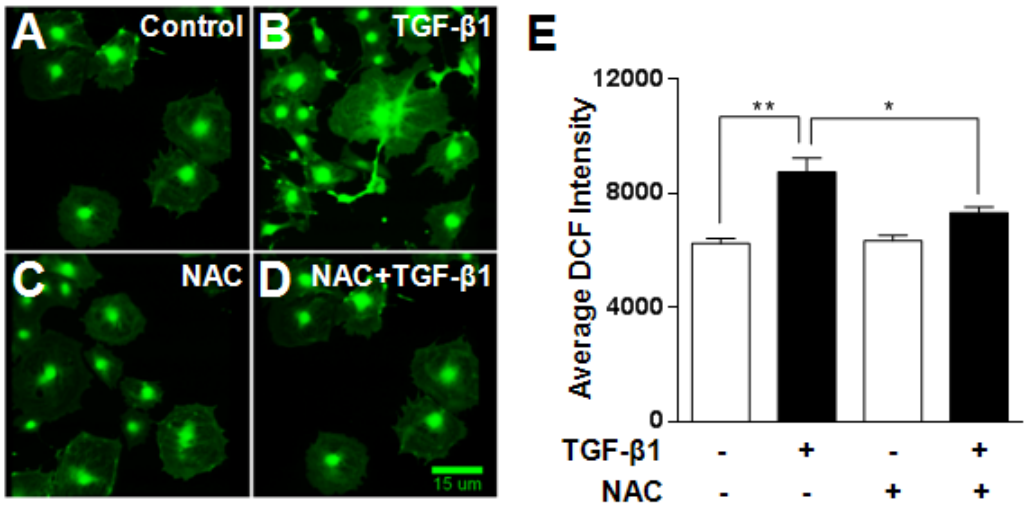

Fig. 14. TGF-β1 treatment increased reactive oxygen species which was scavenged by antioxidant in mouse podocytes.

Cells were grown on 18 mm coverslips for 14 days in non-permissive condition. Effect of TGF-β1 and antioxidant (NAC) were checked for ROS generation using DCF. *A-D,* Representative figures of ROS measurement in podocytes in different groups including control, TGF-β1 (5 ng/ml), NAC (2.5 mM) and NAC+TGF-β1. (E) Bar graphs represents summary of figures *A-D*. All the values are the mean ± SEM and *, ** denote $p<0.05$ and $p<0.01$, respectively.

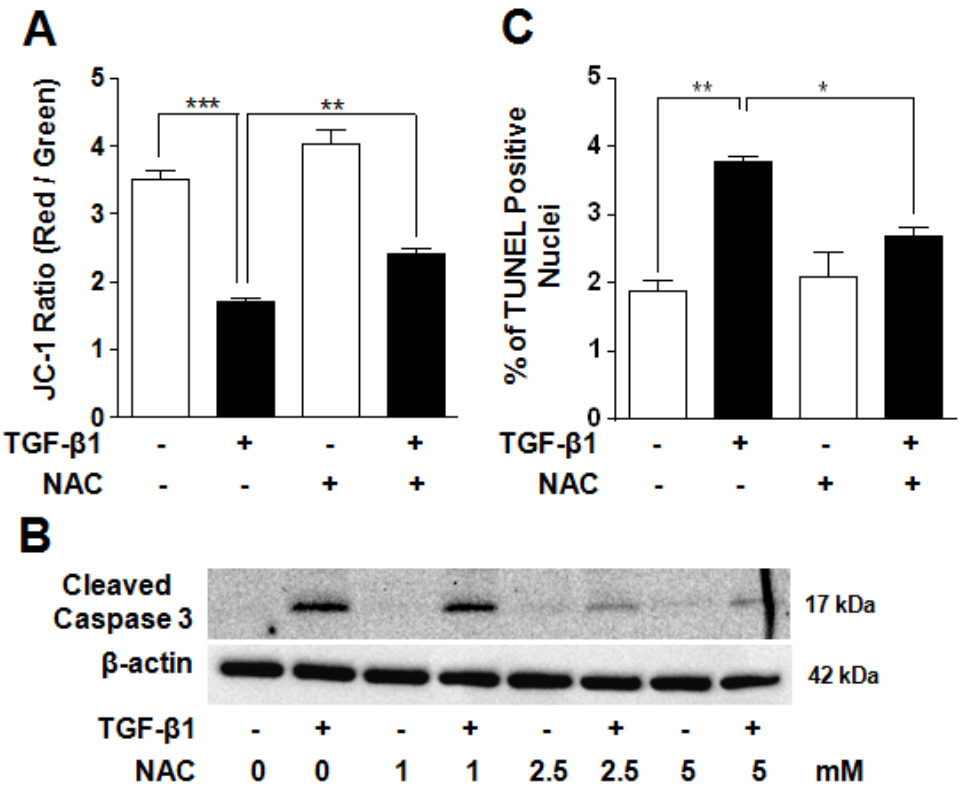

Fig. 15. Antioxidant treatment recovered TGF-β1-induced loss of $\Delta\Psi_m$ and apoptosis in mouse podocytes.

Podocytes were differentiated for 14 days at 37°C. Cells were treated with 0.25% FBS for 24 hr before TGF-β1 application. *A,* Measurement of mitochondrial membrane potential using JC-1 (300 nM) among groups treated with/without TGF-β1 (5 ng/ml) and NAC (2.5 mM). *B,* Western blots showing the effect of NAC on TGF-β1-induced caspase-3 cleavage. *C,* Detection of podocyte cell death by TUNEL assays in the presence and/or absence of TGF-β1 and NAC. All the values are the mean ± SEM and *, **, *** denotes $p<0.05$, $p<0.01$, and $p<0.001$, respectively.

4.5. TGF-β1 elevated Nox4 expression and total Nox activity in mouse podocytes

To identify the possible ROS generating enzyme, semi-quantitative PCR was carried out for Nox1, Nox2, Nox4, and cytochrome P450 4A (CYP4A) in control and TGF-β1-treated podocytes (Fig. 16A). Expression of Nox1 was not detected in differentiated podocytes. TGF-β1 application reduced mRNA level of Nox2 and CYP4A, whereas only Nox4 mRNA was increased by TGF-β1. To confirm the semi-quantitative PCR data, real-time PCR was performed for Nox2, Nox4 and CYP4A. There was a pronounced reduction in Nox2 (0.13 ± 0.09, N=3) and CYP4A (0.03 ± 0.08, N=3) expression, whereas Nox4 mRNA level increased after TGF-β1 treatment (5.66 ± 0.33, N=10) (Fig. 16B-D). Expressions of p22phox (0.42 ± 0.05, N=3, Fig. 16E) and Poldip2 (0.66 ± 0.10, N=3, Fig. 16F) were also decreased by TGF-β1 incubation. Consistent with the elevation of Nox4 transcripts, Nox4 protein level was also increased by TGF-β1 (1.68 ± 0.11, N=3, Fig. 17A-B). In addition, total Nox activity was also significantly augmented following TGF-β1 application (1.83 ± 0.12 fold increase, N=3) (Fig.17C).

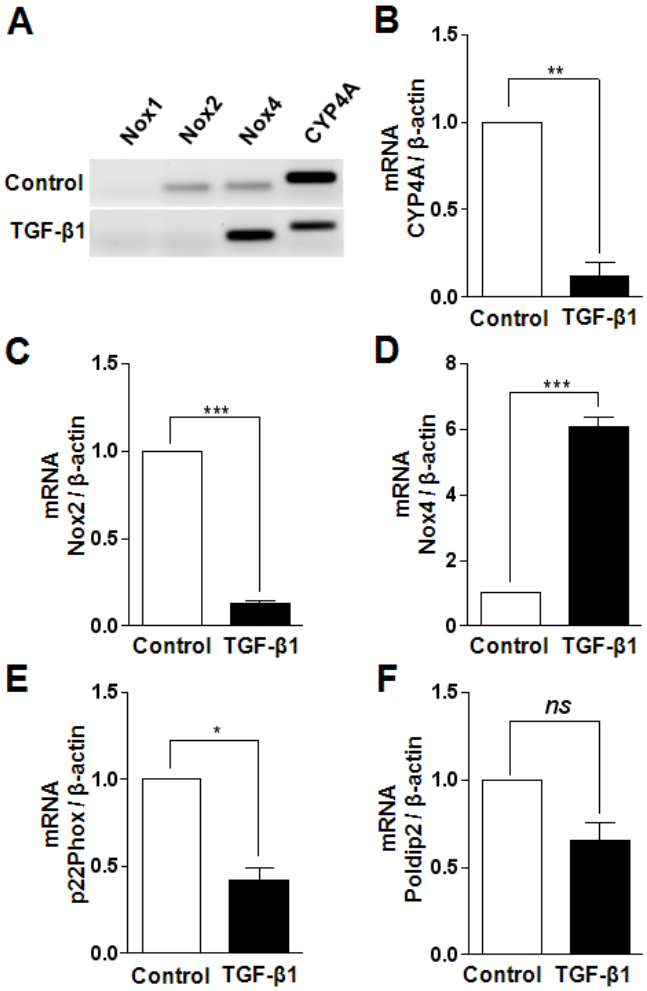

Fig. 16. TGF-β1 upregulated Nox4 mRNA level in mouse podocytes.

RNA was isolated from podocytes grown on 100 mm dishes from control and TGF-β1 (5ng/ml)-treated groups. *A,* RT-PCR data demonstrates the comparative expression level of Nox1, Nox2, Nox4 and CYP4A between control and TGF-β1-treated podocyte. *B-F,* Real-time PCR analysis of CYP4A, Nox2, Nox4, p22Phox and Poldip2 mRNA levels between control and TGF-β1-treated groups. Values are the mean ± SEM and *, **, *** denotes $p<0.05$, $p<0.01$, and $p<0.001$, respectively.

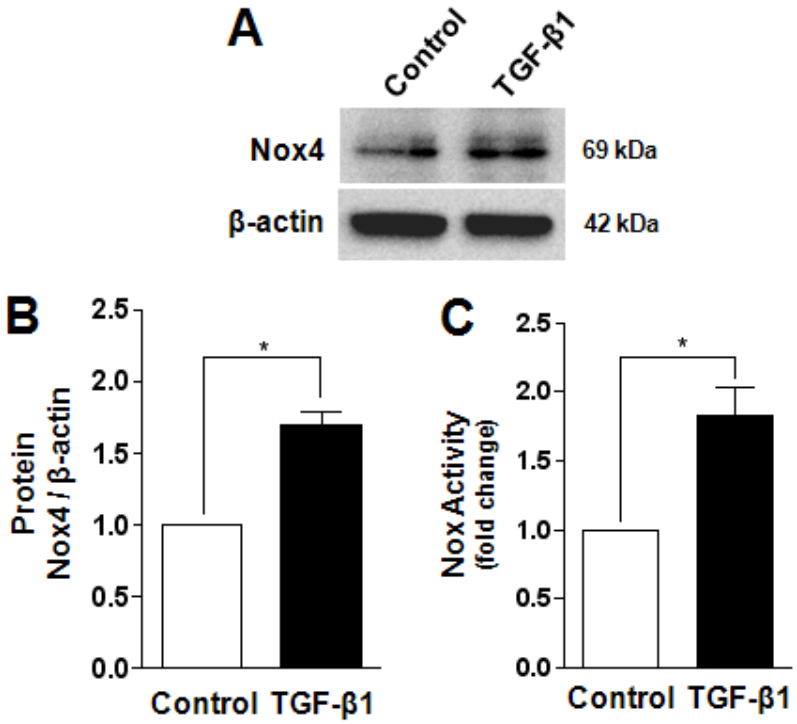

Fig. 17. Nox4 protein level and total Nox activity were increased following TGF-β1 treatment in mouse podocytes.

Podocytes were grown on 100 mm dishes for isolation of total protein for Western blots and Nox activity assay. Cells were deprived with 0.25% serum for 24 hr before TGF-β1 (5 ng/ml) treatment. *A,* Western blots showing Nox4 protein levels in control and TGF-β1 treated groups. *B,* Densitometry analysis of Nox4 protein levels in control and TGF-β1 treated group. *C,* Measurement of total Nox activity in control and TGF-β1-treated groups. Values are the mean ± SEM and *denotes $p<0.05$.

4.6. Nox4 was predominantly localized to mitochondria in podocytes

A recent study showed that Nox4 is localized to mitochondria and Nox4-induced ROS production is responsible for mitochondrial dysfunction[53]. In other cell types, however, Nox4 is present in the ER where it plays an important role in cellular signaling[123]. Intracellular distributions of Nox4 into podocytes were examined by co-localization analysis using mitochondria and ER specific markers. To confirm co-localization, relative intensities of the two fluorescent signals were plotted along a line drawn on the merged images. Co-localization of the two proteins was determined to be where the peaks of the two different intensities overlapped. Mitochondria-targeted cyan fluorescent protein (mitoCFP) was visualized in differentiated podocytes by adenovirus-mediated over-expression system (Fig. 18A and C). Immunostaining of Nox4 using rabbit polyclonal antibody clearly co-localized with mitoCFP as indicated by the presence of multiple yellow puncta in the merged image (Fig. 18C-D). Endogenous mitochondrial protein Cox1 (mitochondrial complex IV, subunit I) labeled with a mouse monoclonal Cox1 antibody was co-localized with Nox4 (Fig. 18E-F). In the presence of rabbit isotype control IgG antibody, however, no signal was detected, indicating the specificity of Nox4 antibody (Fig. 18A-B). We also considered the possibility that Nox4 might be localized in the ER of podocytes. To address that question, the ER was labeled by transfecting D1ER fluorescent protein which is specifically targeted to the luminal side of ER. As shown in Fig. 18G-H, D1ER fluorescence did not co-localize with Nox4 implying that Nox4 was primarily localized to mitochondria, not the ER. In a different approach, podocytes were fractionated into mitochondrial and cytosolic fraction and Nox4 protein level were checked using Western blots. Antibody against Complex I and β-actin were used to check purity of mitochondrial and cytosolic fraction, respectively. Compared to cytosolic fraction,

maximum amount of Nox4 was detected in mitochondrial fraction (Fig. 19A). The protein level of Nox4 in mitochondrial fraction was increased by TGF-β1 (Fig. 19B, 64.5%, N=3) which was consistent to the changes of total Nox4 protein level.

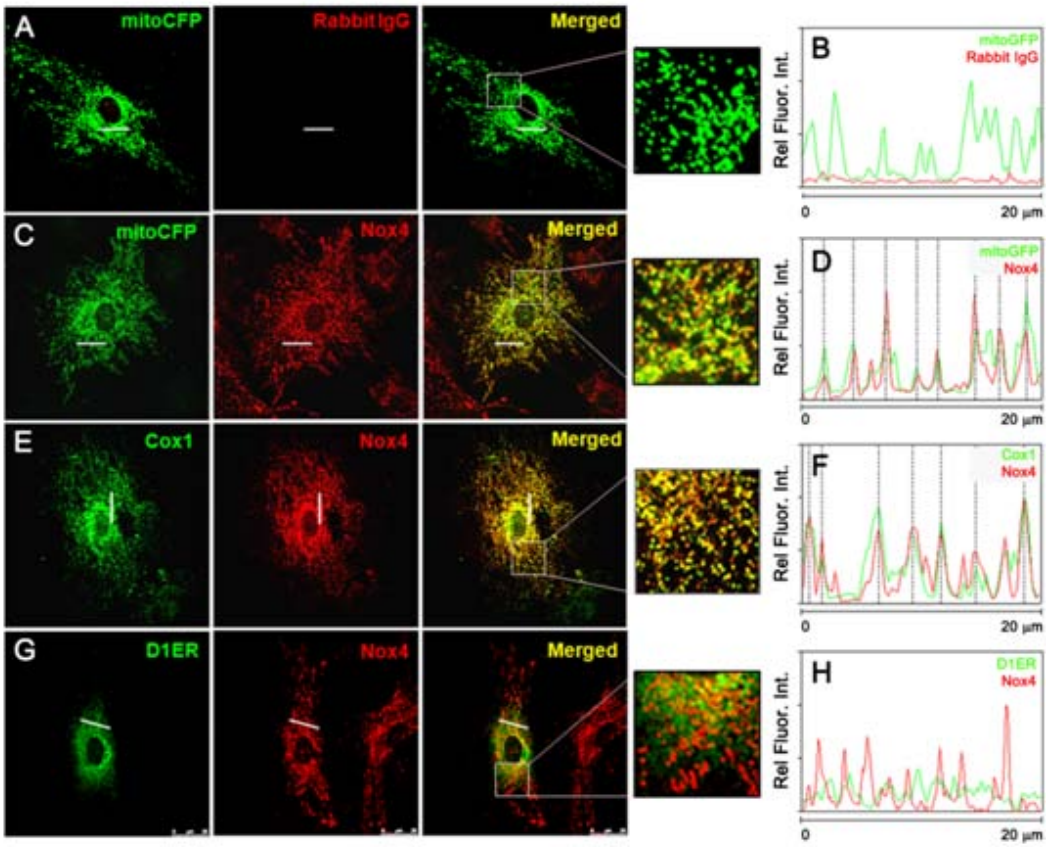

Fig. 18. Nox4 was predominantly localized to mitochondria in mouse podocytes.

Localization of Nox4 in mouse podocytes was detected by immunocytochemistry. Podocytes were differentiated on 18 mm coverslips for 14 days. *A,* Mitochondria in podocytes labeled with mitoCFP (left panel), rabbit isotype control IgG (middle panel) and the merged image (right panel). *C,* Podocytes were infected with mitoCFP adenovirus (left panel), labeled with Nox4 antibody (middle panel) and the merged image (right panel). *E,* Podocytes stained with endogenous mitochondrial protein Cox1 (left panel), Nox4 (middle panel) and the merged image (right panel). *G,* Mouse podocytes transfected with D1ER plasmid (left panel), Nox4 (middle panel) and the merged image

(right panel). *B, D, F* and *H* represent relative fluorescence intensity plots along the line in the merged images in figure *A, C, E* and *G*, respectively.

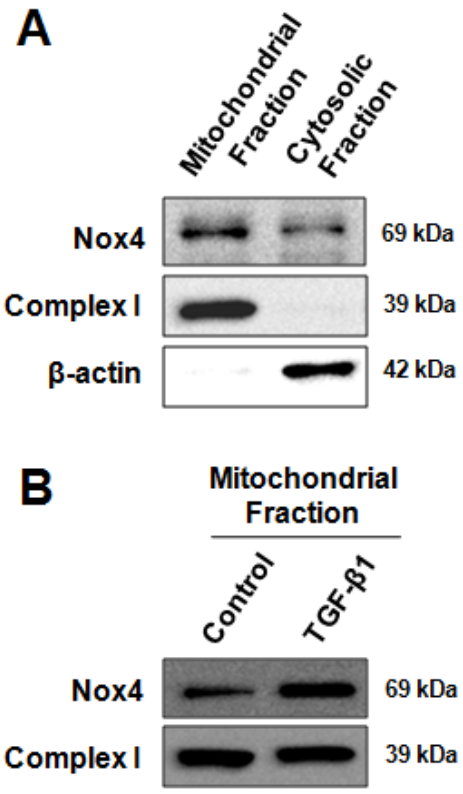

Fig. 19. Nox4 was identified in mitochondrial fraction of mouse podocytes and its expression was increased by TGF-β1 treatment.

Mitochondria were isolated from differentiated podocytes using a commercial kit. *A,* Western blots showing expression of Nox4 protein level in mitochondrial and cytosolic fraction. Antibody against Complex I and β-actin were used to check purity of mitochondrial and cytosolic fraction, respectively. *B,* Western blots showing the increase of mitochondrial Nox4 protein level by TGF-β1 (5 ng/ml) stimulation.

4.7. TGF-β1-induced oxidative stress and apoptosis were Nox4 dependent

To confirm the role of Nox4 in TGF-β1-induced apoptosis, effects of Nox inhibitor DPI and siRNA for Nox4 were examined. Pre-incubation of DPI for 1 hr successfully attenuated TGF-β1-mediated cytosolic ROS increase (87.3% inhibition of Δ increase, N=3, Fig. 20A). Total Nox activity was measured from mitochondrial fraction of podocytes and DPI markedly reduced the basal Nox activities (86.5 ± 7.6% inhibition, N=3, Fig. 20B). Moreover, increased mitochondrial Nox activities mediated by TGF-β1 were completely abolished by DPI pretreatment (N=3, Fig. 20B). Mitochondrial ROS production is known to depolarize the mitochondrial membrane potential which may further deteriorate mitochondrial function and induce apoptosis[2]. DPI rescued the TGF-β1-induced loss of $\Delta\Psi_m$ (75.0% recovery, N=5, $p<0.01$) (Fig. 20C). As a consequence, pre-treatment with DPI blocked the activation of caspase-3 by TGF-β1 (7.73 ± 1.42 fold by TGF-β1 only, 2.32 ± 0.66 fold by TGF-β1 with DPI, N=3, $p<0.01$, Fig. 20D-E). Apocynin, another Nox inhibitor, did not protect podocytes from TGF-β1 induced caspase-3 activation (Fig. 20F). To identify the specific action of Nox4, siRNA for Nox4 was transfected into podocytes. The mRNA level of Nox4 in siNox4-treated cells was reduced by 73.5 ± 8.9% compared to control siRNA (Fig. 21A). Knockdown of Nox4 protein level by siNox4 was also confirmed by Western blotting (55.3 ± 9.3% reduction, N=3) (Fig. 21B-C). Specific knockdown of Nox4 in podocytes prevented TGF-β1-mediated ROS increase (84.0% reduction of Δ increase, N=3, $p<0.05$, Fig. 22A), $\Delta\Psi_m$ depolarization (54% recovery, N=4, $p<0.05$, Fig. 22B), cleaved caspase-3 activation (Fig. 22C) and significantly decreased TUNEL positive nuclei (68.93% reduction of Δ increase, N=3, $p<0.05$, Fig. 22D).

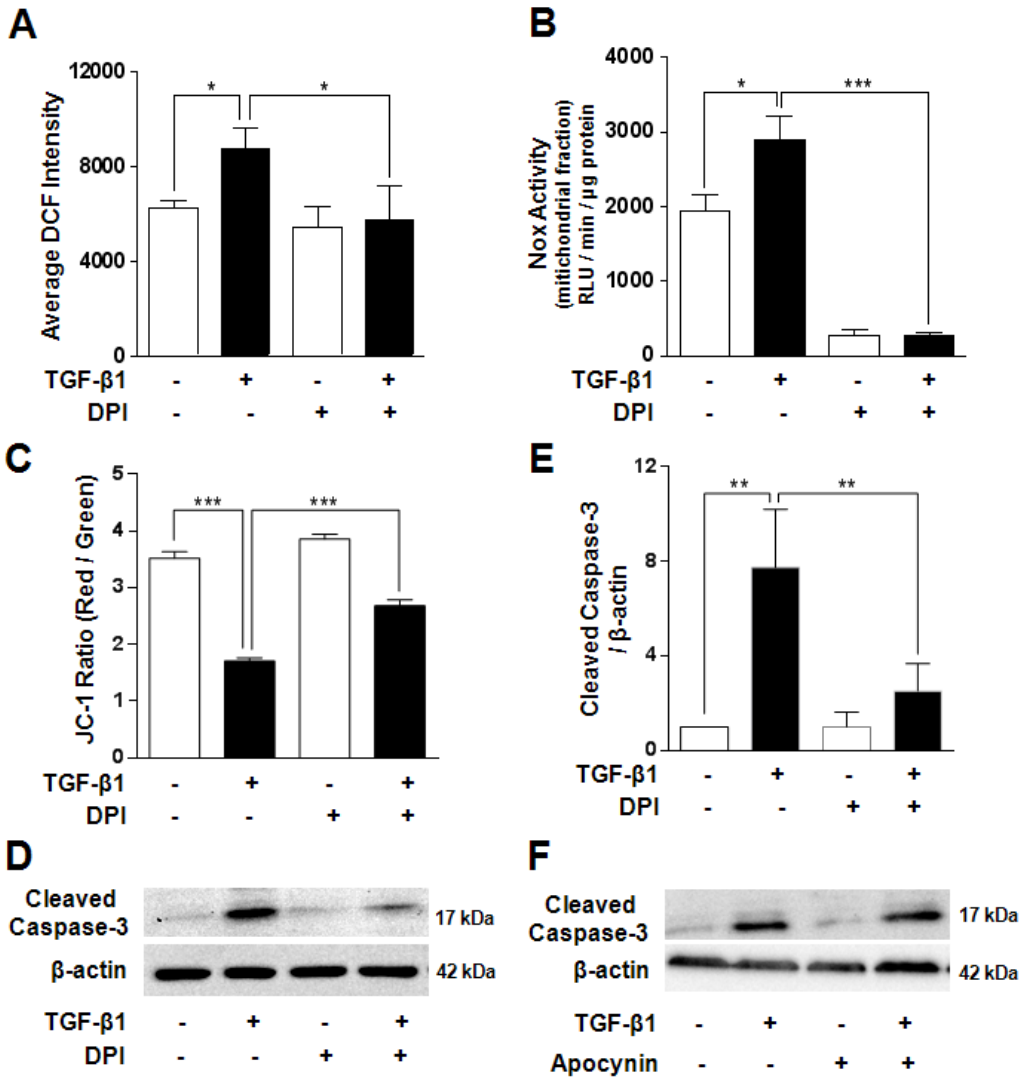

Fig. 20. NADPH oxidase inhibitor abolished podocyte apoptosis by TGF-β1.

Role of Nox4 in TGF-β1 (5ng/ml)-induced apoptosis were checked by inhibiting Nox activity using DPI (2.5 μM). *A,* Measurement of ROS generation using DCF. *B,* Mitochondrial Nox activity measurement. *C,* Mitochondrial membrane potential using JC-1. *D,* Western blots for cleaved caspase-3 in with and without TGFβ1 and DPI. *E,*

Densitometry analysis of figure *D*. *F,* Western blots for cleaved caspase-3 with and without TGFβ1 and apocynin (500 μM). All values are the mean ± SEM and *, **, *** denotes $p<0.05$, $p<0.01$, and $p<0.001$, respectively.

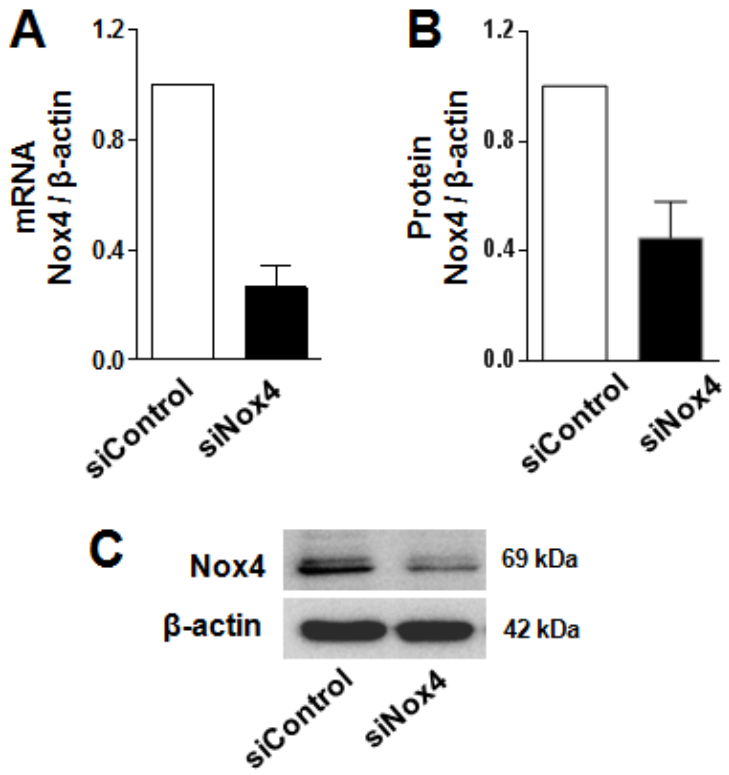

Fig. 21. Nox4 was knocked-down by siRNA for Nox4 in mouse podocytes.

siRNA experiments were carried out with differentiated podocytes grown on 35 mm 6-well dishes. *A,* Real-time PCR data showing knockdown of Nox4 mRNA expression by siRNA Nox4 (siNox4). *B,* Western blots demonstrating reduction in Nox4 protein level by siNox4. *C,* Densitometry analysis of Nox4 protein level after siNox4 treatment. All values are the mean ± SEM.

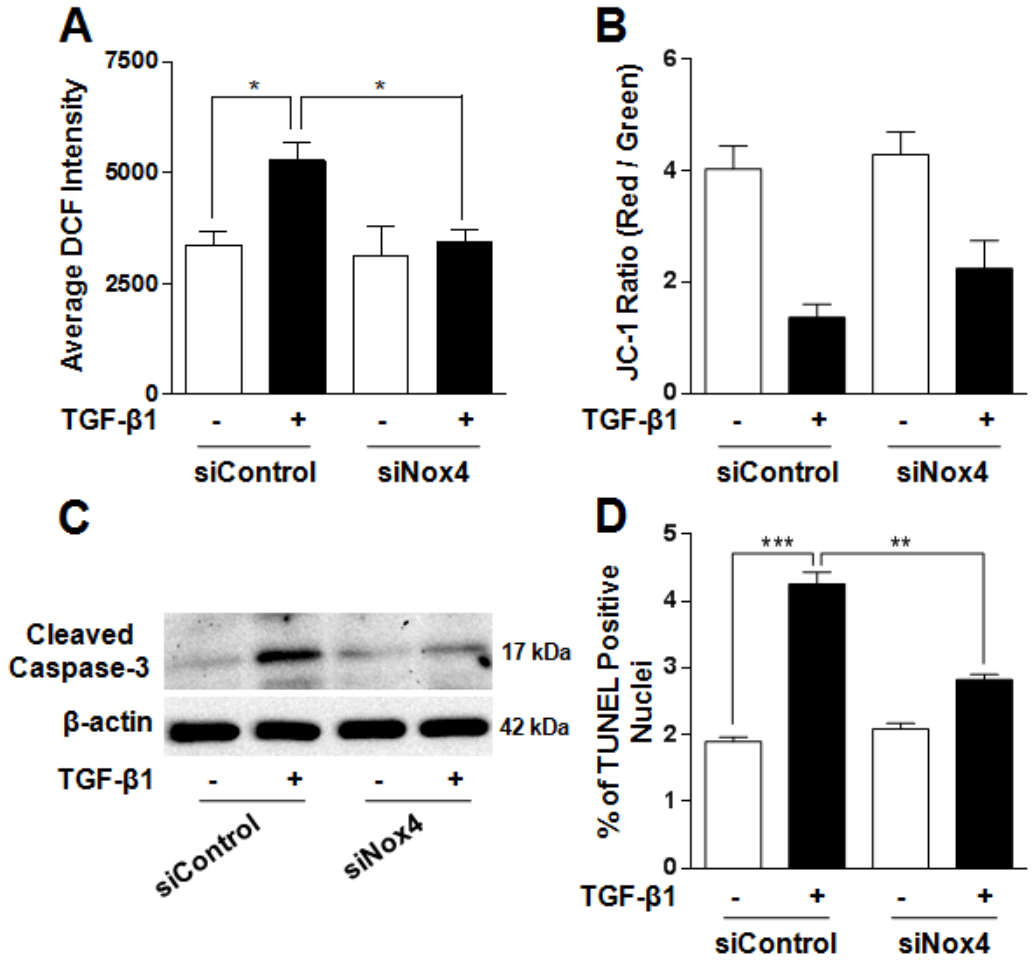

Fig. 22: Nox4 specific siRNA inhibited podocyte apoptosis by TGF-β1.

Effects of Nox4 silencing were checked for TGF-β1 (5 ng/ml)-induced apoptosis in mouse podocytes. *A-D,* Measurement of ROS generation, mitochondrial membrane potential, caspase-3 activation and apoptosis by TUNEL assay, respectively. All values are the mean ± SEM and *, **, *** denotes $p<0.05$, $p<0.01$, and $p<0.001$, respectively.

4.8. TGF-β receptor I-Smad2/3 signaling cascades mediated TGF-β1-induced apoptosis via Nox4 upregulation

Upon binding of ligands to TGF-β receptor II, TGF-β receptor I is phosphorylated. TGF-β1-mediated Nox4 upregulation was completely blocked by SB431542, a potent TGF-β receptor I inhibitor (4.86 ± 0.65 fold increase by TGF-β1 only, 1.01 ± 0.06 fold by TGF-β1 with SB431542, N=4, $p<0.001$, Fig. 23A). Treatment with SB431542 also abrogated TGF-β1-stimulated ROS generation (N=5, Fig. 23B), and prevented mitochondrial membrane depolarization (N=5, Fig. 23C) and caspase-3 activation in the presence of TGF- β1 (Fig. 23D).

TGF-β1 is known to activate both Smad-dependent and Smad-independent apoptotic pathways in podocytes[111]. Both Smad2 and Smad3 phosphorylation were detected within 10 min (0.17 hr) after TGF-β1 stimulation, which reached a peak at 30 min (0.5 hr) and gradually decreased over time (Fig. 24A). To figure out the involvement of Smads in regulating the expression of Nox4, Smad2 and Smad3 were separately knocked down using specific siRNA, and the transcriptional levels of Smad2 and Smad3 were successfully reduced by 73.34 ± 1.2% and 77.0 ± 4.58%, respectively (Fig. 25A-B). Knockdowns of Smad2 and Smad3 were also evaluated at the protein level, which showed 57.49 ± 2.72% and 63.63 ± 12.54% reduction, respectively (Fig. 25C-D). TGF-β1-induced Nox4 upregulation was clearly prevented by siRNA for either Smad2 or Smad3 (Fig. 25E). Knockdown of Smad2 and Smad3 showed >100% (N=3) and 72.4% (N=4) reduction of ROS increase (Fig. 26A), and 76.2% (N=3) and 74.2% (N=3) recovery of mitochondrial membrane potential loss induced by TGF-β1, respectively (Fig. 26B). Both siSmad2 and siSmad3 independently reduced TGF-β1-induced podocyte apoptosis demonstrated by caspase-3 activation (7.35 ± 2.89 fold by control siRNA with TGF-β1;

2.12 ± 1.23 fold by siSmad3 with TGF-β1, N=3) (Fig. 26C) and TUNEL positive nucleus (66.53% and 72.74% reduction of Δ increase by siSmad2 and siSmad3, respectively, N=3, Fig. 26D).

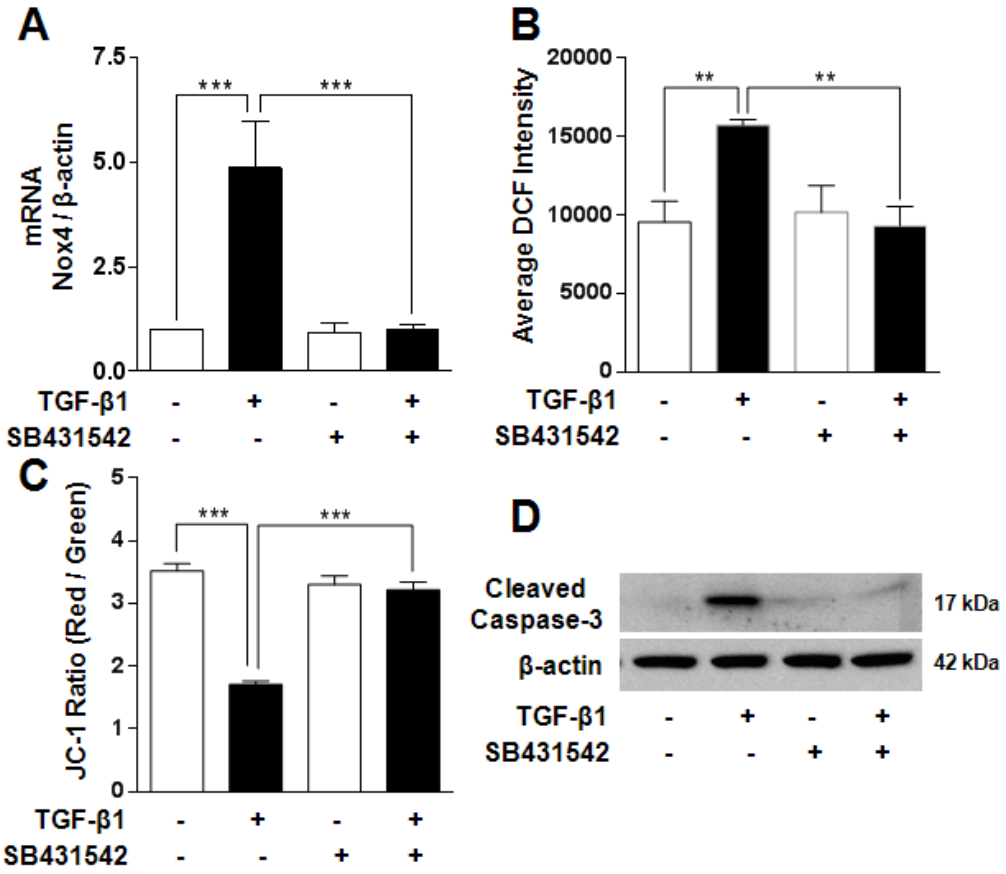

Fig. 23. TGF-β receptor I blocker inhibited TGF-β1-induced podocyte apoptosis.

Pretreatment with SB431542 (10 μM) completely abrogated TGF-β1 (5 ng/ml)-induced apoptotic changes in podocytes. *A-D,* Measurement of Nox4 mRNA level, ROS generation, mitochondrial membrane potential and caspase-3 activation, respectively. Data are presented as mean ± SEM ** and *** denotes $p<0.01$ and $p<0.001$, respectively.

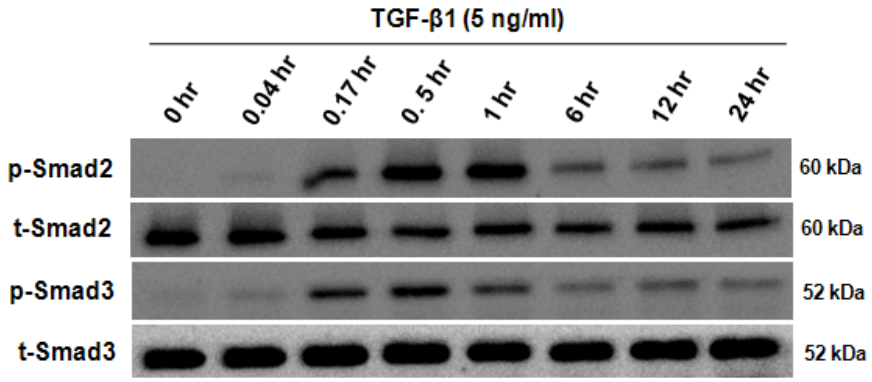

Fig. 24. TGF-β1 phosphorylated both Smad2 and Smad3 in mouse podocytes.

Podocytes were treated with 5 ng/ml of TGF-β1 at different time points. Western blots showing phosphorylation of Smad2 and Smad3 by TGF-β1 at different time points.

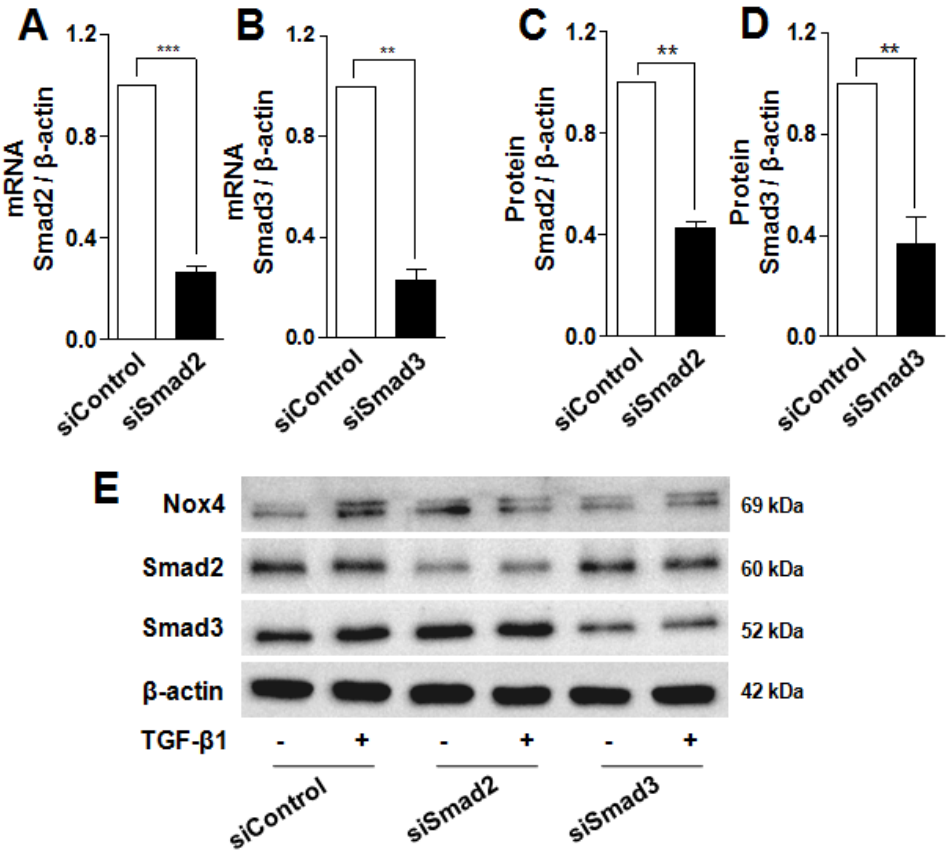

Fig. 25. Smad2/3-dependent signaling contributed to TGF-β1-induced Nox4 upregulation in mouse podocytes.

Roles of Smad2 and Smad3 in TGF-β1 (5 ng/ml)-stimulated Nox4 upregulation were investigated using Smad2 siRNA (siSmad2) and Smad3 siRNA (siSmad3). *A-B,* Real-time PCR data showing knock-down of Smad2 and Smad3 mRNA in podocytes. *C-D,* Densitometry analysis of Western blots showing siRNA mediated knock-down of Smad2 and Smad3 proteins in podocytes. *E,* Western blots showing the effect of siSmad2 and siSmad3 on Nox4 protein expression. All data are presented as mean ± SEM **, *** denotes $p<0.01$ and $p<0.001$, respectively.

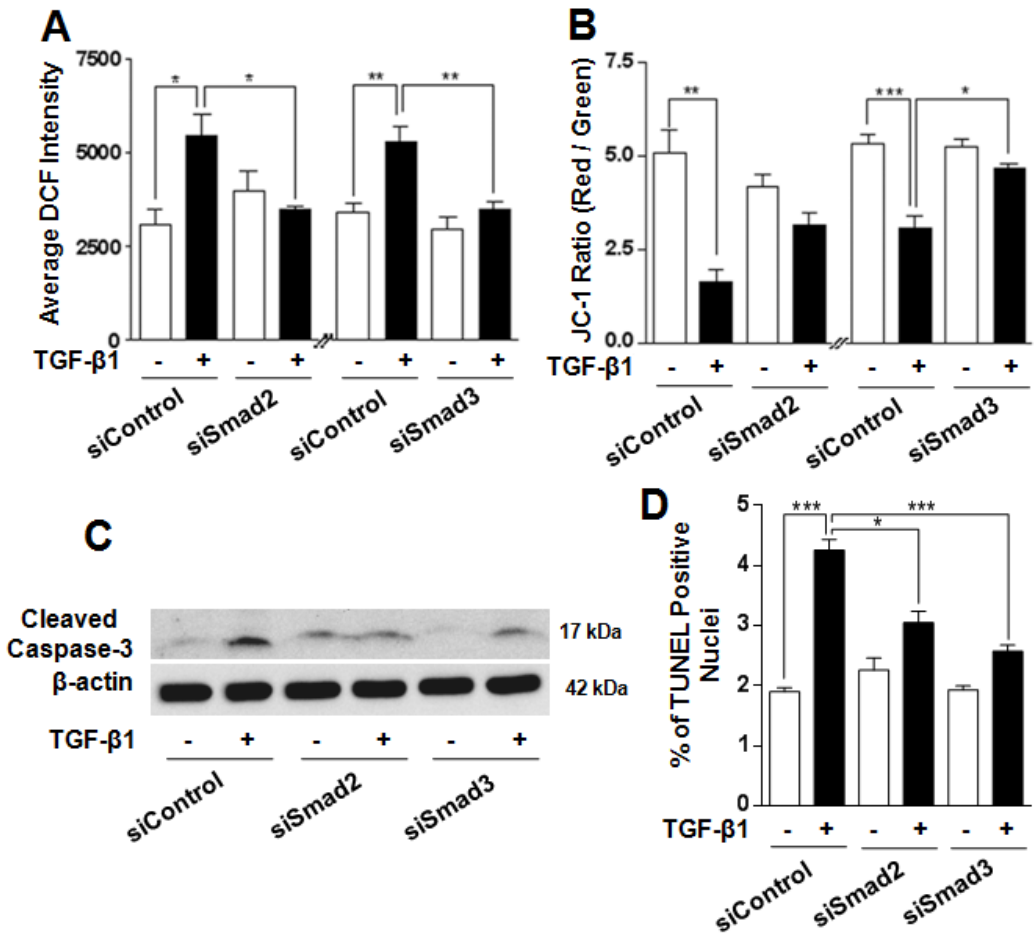

Fig. 26. Smad-dependent signaling contributed to TGF-β1-induced podocyte apoptosis.

Effects of Smad2/3 silencing were tested for ROS generation, mitochondrial membrane potential, caspase-3 activation and TUNEL staining for podocyte apoptosis in control and TGF-β1 (5 ng/ml) treated groups. *A.* Bar graph representing inhibition of ROS generation

by TGF-β1 in siSmad2 and siSmad3-treated podocytes. *B,* Measurement of mitochondrial membrane potential using JC-1 in TGF-β1-stimulated cells after siSmad2 and siSmad3 treatment. *C,* Western blots for cleaved caspase-3 from podocytes transfected with siSmad2 and siSmad3 in the absence or presence of TGF-β1. *D,* Summary of TUNEL assay with siSmad2 and siSmad3 in absence or presence of TGF-β1. All values are the mean ± SEM and *, **, *** denotes $p<0.05$, $p<0.01$, and $p<0.001$, respectively.

4.9. mTOR activation by TGF-β1 elevated Nox activity and podocyte apoptosis

Though mTOR plays an important role in maintenance of podocyte homeostasis, recent studies indicated that increased mTOR activity is associated with podocyte injury in diabetic nephropathy[33, 43]. Western blotting showed that time dependent treatment of TGF-β1 increased phosphorylation of mTOR and its downstream target p70S6K (Fig. 27A). Densitometry analysis revealed that mTOR was phosphorylated very early and reached maximum after 1 hr (1.87 fold increase), while the peak of p70S6K was detected after 6 hr of TGF-β1 treatment (1.82 fold increase) (Fig. 27B). Inhibition of mTOR activity by rapamycin alleviated TGF-β1-induced ROS generation by 91.37% (N=2) and total Nox activity (reduction of 69.6%, N=2) (Fig 28A and B, respectively). Rapamycin treatment also partially recovered loss of $\Delta\Psi_m$ by TGF-β1 (57.88% recovery, N=4, $p<0.01$, Fig 28C). Activation of caspase-3 was also inhibited by mTOR inhibition (Fig. 28D). Interestingly, Nox4 mRNA upregulation by TGF-β1 was not altered by rapamycin treatment (Δ increase 4.75 fold by TGF-β1 and 4.45 fold by rapamycin+TGF-β1, Fig. 30A).

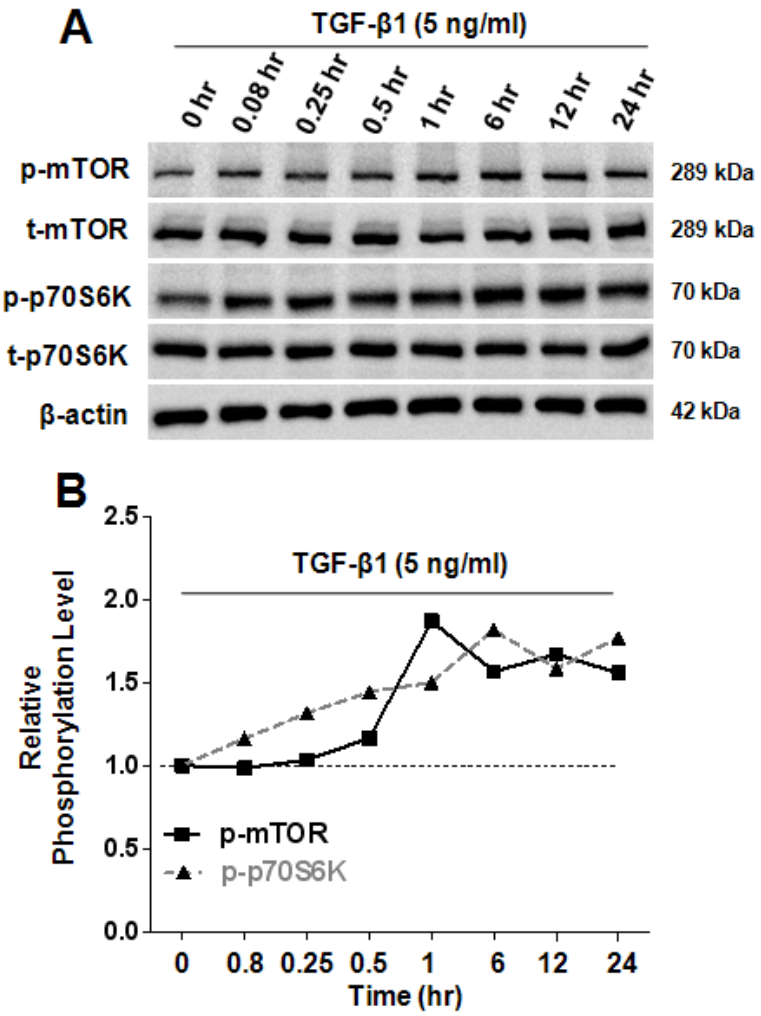

Fig. 27. TGF-β1 activated mTOR signaling in mouse podocytes.

Podocytes were differentiated on 6-well dishes and starved with 0.25% serum for 24 hr before TGF-β1 (5 ng/ml) treatment. Proteins were isolated at different time-points to check mTOR activation. *A,* Western blots showing phosphorylation status of mTOR and its downstream target p70S6K. *B,* Densitometry analysis of figure *A*. Y-axis denotes fold change of phosphorylation level of mTOR and p70S6K by TGF-β1 compared to control, and the values were normalized against total mTOR and total p70S6K, respectively.

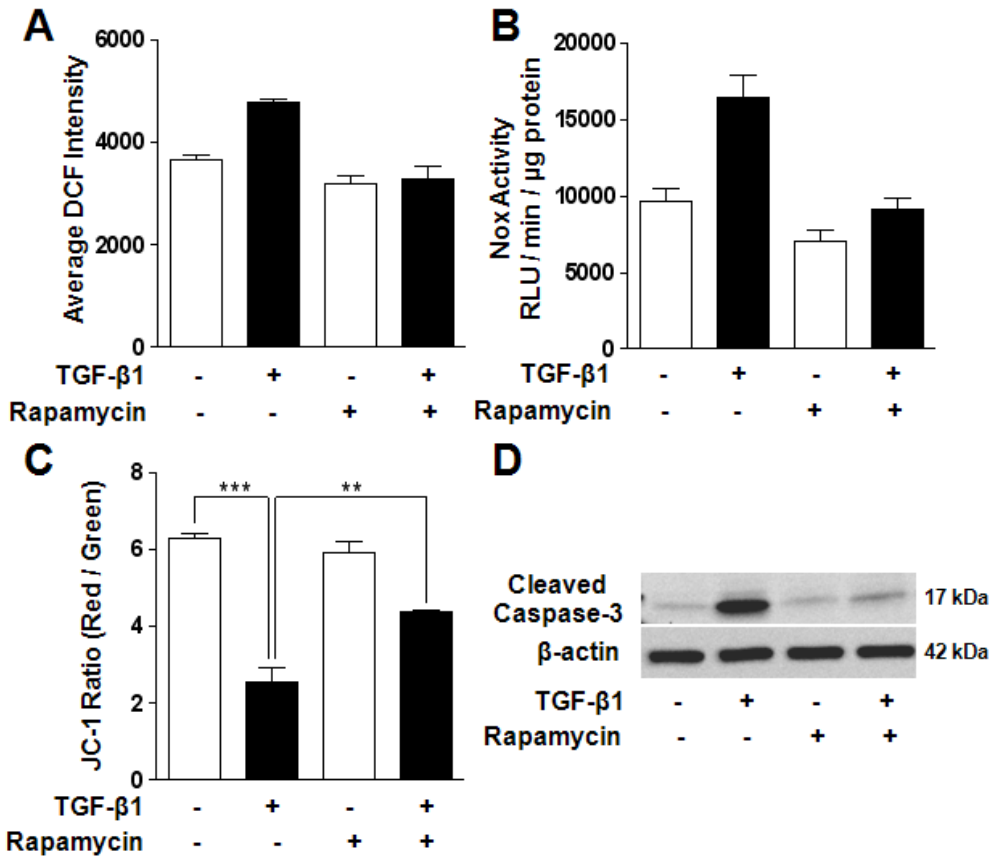

Fig. 28. Inhibition of mTOR pathway by rapamycin protected podocytes from TGF-β1-induced oxidative stress.

Effects of rapamycin (50 nM) were verified on podocytes of control and TGF-β1 (5 ng/ml)-treated groups. *A,* Histogram representing measurement of ROS using DCF in presence and/or absence of rapamycin and TGF-β1. *B,* Effect of rapamycin was checked for total Nox activity in cells with TGF-β1-stimulation. *C,* Measurement of mitochondrial membrane potential in TGF-β1 and/or rapamycin-treated podocytes. *D,* Detection of cleaved caspase-3 in podocytes treated with TGF-β1 and/or rapamycin by Western blots. All values are the mean ± SEM and **, *** denotes $p<0.01$ and $p<0.001$, respectively.

4.10. TGF-β1-induced ERK1/2 phosphorylation regulated total Nox activity and podocyte apoptosis

TGF-β1 treatment rapidly phosphorylated ERK1/2 MAPK in cultured podocytes. ERK1/2 phosphorylation was easily detected at 5 min and reached maximum level at 30 min following decrease of phosphorylated ERK1/2 which reached to basal level at 24 hr (Fig. 29A). To clarify the signaling role of ERK1/2 phosphorylation on Nox4 upregulation, U0126 (a MEK1/2 inhibitor thereby inhibiting ERK1/2 activation) was tested on TGF-β1-triggered Nox4 upregulation. Application of U0126 reduced TGF-β1 induced Nox activity (reduction of 86.57%, N=2, Fig. 29B), recovered loss of mitochondrial membrane potential (54.13% recovery, N=3, $p<0.05$, Fig. 29C), and inhibited caspase-3 activation (Fig. 29D). Similar to rapamycin, ERK1/2 inhibition with different doses of U0126 (5 μM and 10 μM), did not change the expression of Nox4 mRNA level increased by TGF-β1 (Fig. 30B).

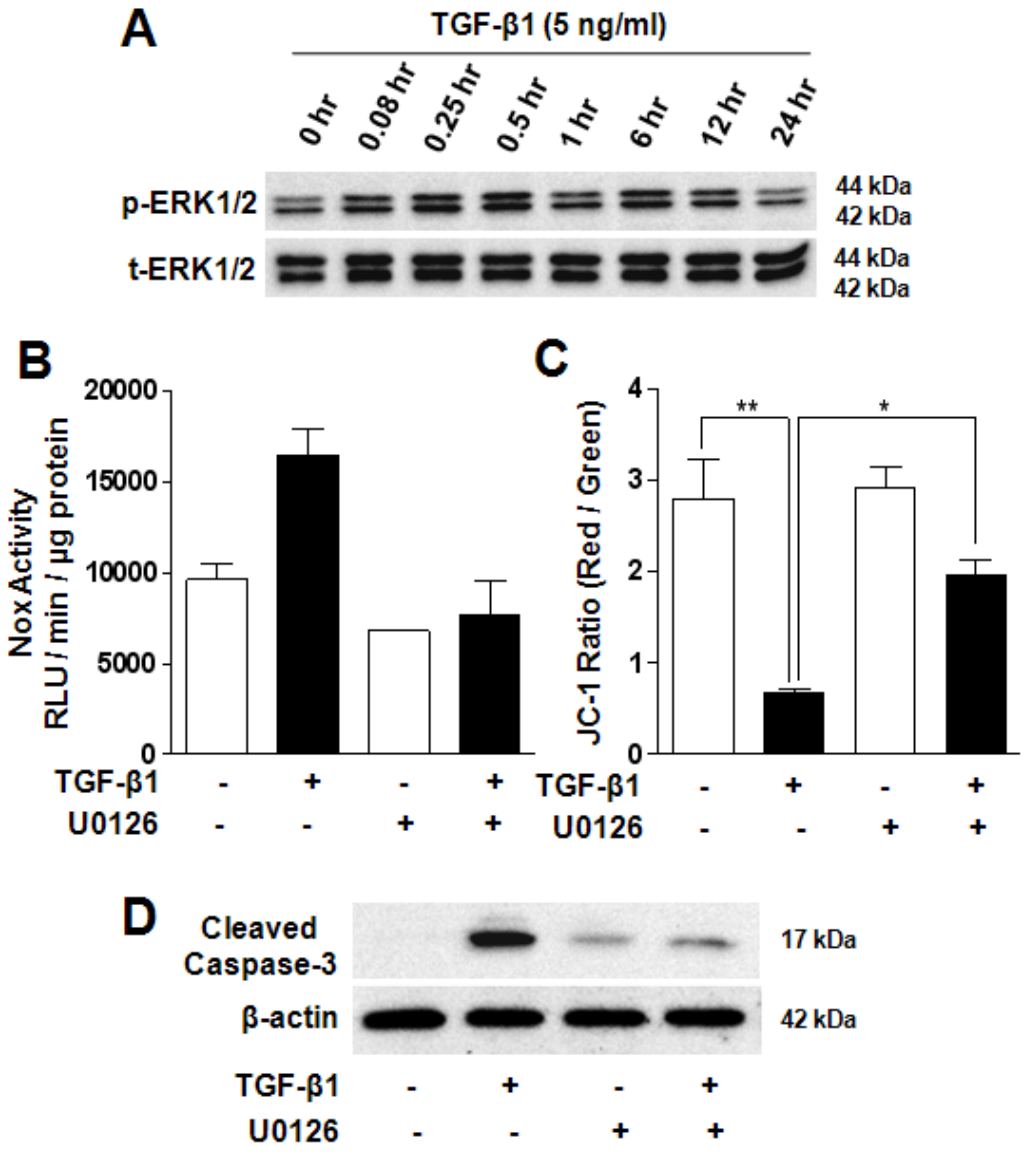

Fig. 29. Inhibition of ERK1/2 activation protected podocytes from TGF-β1-induced oxidative stress.

Podocytes were treated with TGF-β1 for different time-points and proteins were isolated. *A,* Western blots representing activation of ERK1/2 signaling by TGF-β1 in podocytes. *B,*

Pretreatment with U0126 (5 μM) reduced TGF-β1-induced total Nox activity. *C-D,* U0126 treatment recovered loss of mitochondrial membrane potential and protected cells from apoptosis by reducing activation of cleaved caspase-3. All values are the mean ± SEM and *, ** denotes $p<0.05$ and $p<0.01$, respectively.

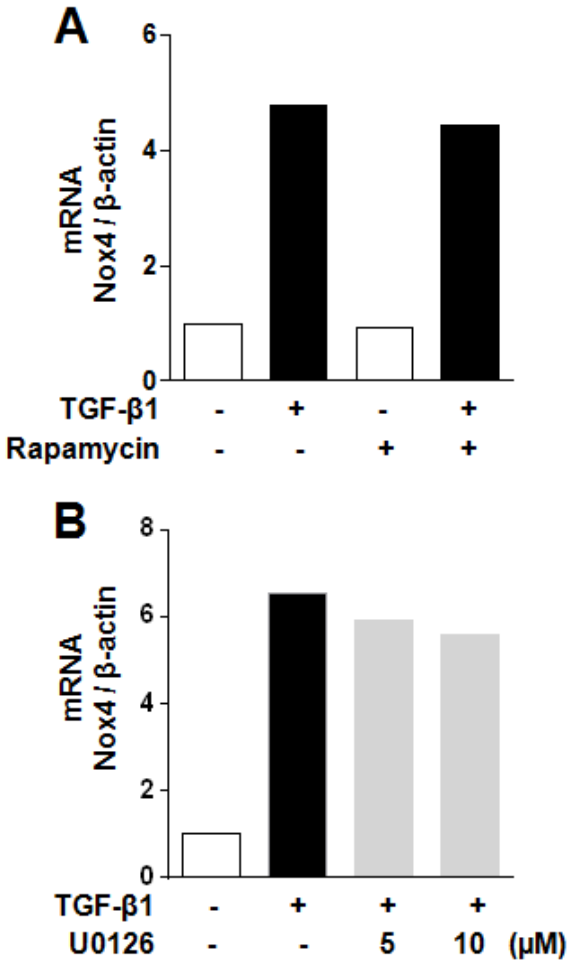

Fig. 30. Inhibition of mTOR or ERK1/2 did not suppress TGF-β1-induced Nox4 mRNA upregulation.

Total RNA was isolated from podocytes treated with TGF-β1 (5 ng/ml) for 24hr along with rapamycin (50 nM) or ERK1/2 inhibitor (5 μM). *A,* Real-time PCR showing the effect of rapamycin on Nox4 mRNA expression in the presence of TGF-β1. *B,* Real-time PCR showing the effect of U0126 on Nox4 mRNA expression after TGF-β1 treatment.

4.11. TGF-β1-simulated mTOR signaling was regulated by ERK1/2 MAPK in podocytes

ERK1/2 and mTOR inhibitors completely abrogated TGF-β1-induced total Nox activity in podocytes. So experiments were considered to find out relationship between them. For that purpose, an ERK1/2 inhibitor was used to check the phosphorylation level of mTOR and its immediate downstream molecule p70S6K in presence of TGF-β1. Podocytes were treated with 2.5 μM of U0126 1 hr before TGF-β1 addition and total protein was isolated after 6 hr. Phosphorylation levels of both mTOR and p70S6K were markedly increased after 6 hr of TGF-β1 treatment and was completely inhibited by pretreatment with U0126 (Fig. 31A).

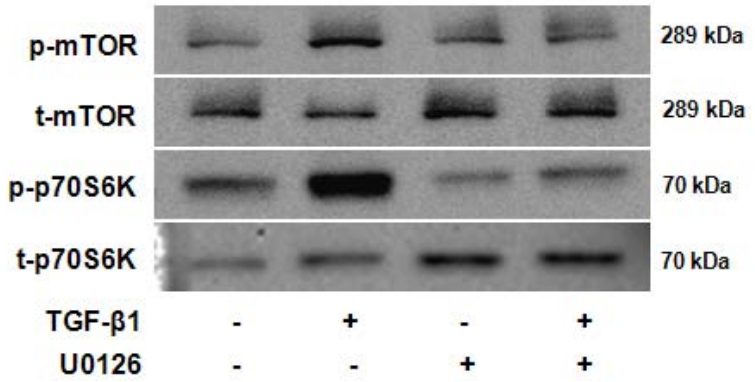

Fig. 31. ERK inhibitor blocked TGF-β1-induced mTOR signaling in podocytes.

Cells were pre-treated with ERK inhibitor (U0126) (5 μM) for 1 hr before TGF-β1 (5 ng/ml) treatment. Protein was isolated 6 hr after TGF-β1 addition. Western blots showing result of p-mTOR, total-mTOR, p-p70S6K and total-p70S6K in presence or absence of TGF-β1 and U0126.

4.12. Activation of Smad7 did not participate in TGF-β1-induced Nox4 upregulation

In podocytes, Smad7 has been demonstrated to act as a pro-apoptotic factor and its expression is increased by TGF-β1 in podocytes[94]. Transcriptional level of Smad7 was measured by quantitative PCR, which was peaked (8 fold increase) at 1 hr after TGF-β1 treatment (Fig. 32A). To identify the role of Smad7 on TGF-β1-induced Nox4 upregulation, we applied siRNA for Smad7 which successfully knocked down the mRNA level of Smad7 (0.25 ± 0.08, N=3, Fig. 32B). However, TGF-β1-induced Nox4 upregulation (6.68 ± 0.73 fold, N=3) was not attenuated but, in fact, was increased by siSmad7 (10.45 ± 2.79 fold, N=2, Fig. 32C). Knockdown with siSmad7 did not prevent the mitochondrial depolarization elicited by TGF-β1 (N=3, Fig. 32D) and caspase-3 activation (Fig. 32E), though a small reduction of TUNEL positive nuclei were observed (4.26% by TGF-β1 in siControl group and 3.58% by TGF-β1 in siSmad7-treated group, N=2, Fig. 32F).

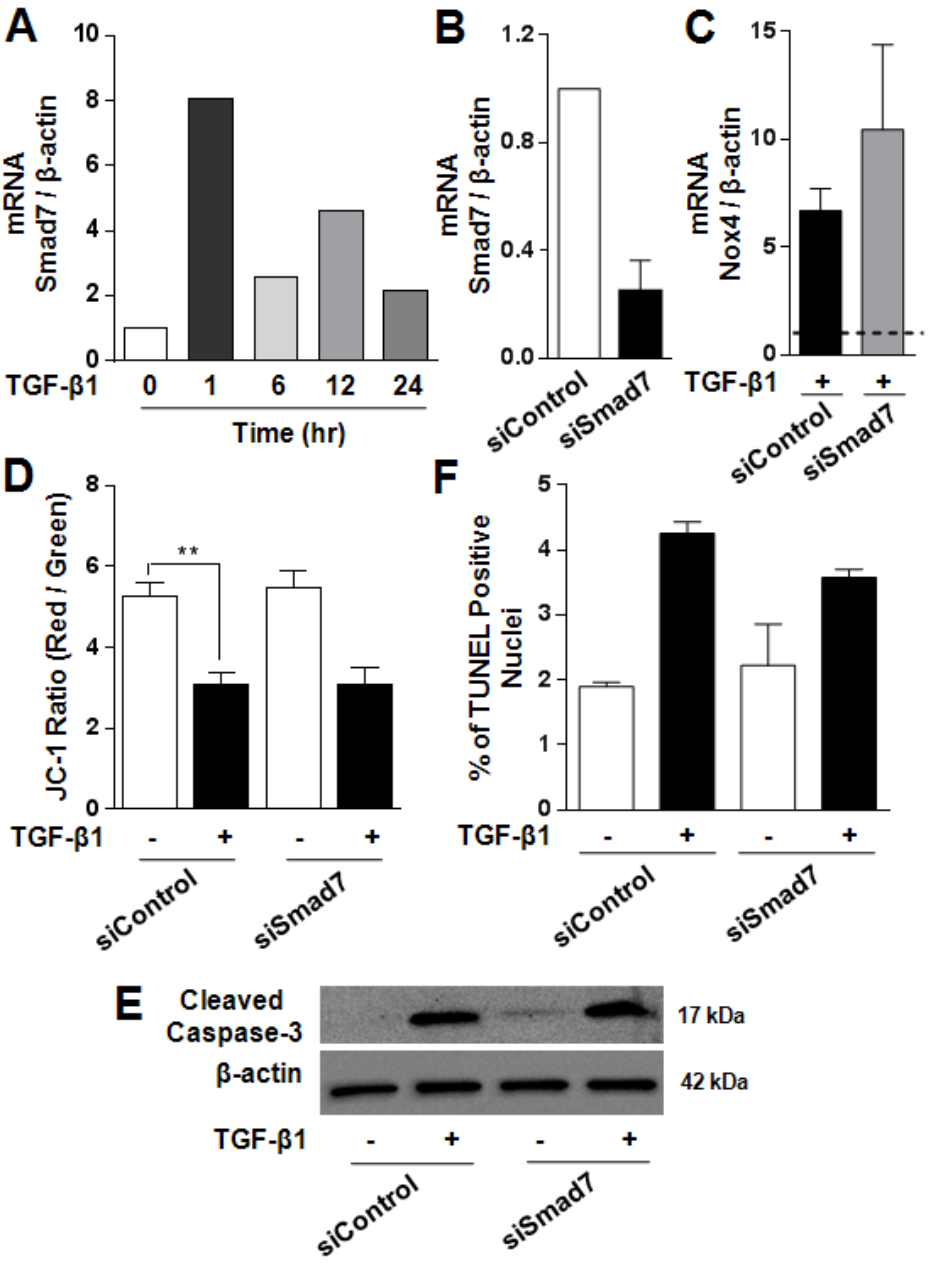

Fig. 32. Nox4 mRNA upregulation upon TGF-β1-stimulation was independent of Smad7 expression in podocytes.

Effects of Smad7 silencing (using siSmad7) were checked for TGF-β1 (5 ng/ml)-induced Nox4 upregulation and podocyte apoptosis. *A,* Real-time PCR analysis of Smad7 mRNA level after TGF-β1 treatment in podocytes. *B,* mRNA expression analysis of Smad7 mRNA level by using real-time PCR after siRNA-mediated knockdown of Smad7. *C,* TGF-β1-induced upregulation of Nox4 was compared in control siRNA and siSmad7 treated cells. *D,* Measurement of mitochondrial membrane potential using JC-1 in siControl and siSmad7-treated groups in the presence or absence of TGF-β1. *E,* Western blots showing activation of caspase-3 in siControl and siSmad7 treated groups in presence and/or absence of TGF-β1. *F,* Assessment of podocyte apoptosis by TUNEL assay in siControl and siSmad7 treated groups in presence and/or absence of TGF-β1. All values are the mean ± SEM.

4.13. p38 MAPK signaling did not interfere with TGF-β1-induced Nox4 upregulation

As a Smad-independent pathway, activation of p38 MAPK has been known to mediate TGF-β-induced apoptosis in podocytes[94]. Phosphorylation of p38 MAPK became evident at 30 min after TGF-β1 application and started decreasing after 6 hr, though it was detected till 24 hr after treatment (Fig. 33A). To check the effect of p38 MAPK activation on Nox4 mRNA upregulation, a selective inhibitor for p38 MAPK was employed. Though SB202190 partially reduced caspase-3 activation (Fig. 33B) and apoptosis detected by TUNEL staining (3.77% with TGF-β1 and 3.34% with SB202190+TGF-β1 treatment, Fig. 33C), it had no effect on Nox4 mRNA upregulation (6.86 fold by TGF-β1 and 11.39 fold with SB202190+TGF-β1, Fig. 33D) and mitochondrial depolarization induced by TGF-β1 (Fig. 33E). SB202190 also did not alleviate cytosolic ROS production by TGF-β1 (data not shown), which is consistent with it being a result of Nox4 upregulation. In a cross examination, effect of ROS inhibition was checked for p38 MAPK activation, but TGF-β1-induced p38 MAPK phosphorylation was not blocked by the Nox inhibitor DPI (Fig. 33F).

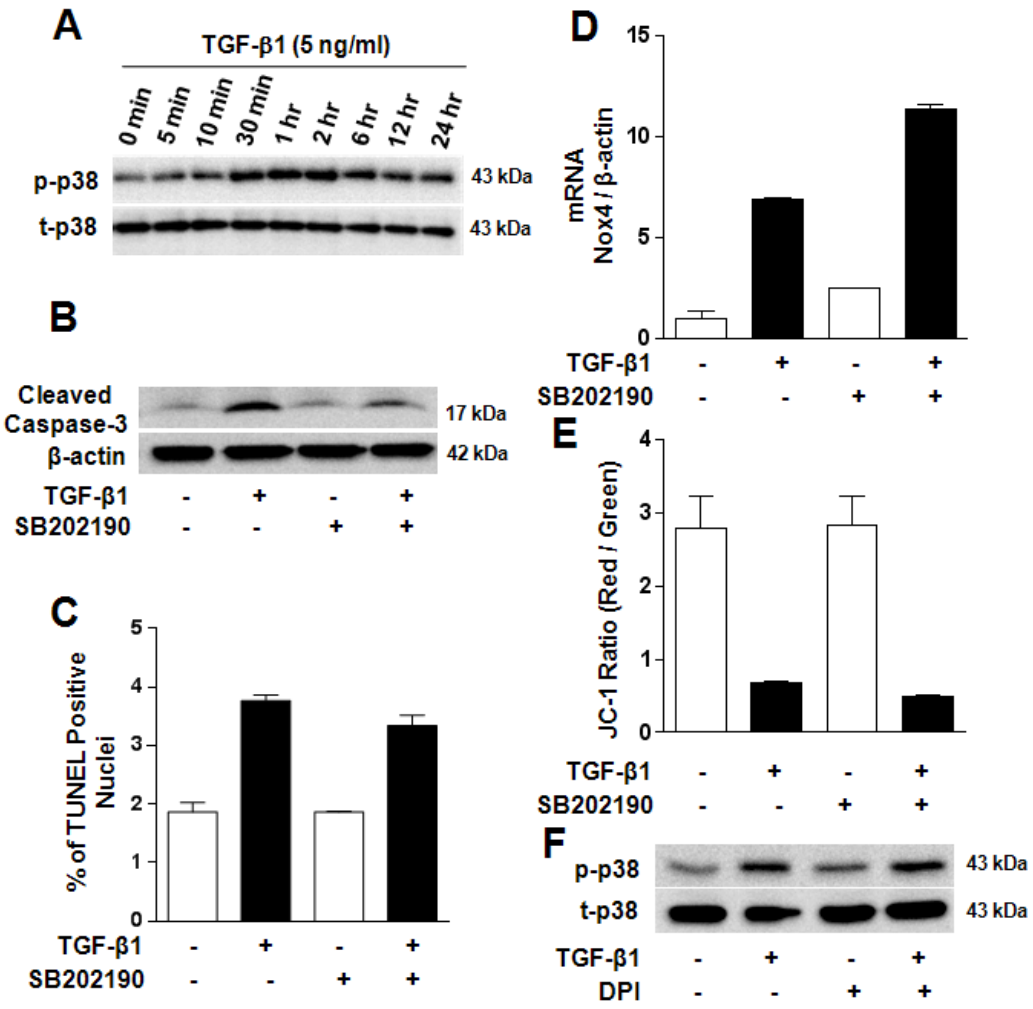

Fig. 33. p38 MAPK activation was not involved in TGF-β1-induced Nox4 mRNA upregulation.

Podocytes were differentiated for 14 days in non-permissive condition before serum starvation (0.25% FBS) for 24 hr and TGF-β1 treatment. *A,* Western blot showing phosphorylation of p38 MAPK after TGF-β1 treatment at different time points. *B,* Western blots showing partial inhibition of caspase-3 activation by p38 MAPK inhibitor (SB202190) (2.5 μM) in podocytes treated with TGF-β1. *C,* Detection of podocyte apoptosis by TUNEL assay under TGF-β1 and SB202190 treatment. *D,* Real-time PCR showing Nox4 mRNA expression by TGF-β1 and/or SB202190 treatment. *E,* Measurement of mitochondrial membrane potential after TGF-β1 application in presence or absence of SB202190. *F,* Western blots representing effect of DPI on p38 MAPK phosphorylation. All values are the mean ± SEM.

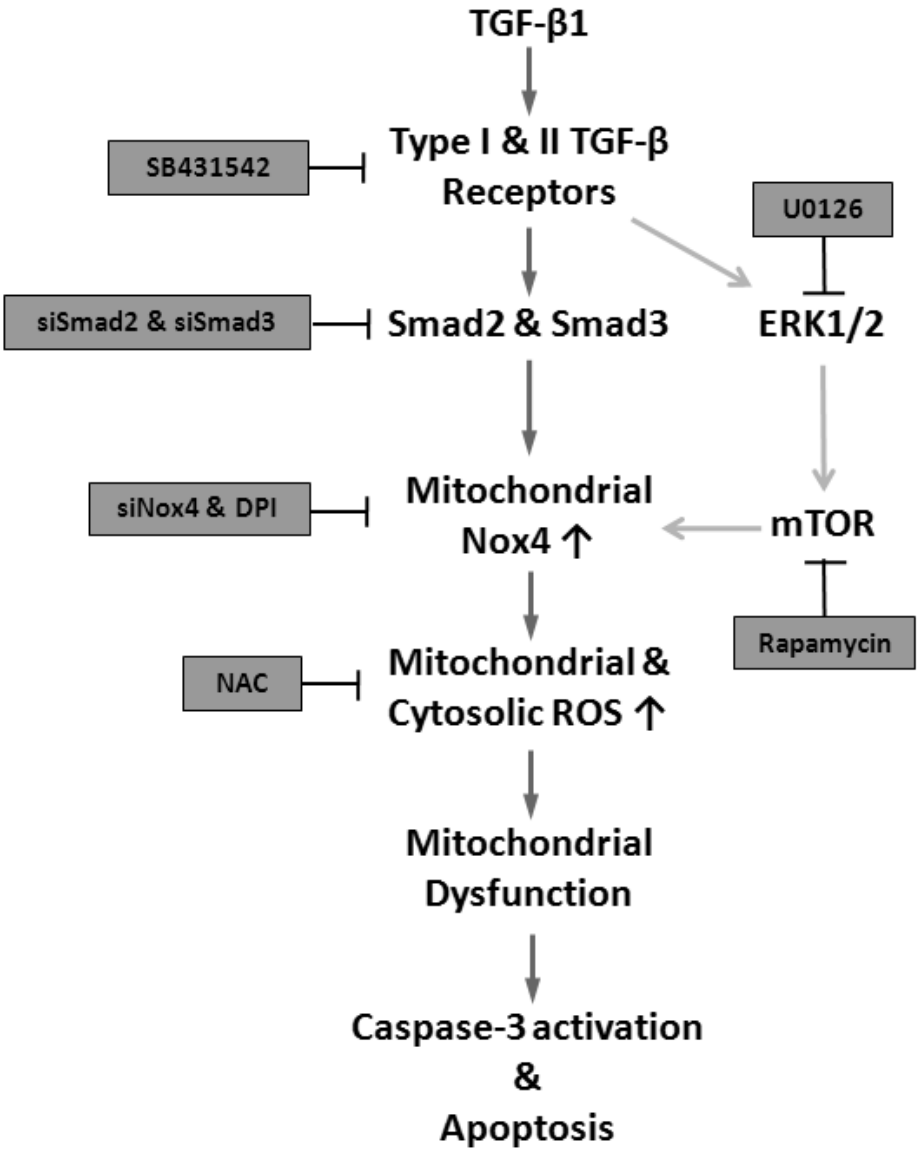

Fig. 34. Proposed mechanisms of TGF-β1-induced podocyte apoptosis.

V. DISCUSSION

One of the primary reasons for progressive chronic kidney diseases is loss of glomerular podocytes characterized by increased proteinuria followed by renal dysfunction. Ongoing studies also reflect that epithelial micro-injuries result in unbalanced epithelial to mesenchymal transition that initiates fibrotic changes in podocytes[9]. High glucose[29, 30], TGF-β1[41, 63] and ANG II[22, 100] are well known players of podocyte pathogenesis. TGF-β constitutes a large family of cytokines that control key cellular processes in development and tissue repair. In various kidney diseases, accumulation of TGF-β is reported in human patients[8] and is responsible for activation of numerous signaling pathways leading to kidney injuries. Podocytes, accounted for early stage of renal injuries, are affected by pathogenic activation of TGF-β signaling leading to apoptosis, EMT, fibrosis, hypertrophy etc.

In the present study, novel molecular pathways have been demonstrated that involves TGF-β-induced oxidative stress and podocyte apoptosis through the upregulation of mitochondrial Nox4. It is proved that TGF-β receptor-Smad2/3 pathway mediates the transcriptional regulation of Nox4 by TGF-β1, which is not affected by Smad-independent p38 MAPK activation. Though Nox4 mRNA upregulation is exclusively dependent on Smad2/3 activation, simultaneous activation of ERK1/2 and mTOR participates in TGF-β1-stimulated total Nox activity and caspase-3 activation. These results are also quite different from previous reports in podocytes that argued for a Smad-dependent apoptotic pathway that is caspase-independent and primarily mediated by Smad7[94, 111].

Mouse podocyte cell line (MPC-5) was thoroughly characterized before starting of experiments as described elsewhere[72]. When cells were thermoshifted to 37°C,

phenotypical changes and growth restriction were very clear and these changes are characteristics of proper podocyte differentiation. During this period, cytoplasmic to nuclear ratio of cells increased substantially and cobblestone morphology of podocytes (33°C) changed into arborized cell bearing highly branched processes (37°C) (Fig. 3). In molecular level, expression of differentiation marker synaptopodin expression was evident (Fig. 4). Podocyte marker protein, nephrin is very crucial for podocyte functions[112]. Several articles report the loss of nephrin expression during podocyte sub-culture[108]. So the expressions of nephrin (both in permissive and non-permissive conditions) and its organization on the plasma membrane of differentiated podocytes was verified (Fig. 5). Podocytes are actin-rich cells with bundles of actin fibers extend along the cell axis giving the arborized morphology of podocytes. Characteristic organization of stress fibers and formation of vimentin network were also observed in differentiated podocytes (Fig. 6-7, respectively). With all these evidences, podocyte differentiation was confirmed and further experiments were carried out. Expression of nephrin was routinely checked whenever new stocks of cells were used.

In a strategy to identify pathogenic changes by TGF-β1 in mouse podocytes, expression of genes, already known to associate with podocyte disorders and some of other genes whose pathogenic effects are still unknown in podocytes, were analyzed by real-time PCR. Though the increased expression of EMT related genes in podocytes (MMP-9, MMP-2, Fibronectin, α-SMA, and collagen, Fig. 8) is mediated by TGF-β1[131], the precise mechanisms of their regulation are still unclear. Moreover, these changes are already known indicators of pathogenic changes by TGF-β1 and, thus, significant alteration of other genes may be considered to be associated with podocyte disorders under the similar conditions. Expression of inflammatory gene cyclooxygenase-2 (Cox2)

is associated with podocyte damage and diabetic nephropathy[18, 68] and experiment showed that TGF-β1 treatment highly alters Cox2 mRNA expression in cultured podocytes (Fig. 9B). Caveolins are important molecules of signal transduction and caveolae-mediated endocytosis. Physiological meaning of Caveolin-1 suppression by TGF-β1 (Fig. 9C) needs to be resolved in future, though diet-induced obesity and type II diabetes has been described in caveolin-1 deficient mice elsewhere[90]. Integrins α3β1 are the major integrin in podocytes involved not only for podocyte attachment to GBM, but also for the signal transduction in–and-out of podocytes[32]. TGF-β1 does not significantly alter integrins expressions in these experiments (Fig. 10A-B). Expression of another anchoring protein dystroglycan is reduced by TGF-β1 (Fig. 10C). Role of dystroglycan in podocytopathy is contradictory. Loss of dystroglycan has been reported in minimal change disease but not in FSGS[91]. But a study with podocyte specific dystroglycan null$^{-/-}$ mice does not signify its contribution to kidney development or function in healthy or injured mice[44]. It is anticipated that loss of anchoring protein may lead to podocyte detachment but the physiological significance of dystroglycan reduction by TGF-β1 remains elusive. Expression of TGF-β1, its receptors, and downstream target molecules were also measured after TGF-β1 treatment. TGF-β-receptor-I is divided into Alk-1 (downstream molecule; id-1) and Alk-5 (downstream molecule; PAI-1). Transient expression of id1 indicates immediate activation of Alk-1 mediated Smad1/5/8 activation which may be inactivated early, whereas Alk-5-Smad2/3-PAI-1 signaling axis sustained till 48 hr indicating prolonged effect of TGF-β1 mediated Smad2/3 signaling podocytes (Fig. 11D-E). Recent studies show that Alk-1 is associated with diabetic nephropathy[3]. Expression of Alk-1 was markedly changed by TGF-β1 (Fig. 11B), but this significance is unknown in podocyte pathophysiology. Expression of TGF-βRII was significantly

reduced (Fig. 11A) implicating probable role in signal termination. TGF-β mRNA level was slightly increased (Fig. 11F) which may further lead to autocrine and/or paracrine signal activation and, thereby, augment renal pathogenesis. Interestingly, TGF-β1-induced transcriptional alteration of all the genes was significantly inhibited by Alk-5 inhibitor SB431542 (Fig. 11). This indicates the importance of Smad2/3 signaling in regulation of gene expression by TGF-β1 in mouse podocytes in pathological context.

In gene expression experiments, highly elevated expression of ROS producing enzyme Nox4 was detected (Fig. 9A) and production of ROS was also detected in one of the preliminary experiments (data not shown). Nox4 is previously shown to be involved in apoptosis of myocytes and hepatocytes[2, 14]. These co-incidents led to find role of Nox4 in TGF-β1 mediated podocyte apoptosis. TGF-β1 treatment increased caspase-3 activation (Fig. 13A), DAPI-stained condensed and apoptotic nuclei (Fig. 12) and TUNEL positive nuclei (Fig. 13B-D) confirming role of TGF-β1 in podocyte cell death. In an effort to screen possible ROS generating enzymes, mRNA levels of CYP4A, Nox1, Nox2, Nox4 and p22phox were determined by real-time PCR (Fig. 16A). These enzymes were previously shown to increase ROS levels in podocytes under various conditions related to diabetes[29]. Of note, Nox1 mRNA expression was not detected in our culture condition. CYP4A, one of the family members of cytochrome 450, produces 20-hydroxyeicosatetraenoic acids (20-HETE) through arachidonic acid metabolism. Eid *et al.* has shown that high glucose increases 20-HETE production which subsequently upregulates Nox1 and Nox4 expression and triggers ROS-induced podocyte apoptosis[29]. Activation of mTOR also increases Nox4 activity[31], whereas activation of AMP-activated protein kinase (AMPK) negatively regulates Nox4 in hyperglycemia[30]. We showed that only Nox4 expression is elevated by TGF-β1 treatment in podocytes, whereas CYP4A, Nox2 and p22phox are

strongly down-regulated under the same condition. However, increased Nox4 expression seems not to be a mere compensatory mechanism following downregulation of other counterparts because TGF-β1 increased total Nox activity (Fig. 17C). In addition, ROS induced podocyte apoptosis was further strengthened as antioxidant NAC reversed all the changes of apoptotic features induced by TGF-β1 (Fig. 14 and Fig.15).

Several lines of evidences suggest that Nox4 is expressed in the ER[123], mitochondria[2, 6], and the plasma membrane[50], which might be cell-type dependent. Karen *et al.* observed the presence of Nox4 in the mitochondria of mesangial cells and podocytes[6]. To our knowledge, the role of mitochondrial Nox4 in podocytes has not been examined in detail. Our co-localization analysis which used mitoCFP adenovirus targeted to mitochondria and the endogenous mitochondrial marker protein, Cox1, of mitochondrial electron transport chain complex IV, showed that Nox4 is localized to mitochondria. In addition, majority of Nox4 protein was detected in mitochondrial fraction (Fig. 19A) supporting the notion that Nox4 is localized to mitochondria. Mitochondrial Nox4 in podocyte is fully functional as TGF-β1 treatment increased a substantial degree of Nox activity in mitochondrial fraction which was almost completely suppressed by a Nox inhibitor (Fig. 20B). It has been known that mitochondrial ROS precipitates in collapse of mitochondrial trans-membrane potential preceding cytochrome c release and caspase activation[36, 60]. ROS produced by mitochondrial Nox4 has been already shown to induce mitochondrial dysfunction and apoptosis in cardiac myocytes[2].

To clarify the role of mitochondrial Nox4 in TGF-β1-induced podocyte apoptosis, we used the Nox inhibitor DPI and Nox4 siRNA. The flavoprotein inhibitor, DPI, causes inhibition by reversing TGF-β1-stimulated ROS production, mitochondrial Nox activity, loss of mitochondrial membrane potential, and caspase-3 activation (Fig. 20A-E).

Interestingly, apocynin does not prevent cleavage of caspase-3 by TGF-β1 (Fig. 20F). This might be due to the different mode of action of DPI and apocynin. DPI prevents flow of electrons by extracting electrons from flavin adenine dinucleotide (FAD) at its carboxy-terminal tail, while apocynin prevents the assembly of p47phox with membrane bound components[26]. Though contrasting evidence exists[53], this observation indicates that mitochondrial Nox4 does not require cytosolic subunit p47phox for its activity in podocytes upon TGF-β1 treatment. The subunit requirement for Nox4 activity is controversial in renal cells[34]. p22phox is the membrane bound subunit of Nox4 and has been demonstrated to be upregulated in the renal cortex of *db/db* mice[98] and high glucose-treated mesangial cells[126]. Poldip2 is another regulatory cytosolic subunit for Nox4 and regulates its activity in vascular smooth muscle cells[67]. Interestingly, mRNA levels of none of those Nox4 subunits were upregulated in TGF-β1 treated podocytes, which suggests that increase in Nox4 protein is sufficient for ROS-mediated podocyte apoptosis. Similar to the effects of DPI, knock-down of Nox4 using siRNA protected podocytes from TGF-β1-mediated ROS generation, loss of $\Delta\Psi_m$, activation of caspase-3 and apoptosis detected by TUNEL assay (Fig. 22). Thus, pharmacologic and genetic inhibition clearly demonstrates the importance of Nox4 upregulation in podocyte apoptosis upon TGF-β1 stimulation.

Even though DPI markedly reduces Nox-induced superoxide production in the mitochondrial fraction (Fig. 20B), but it does only small reduction of DCF intensity in control cells (Figure 20A). Similar effect of DPI has been reported by Parinandi *et al.* showing that DPI completely inhibited Nox activity in human lung endothelial cells, while intracellular ROS level measured by DCF-DA was not significantly altered under same condition[81]. It is conceivable that the necessity of maintaining basal ROS level is

indispensible for cell survival which may be compensated by other ROS producing systems in the absence of Nox-derived ROS. Needless to say, apart from NADPH oxidases, other ROS-generating enzymes exist in the cells including xanthine oxidase, proteins of mitochondrial electron transport chain (ETC), cyclooxygenase, and cytochrome P450. Our observation shows that inhibiting Nox activity by DPI in the absence of TGF-β1 has very minimal effect on mitochondrial membrane potential (Fig. 20C). This is consistent to the finding that total ROS level was not greatly affected by eliminating basal Nox activities.

A previous report showed that TGF-β1 induces mitochondrial dysfunction in podocytes by reducing citrate synthase activity and mitochondrial complex IV and V activity, and increases total nicotinamide adenine dinucleotide (NADH) content[106]. Simultaneously they observed that Nox4 in the mitochondrial fraction can utilize NADH more efficiently than NADPH to produce superoxide[2]. Here, it is also speculated that elevated NADH by TGF-β1 treatment would be a better substrate for superoxide production by Nox4 in mitochondria. Oxidative stress in mitochondria can trigger leakage of electrons from mitochondria and accelerate further oxidative stress causing “ROS induced ROS release”. This vicious cycle, therefore, may promote mitochondrial depolarization, oxidation modification of mitochondrial permeability transition pore (MPTP)components, release of cytochrome c, activation of caspase-3, and apoptosis[41, 134].

Multifunctional cytokine TGF-β acts through its binding with membrane bound TGF-β receptor. Upon ligand stimulation, TGF-β receptor type I (TGF-βRI) and type II (TGF-βRII) form heteromeric complexes and phosphorylate Smads through the canonical pathway[111, 122]. Phosphorylated Smad2 and Smad3 bind to Smad4 and this complex translocates from cytosol to nucleus to act as a transcription factor. In addition to the Smad-dependent

pathway, TGF-β activates TGF-β-activated kinase 1 (TAK1), phosphorylation of which activates p38 MAP kinase, ERK1/2, and c-Jun N-terminal kinase (JNK) by the Smad-independent pathway[52]. Interestingly, a TGF-βRI kinase inhibitor, SB431542, does not block Smad-independent TAK1 activation, but completely abrogates Smad2/3 phosphorylation[52]. In our study, SB431542 completely reverses TGF-β1-induced changes (Fig. 23) further emphasizing the importance of the Smad during TGF-β1-induced apoptosis. It is noteworthy that the Smad2/3 double knock-out podocytes are resistant to TGF-β1 induced cell death[125]. However, the molecular mechanism seems unclear as $Smad3^{-/-}$ podocyte clones show reduced p38 MAPK activation[122] even though p38 MAPK-induced apoptosis is Smad-independent[94].

Previous studies show that the Smad3-Nox4 axis is involved in renal myofibroblast activation[7], epithelial to mesenchymal transition, and migration of breast epithelial cells[10]. On the other hand, Smad2 phosphorylation is responsible for Nox4 mediated epithelial cell death during development of lung fibrosis[15]. Moreover, evidence shows that both Smad2 and Smad3 can also regulate the expression of a single gene, for example STAT5 in mammary epithelial cells[21]. In this study using siRNAs for Smad2 and Smad3, we clearly demonstrate that Smad2 and Smad3 are responsible for TGF-β1-induced Nox4 expression (Fig 25E), ROS generation, mitochondrial membrane depolarization, cleavage of caspase-3, and reduction of TUNEL positive nuclei (Fig. 26). Thus, contrary to previous findings[94, 95], this mode of apoptosis by Smads follows a caspase-dependent mechanism that is activated by Nox4-induced oxidative stress. Moreover, Irene *et al.* have shown that the rat Nox4 promoter region contains putative Smad binding elements[14] implying direct regulation of Nox4 transcription by Smad2 and Smad3. We have also observed down-regulation of Nox4 transcripts in siSmad3-treated cells in the presence of TGF-β1 (data

not shown).

Activation of mTOR plays important role in protein synthesis and its roles in podocytes are not clearly understood. Studies by Davide *et al.* showed that inhibition of mTOR disrupts autophagic flux in cultured podocytes and induces proteinuria in patients[20]. Genetic ablation of mTOR complex 1 in podocytes induced proteinuria and progressive glomerulosclerosis[33]. In contrasts, mTOR activity is enhanced in human diabetic subjects and genetic reduction of mTORC1 copy number or knock-out of upstream regulator tuberous sclerosis proteins 1 (Tsc1) protected mice from glomerular injuries[33, 43]. It was also reported that high glucose stimulated Nox4 upregulation and podocyte depletion are mediated by mTOR[31] and a recent article showed that TGF-β1 increases ROS partially by mTOR activation which is independent of Nox4 upregulation in podocytes[1]. In this study, mTOR inhibitor rapamycin significantly blocked TGF-β-induced ROS generation, total Nox activity, loss of $\Delta\Psi_m$, and caspase-3 activation (Fig. 28A-D), suggesting a clear role of mTOR activation in oxidative stress-induced podocyte apoptosis. Yu *et al.* showed that the Smad3-ERK1/2-NF-κB axis mediates TGF-β-induced podocyte apoptosis through membrane translocation of TRPC6[129]. They clearly demonstrate sequential activation of ERK1/2 after Smad3 activation, which could possibly involve ERK1/2-mediated Rel/p65 translocation to the nucleus. However, this process of ERK1/2 activation by Smad3 is not well understood due to the lack of inhibitory studies on Smad3. In contrast, TGF-β1 stimulates rapid ERK1/2 phosphorylation in a Smad-independent manner in mouse podocytes[96, 125]. In this study, inhibition of ERK1/2 did not affect TGF-β1-stimulated Nox4 mRNA upregulation (Fig. 30B). Similar to mTOR, ERK1/2 inhibition completely inhibited Nox activity, loss of $\Delta\Psi_m$, and caspase-3 activation (Fig. 29B-D). These results raise the possibilities that transcriptional regulation of Nox4 is under the control of transcription

factors Smad2/3; on the other hand ERK1/2, and mTOR activation by TGF-β1 regulates Nox activity either by augmentation of protein synthesis or by the modification Nox4 protein. Thus, regulation of Nox4 activity by ERK1/2 MAPK needs further investigation. Ma *et al.* has shown that ERK1/2 may enhance mTOR activity by dissociation of Tsc1-Tsc2 complex which is a negative regulator of mTOR[69], suggesting that ERK1/2 activation is an upstream of mTOR activation and, therefore, may regulate Nox activity through ERK1/2-mTOR signaling cascade in podocytes. In fact, inhibition of ERK1/2 by U0126 completely blocked mTOR and p70S6K phosphorylation (Fig. 31) implying that ERK1/2 is an upstream regulator of TGF-β1-induced mTOR activation in podocytes. Moreover, Carriere *et al.* has shown that ERK1/2 can phosphorylate Raptor which positively regulates mTORC1 activity[16]. Thus, more studies are needed to find out the molecular mechanisms of mTOR activation by ERK1/2 MAPK in podocytes.

Smad7 is one of the inhibitory Smads that negatively regulates Smad2 and Smad3 signaling in podocytes. It has also been shown to be upregulated in different glomerular diseases[95] and recognized as a pro-apoptotic factor induced by TGF-β1[94]. On the other hand, Smad6 expression is not enhanced by TGF-β stimulation in podocytes[95] and is not involved in negative regulation of Smad signaling in podocytes. These observations led us to investigate possible crosstalk between Smad7 and Nox4 and determine if there is a functional link between these signaling molecules in regulating apoptotic signaling. Time kinetic mRNA analysis reveals that TGF-β1 stimulates Smad7 mRNA expression earlier than that of Nox4. Therefore, it is possible that Smad7 could positively or negatively control the transcription of Nox4. We expected either one of these two outcomes from siRNA-mediated Smad7 knock-down experiments. Firstly, if Nox4 is downstream target of Smad7, knock-down of Smad7 would reduce expression and functional activity of Nox4.

Secondly, if Nox4 is regulated by Smad2/Smad3, knock-down of Smad7 might increase expression and activity of Nox4. As expected according to second hypothesis that Nox4 transcription is under the control of Smad2 and Smad3, knockdown of Smad7 unmasked Nox4 upregulation with TGF-β1 stimulation (Fig. 32C). siSmad7 also did not protected podocytes from oxidative stress-induced loss of $\Delta\Psi_m$ and caspase-3 activation (Fig. 32D and 31E), though small reduction of apoptosis was observed (Fig. 32F). This observation suggests that the apoptotic pathway mediated by TGF-β-Smad2/3-Nox4 cascade is independent of Smad7-induced apoptotic pathway.

Among various non-canonical pathways, TGF-β1 also triggers p38 MAPK[132]. It was previously reported that TGF-β1 phosphorylates p38 MAPK, which, in turn, increases expression of proapoptotic Bax protein in podocytes[94]. Bax translocation to mitochondria releases cytochrome c, which activates cleaved caspase-3 resulting in apoptosis. In our observation, TGF-β1 activates p38 MAPK as early as 30 min and activation is sustained for 24 hr. Because p38 MAPK activation could be caused by oxidative stress[12, 45, 98], we investigated the possibility of p38 MAPK activation by Nox4-induced ROS. Our results show that the Nox inhibitor, DPI, has no inhibitory effect on p38 MAPK phosphorylation (Fig. 33F). p38 MAPK is also a multifunctional protein kinase which regulates gene expression. In podocytes, the time kinetics of p38 MAPK activation by TGF-β1 reveals that its phosphorylation occurs earlier than upregulation of Nox4 mRNA under the same stimulus. The possibility of Nox4 up-regulation by p38 MAPK was checked and found that p38 MAPK inhibition does not block TGF-β1-induced Nox4 upregulation (Fig. 33C), mitochondrial membrane potential depolarization (Fig. 33E), and ROS generation (data not shown), indicating that p38 MAPK has no impact on Nox4-mediated ROS production in podocytes.

Using diabetic mice model, Eid *et al.* demonstrated that podocytes undergo foot process effacement, GBM thickening and proteinuria through Nox4-induced oxidative stress[29, 30], while Susztak *et al.* examined that high glucose-induced podocyte apoptosis is mediated by increased ROS[107]. Though the magnitude of apoptotic podocytes is not very high in these cases, but the evidences reflect statistically significant increase of apoptosis in diabetic animal models. In another studies with albumin/TGF-β1 TG mice, Schiffer *et al.* proved that TUNEL positive apoptotic podocyte increased in TGF-β1 TG mice compared to wild type mice and 2 week old TG mice shows significantly higher rate of apoptosis compared to 5 week old TG mice[94]. This observation indicates that age of the experimental animals should be considered for examining podocyte apoptosis in animal models. It is assumed that apoptotic podocytes might be lost with the age of disease progression and excreted out with urine which may decrease the chance to detect apoptosis *in vivo*. Because of limitation of our results using *in vitro* cultured podocytes, further evidence from *in vivo* study is required to strongly suggest the pathogenic mechanism in a diabetic glomerular injury.

Taken together, the present study demonstrates that the 'TGF-β receptor-Smad2/3-Nox4 axis' is a pathophysiologic mechanism of TGF-β-induced podocyte apoptosis independent of Smad7 and p38 MAPK activation (Fig. 34). In particular, ROS generation through mitochondrial Nox4 might be a key inducer of mitochondrial dysfunction and apoptosis. Because TGF-β levels in kidney tissue are elevated in diabetic nephropathy and other chronic renal disease, it is of critical importance to find the possible targets of therapeutic or preventive treatment within the apoptotic cascade triggered by TGF-β1. The pathogenic consequence of Nox4-generating oxidative stress is not restricted to podocyte depletion but is also significant in causing defective glomerular basement

membrane, foot process abnormalities, and fibrotic sclerosis, all of which play a significant role in the development and progression of chronic proteinuric glomerular diseases.

VI. CONCLUSION

TGF-β1 induces apoptosis and oxidative stress in mouse podocytes through elevation of reactive oxygen species resulting from upregulation of Nox4. Nox4 is predominantly localized to mitochondria in podocytes and responsible for mitochondrial dysfunction through ROS generation in presence of TGF-β1. When podocytes are stimulated with TGF-β1, TGF-βRI-Smad2/3 axis mediates upregulation of Nox4. In addition, activation of ERK1/2 and mTOR also contribute to TGF-β1-induced oxidative stress and podocyte apoptosis. Thus, intervention strategy for Nox4 could be a future therapeutic target to prevent podocyte specific glomerular diseases.

VII. REFERENCES

1. Abe Y, Sakairi T, Beeson C, Kopp JB. TGF-β1 stimulates mitochondrial oxidative phosphorylation and generation of reactive oxygen species in cultured mouse podocytes, mediated in part by the mTOR pathway. Am J Physiol Renal Physiol 2013;305:F1477-90.

2. Ago T, Kuroda J, Pain J, Fu C, Li H, Sadoshima J. Upregulation of Nox4 by hypertrophic stimuli promotes apoptosis and mitochondrial dysfunction in cardiac myocytes. Circ Res 2010;106:1253-64.

3. Araoka T, Abe H, Tominaga T, Mima A, Matsubara T, Murakami T, et al. Transcription factor 7-like 2 (TCF7L2) regulates activin receptor-like kinase 1 (ALK1)/Smad1 pathway for development of diabetic nephropathy. Mol Cells 2010;30:209-18.

4. Bai Y, Wang L, Li Y, Liu S, Li J, Wang H, et al. High ambient glucose levels modulates the production of MMP-9 and α5(IV) collagen by cultured podocytes. Cell Physiol Biochem 2006;17:57-68.

5. Bhathena DB. Glomerular basement membrane length to podocyte ratio in human nephronopenia: implications for focal segmental glomerulosclerosis. Am J Kidney Dis 2003;41:1179-88.

6. Block K, Gorin Y, Abboud HE. Subcellular localization of Nox4 and regulation in diabetes. Proc Natl Acad Sci U S A 2009;106:14385-90.

7. Bondi CD, Manickam N, Lee DY, Block K, Gorin Y, Abboud HE, et al. NAD(P)H oxidase mediates TGF-β1-induced activation of kidney myofibroblasts. J Am Soc Nephrol 2010;21:93-102.

8. Border WA, Noble NA. Transforming growth factor β in tissue fibrosis. N Engl J Med 1994;331:1286-92.

9. Bottinger EP. TGF-β in renal injury and disease. Semin Nephrol 2007;27:309-20.

10. Boudreau HE, Casterline BW, Rada B, Korzeniowska A, Leto TL. Nox4

involvement in TGF-β and SMAD3-driven induction of the epithelial-to-mesenchymal transition and migration of breast epithelial cells. Free Radic Biol Med 2012;53:1489-99.

11. Boute N, Gribouval O, Roselli S, Benessy F, Lee H, Fuchshuber A, et al. NPHS2, encoding the glomerular protein podocin, is mutated in autosomal recessive steroid-resistant nephrotic syndrome. Nat Genet 2000;24:349-54.

12. Breton-Romero R, Gonzalez de Orduna C, Romero N, Sanchez-Gomez FJ, de Alvaro C, Porras A, et al. Critical role of hydrogen peroxide signaling in the sequential activation of p38 MAPK and eNOS in laminar shear stress. Free Radic Biol Med 2012;52:1093-100.

13. Campbell DJ, Rong P, Kladis A, Rees B, Ganten D, Skinner SL. Angiotensin and bradykinin peptides in the TGR(mRen-2)27 rat. Hypertension 1995;25:1014-20.

14. Carmona-Cuenca I, Roncero C, Sancho P, Caja L, Fausto N, Fernandez M, et al. Upregulation of the NADPH oxidase NOX4 by TGF-β in hepatocytes is required for its pro-apoptotic activity. J Hepatol 2008;49:965-76.

15. Carnesecchi S, Deffert C, Donati Y, Basset O, Hinz B, Preynat-Seauve O, et al. A key role for NOX4 in epithelial cell death during development of lung fibrosis. Antioxid Redox Signal 2011;15:607-19.

16. Carriere A, Romeo Y, Acosta-Jaquez HA, Moreau J, Bonneil E, Thibault P, et al. ERK1/2 phosphorylate Raptor to promote Ras-dependent activation of mTOR complex 1 (mTORC1). J Biol Chem 2011;286:567-77.

17. Chen S, Kasama Y, Lee JS, Jim B, Marin M, Ziyadeh FN. Podocyte-derived vascular endothelial growth factor mediates the stimulation of α3(IV) collagen production by transforming growth factor-β1 in mouse podocytes. Diabetes 2004;53:2939-49.

18. Cheng H, Wang S, Jo YI, Hao CM, Zhang M, Fan X, et al. Overexpression of cyclooxygenase-2 predisposes to podocyte injury. J Am Soc Nephrol 2007;18:551-9.

19. Chesebro B, Wehrly K. Studies on the role of the host immune response in recovery from Friend virus leukemia. I. Antiviral and antileukemia cell antibodies. J Exp Med 1976;143:73-84.

20. Cina DP, Onay T, Paltoo A, Li C, Maezawa Y, De Arteaga J, et al. Inhibition of MTOR disrupts autophagic flux in podocytes. J Am Soc Nephrol 2012;23:412-20.

21. Cocolakis E, Dai M, Drevet L, Ho J, Haines E, Ali S, et al. Smad signaling antagonizes STAT5-mediated gene transcription and mammary epithelial cell differentiation. J Biol Chem 2008;283:1293-307.

22. Debiec H, Nauta J, Coulet F, van der Burg M, Guigonis V, Schurmans T, et al. Role of truncating mutations in MME gene in fetomaternal alloimmunisation and antenatal glomerulopathies. Lancet 2004;364:1252-9.

23. Dessapt C, Baradez MO, Hayward A, Dei Cas A, Thomas SM, Viberti G, et al. Mechanical forces and TGF-β1 reduce podocyte adhesion through α3β1 integrin downregulation. Nephrol Dial Transplant 2009;24:2645-55.

24. Ding G, Reddy K, Kapasi AA, Franki N, Gibbons N, Kasinath BS, et al. Angiotensin II induces apoptosis in rat glomerular epithelial cells. Am J Physiol Renal Physiol 2002;283:F173-80.

25. Djamali A, Reese S, Hafez O, Vidyasagar A, Jacobson L, Swain W, et al. Nox2 is a mediator of chronic CsA nephrotoxicity. Am J Transplant 2012;12:1997-2007.

26. Drummond GR, Selemidis S, Griendling KK, Sobey CG. Combating oxidative stress in vascular disease: NADPH oxidases as therapeutic targets. Nat Rev Drug Discov 2011;10:453-71.

27. Durvasula RV, Petermann AT, Hiromura K, Blonski M, Pippin J, Mundel P, et al. Activation of a local tissue angiotensin system in podocytes by mechanical strain. Kidney Int 2004;65:30-9.

28. Economou CG, Kitsiou PV, Tzinia AK, Panagopoulou E, Marinos E, Kershaw DB, et al. Enhanced podocalyxin expression alters the structure of podocyte basal surface. J Cell Sci 2004;117:3281-94.

29. Eid AA, Gorin Y, Fagg BM, Maalouf R, Barnes JL, Block K, et al. Mechanisms of podocyte injury in diabetes: role of cytochrome P450 and NADPH oxidases. Diabetes 2009;58:1201-11.

30. Eid AA, Ford BM, Block K, Kasinath BS, Gorin Y, Ghosh-Choudhury G, et al. AMP-activated protein kinase (AMPK) negatively regulates Nox4-dependent activation of p53 and epithelial cell apoptosis in diabetes. J Biol Chem 2010;285:37503-12.

31. Eid AA, Ford BM, Bhandary B, de Cassia Cavaglieri R, Block K, Barnes JL, et al. Mammalian target of rapamycin regulates Nox4-mediated podocyte depletion in diabetic renal injury. Diabetes 2013;62:2935-47.

32. Faul C, Asanuma K, Yanagida-Asanuma E, Kim K, Mundel P. Actin up: regulation of podocyte structure and function by components of the actin cytoskeleton. Trends Cell Biol 2007;17:428-37.

33. Godel M, Hartleben B, Herbach N, Liu S, Zschiedrich S, Lu S, et al. Role of mTOR in podocyte function and diabetic nephropathy in humans and mice. J Clin Invest 2011;121:2197-209.

34. Gorin Y, Block K. Nox4 and diabetic nephropathy: With a friend like this, who needs enemies? Free Radic Biol Med 2013;61C:130-42.

35. Grahammer F, Schell C, Huber TB. The podocyte slit diaphragm - from a thin grey line to a complex signalling hub. Nat Rev Nephrol 2013;9:587-98.

36. Green DR, Reed JC. Mitochondria and apoptosis. Science 1998;281:1309-12.

37. Han G, Li AG, Liang YY, Owens P, He W, Lu S, et al. Smad7-induced β-catenin degradation alters epidermal appendage development. Dev Cell 2006;11:301-12.

38. Hara M, Yanagihara T, Kihara I, Higashi K, Fujimoto K, Kajita T. Apical cell membranes are shed into urine from injured podocytes: a novel phenomenon of podocyte injury. J Am Soc Nephrol 2005;16:408-16.

39. Hoshi S, Shu Y, Yoshida F, Inagaki T, Sonoda J, Watanabe T, et al. Podocyte injury promotes progressive nephropathy in zucker diabetic fatty rats. Lab Invest

2002;82:25-35.

40. Hsu HH, Hoffmann S, Endlich N, Velic A, Schwab A, Weide T, et al. Mechanisms of angiotensin II signaling on cytoskeleton of podocytes. J Mol Med (Berl) 2008;86:1379-94.

41. Ide T, Tsutsui H, Kinugawa S, Utsumi H, Kang D, Hattori N, et al. Mitochondrial electron transport complex I is a potential source of oxygen free radicals in the failing myocardium. Circ Res 1999;85:357-63.

42. Iglesias-de la Cruz MC, Ziyadeh FN, Isono M, Kouahou M, Han DC, Kalluri R, et al. Effects of high glucose and TGF-β1 on the expression of collagen IV and vascular endothelial growth factor in mouse podocytes. Kidney Int 2002;62:901-13.

43. Inoki K, Mori H, Wang J, Suzuki T, Hong S, Yoshida S, et al. mTORC1 activation in podocytes is a critical step in the development of diabetic nephropathy in mice. J Clin Invest 2011;121:2181-96.

44. Jarad G, Pippin JW, Shankland SJ, Kreidberg JA, Miner JH. Dystroglycan does not contribute significantly to kidney development or function, in health or after injury. Am J Physiol Renal Physiol 2011;300:F811-20.

45. Jaulmes A, Sansilvestri-Morel P, Rolland-Valognes G, Bernhardt F, Gaertner R, Lockhart BP, et al. Nox4 mediates the expression of plasminogen activator inhibitor-1 via p38 MAPK pathway in cultured human endothelial cells. Thromb Res 2009;124:439-46.

46. Jung KY, Chen K, Kretzler M, Wu C. TGF-β1 regulates the PINCH-1-integrin-linked kinase-α-parvin complex in glomerular cells. J Am Soc Nephrol 2007;18:66-73.

47. Kaplan JM, Kim SH, North KN, Rennke H, Correia LA, Tong HQ, et al. Mutations in ACTN4, encoding α-actinin-4, cause familial focal segmental glomerulosclerosis. Nat Genet 2000;24:251-6.

48. Kerjaschki D. Caught flat-footed: podocyte damage and the molecular bases of

focal glomerulosclerosis. J Clin Invest 2001;108:1583-7.

49. Kestila M, Lenkkeri U, Mannikko M, Lamerdin J, McCready P, Putaala H, et al. Positionally cloned gene for a novel glomerular protein-nephrin is mutated in congenital nephrotic syndrome. Mol Cell 1998;1:575-82.

50. Kim EY, Anderson M, Dryer SE. Insulin increases surface expression of TRPC6 channels in podocytes: role of NADPH oxidases and reactive oxygen species. Am J Physiol Renal Physiol 2012;302:F298-307.

51. Kim JM, Wu H, Green G, Winkler CA, Kopp JB, Miner JH, et al. CD2-associated protein haploinsufficiency is linked to glomerular disease susceptibility. Science 2003;300:1298-300.

52. Kim SI, Kwak JH, Na HJ, Kim JK, Ding Y, Choi ME. Transforming growth factor-β (TGF-β1) activates TAK1 via TAB1-mediated autophosphorylation, independent of TGF-β receptor kinase activity in mesangial cells. J Biol Chem 2009;284:22285-96.

53. Kim SM, Kim YG, Jeong KH, Lee SH, Lee TW, Ihm CG, et al. Angiotensin II-induced mitochondrial Nox4 is a major endogenous source of oxidative stress in kidney tubular cells. PLoS One 2012;7:e39739.

54. Kim YH, Goyal M, Kurnit D, Wharram B, Wiggins J, Holzman L, et al. Podocyte depletion and glomerulosclerosis have a direct relationship in the PAN-treated rat. Kidney Int 2001;60:957-68.

55. Kitamura M. Endoplasmic reticulum stress in the kidney. Clin Exp Nephrol 2008;12:317-25.

56. Kojima K, Davidovits A, Poczewski H, Langer B, Uchida S, Nagy-Bojarski K, et al. Podocyte flattening and disorder of glomerular basement membrane are associated with splitting of dystroglycan-matrix interaction. J Am Soc Nephrol 2004;15:2079-89.

57. Kreidberg JA, Donovan MJ, Goldstein SL, Rennke H, Shepherd K, Jones RC, et al. α3β1 integrin has a crucial role in kidney and lung organogenesis.

Development 1996;122:3537-47.

58. Kretzler M, Teixeira VP, Unschuld PG, Cohen CD, Wanke R, Edenhofer I, et al. Integrin-linked kinase as a candidate downstream effector in proteinuria. FASEB J 2001;15:1843-5.

59. Kriz W, Gretz N, Lemley KV. Progression of glomerular diseases: is the podocyte the culprit? Kidney Int 1998;54:687-97.

60. Kroemer G, Reed JC. Mitochondrial control of cell death. Nat Med 2000;6:513-9.

61. Lee K, Chen QK, Lui C, Cichon MA, Radisky DC, Nelson CM. Matrix compliance regulates Rac1b localization, NADPH oxidase assembly, and epithelial-mesenchymal transition. Mol Biol Cell 2012;23:4097-108.

62. Lemley KV, Lafayette RA, Safai M, Derby G, Blouch K, Squarer A, et al. Podocytopenia and disease severity in IgA nephropathy. Kidney Int 2002;61:1475-85.

63. Li CX, Xia M, Han WQ, Li XX, Zhang C, Boini KM, et al. Reversal by growth hormone of homocysteine-induced epithelial-to-mesenchymal transition through membrane raft-redox signaling in podocytes. Cell Physiol Biochem 2011;27:691-702.

64. Li Y, Kang YS, Dai C, Kiss LP, Wen X, Liu Y. Epithelial-to-mesenchymal transition is a potential pathway leading to podocyte dysfunction and proteinuria. Am J Pathol 2008;172:299-308.

65. Liu F, Gomez Garcia AM, Meyskens FL, Jr. NADPH oxidase 1 overexpression enhances invasion via matrix metalloproteinase-2 and epithelial-mesenchymal transition in melanoma cells. J Invest Dermatol 2012;132:2033-41.

66. Livak KJ, Schmittgen TD. Analysis of relative gene expression data using real-time quantitative PCR and the $2^{-\Delta\Delta C}{}_{T}$ Method. Methods 2001;25:402-8.

67. Lyle AN, Deshpande NN, Taniyama Y, Seidel-Rogol B, Pounkova L, Du P, et al. Poldip2, a novel regulator of Nox4 and cytoskeletal integrity in vascular smooth muscle cells. Circ Res 2009;105:249-59.

68. Ma J, Phillips L, Wang Y, Dai T, LaPage J, Natarajan R, et al. Curcumin activates the p38MPAK-HSP25 pathway in vitro but fails to attenuate diabetic nephropathy in DBA2J mice despite urinary clearance documented by HPLC. BMC Complement Altern Med 2010;10:67.

69. Ma L, Chen Z, Erdjument-Bromage H, Tempst P, Pandolfi PP. Phosphorylation and functional inactivation of TSC2 by Erk implications for tuberous sclerosis and cancer pathogenesis. Cell 2005;121:179-93.

70. Matsui K, Breiteneder-Geleff S, Kerjaschki D. Epitope-specific antibodies to the 43-kD glomerular membrane protein podoplanin cause proteinuria and rapid flattening of podocytes. J Am Soc Nephrol 1998;9:2013-26.

71. Miceli I, Burt D, Tarabra E, Camussi G, Perin PC, Gruden G. Stretch reduces nephrin expression via an angiotensin II-AT(1)-dependent mechanism in human podocytes: effect of rosiglitazone. Am J Physiol Renal Physiol 2010;298:F381-90.

72. Mundel P, Reiser J, Zuniga Mejia Borja A, Pavenstadt H, Davidson GR, Kriz W, et al. Rearrangements of the cytoskeleton and cell contacts induce process formation during differentiation of conditionally immortalized mouse podocyte cell lines. Exp Cell Res 1997;236:248-58.

73. Nagase M, Fujita T. Aldosterone and glomerular podocyte injury. Clin Exp Nephrol 2008;12:233-42.

74. Nakamura T, Ushiyama C, Suzuki S, Hara M, Shimada N, Ebihara I, et al. Urinary excretion of podocytes in patients with diabetic nephropathy. Nephrol Dial Transplant 2000;15:1379-83.

75. Niranjan T, Bielesz B, Gruenwald A, Ponda MP, Kopp JB, Thomas DB, et al. The Notch pathway in podocytes plays a role in the development of glomerular disease. Nat Med 2008;14:290-8.

76. Niranjan T, Murea M, Susztak K. The pathogenic role of Notch activation in podocytes. Nephron Exp Nephrol 2009;111:e73-9.

77. Nohe A, Keating E, Knaus P, Petersen NO. Signal transduction of bone

morphogenetic protein receptors. Cell Signal 2004;16:291-9.

78. Oft M, Peli J, Rudaz C, Schwarz H, Beug H, Reichmann E. TGF-β1 and Ha-Ras collaborate in modulating the phenotypic plasticity and invasiveness of epithelial tumor cells. Genes Dev 1996;10:2462-77.

79. Okuda S, Languino LR, Ruoslahti E, Border WA. Elevated expression of transforming growth factor-β and proteoglycan production in experimental glomerulonephritis. Possible role in expansion of the mesangial extracellular matrix. J Clin Invest 1990;86:453-62.

80. Pagtalunan ME, Miller PL, Jumping-Eagle S, Nelson RG, Myers BD, Rennke HG, et al. Podocyte loss and progressive glomerular injury in type II diabetes. J Clin Invest 1997;99:342-8.

81. Parinandi NL, Kleinberg MA, Usatyuk PV, Cummings RJ, Pennathur A, Cardounel AJ, et al. Hyperoxia-induced NAD(P)H oxidase activation and regulation by MAP kinases in human lung endothelial cells. Am J Physiol Lung Cell Mol Physiol 2003;284:L26-38.

82. Park KS, Wiederkehr A, Kirkpatrick C, Mattenberger Y, Martinou JC, Marchetti P, et al. Selective actions of mitochondrial fission/fusion genes on metabolism-secretion coupling in insulin-releasing cells. J Biol Chem 2008;283:33347-56.

83. Patterson GI, Padgett RW. TGF-β-related pathways. Roles in Caenorhabditis elegans development. Trends Genet 2000;16:27-33.

84. Pavenstadt H, Kriz W, Kretzler M. Cell biology of the glomerular podocyte. Physiol Rev 2003;83:253-307.

85. Perlman R, Schiemann WP, Brooks MW, Lodish HF, Weinberg RA. TGF-β-induced apoptosis is mediated by the adapter protein Daxx that facilitates JNK activation. Nat Cell Biol 2001;3:708-14.

86. Petermann AT, Pippin J, Krofft R, Blonski M, Griffin S, Durvasula R, et al. Viable podocytes detach in experimental diabetic nephropathy: potential mechanism underlying glomerulosclerosis. Nephron Exp Nephrol 2004;98:e114-23.

87. Petermann AT, Pippin J, Durvasula R, Pichler R, Hiromura K, Monkawa T, et al. Mechanical stretch induces podocyte hypertrophy in vitro. Kidney Int 2005;67:157-66.

88. Piwkowska A, Rogacka D, Audzeyenka I, Jankowski M, Angielski S. High glucose concentration affects the oxidant-antioxidant balance in cultured mouse podocytes. J Cell Biochem 2011;112:1661-72.

89. Quan X, Das R, Xu S, Cline GW, Wiederkehr A, Wollheim CB, et al. Mitochondrial phosphate transport during nutrient stimulation of INS-1E insulinoma cells. Mol Cell Endocrinol 2013;381:198-209.

90. Razani B, Combs TP, Wang XB, Frank PG, Park DS, Russell RG, et al. Caveolin-1-deficient mice are lean, resistant to diet-induced obesity, and show hypertriglyceridemia with adipocyte abnormalities. J Biol Chem 2002;277:8635-47.

91. Regele HM, Fillipovic E, Langer B, Poczewki H, Kraxberger I, Bittner RE, et al. Glomerular expression of dystroglycans is reduced in minimal change nephrosis but not in focal segmental glomerulosclerosis. J Am Soc Nephrol 2000;11:403-12.

92. Ronco P, Debiec H. Molecular pathomechanisms of membranous nephropathy: from Heymann nephritis to alloimmunization. J Am Soc Nephrol 2005;16:1205-13.

93. Roselli S, Gribouval O, Boute N, Sich M, Benessy F, Attie T, et al. Podocin localizes in the kidney to the slit diaphragm area. Am J Pathol 2002;160:131-9.

94. Schiffer M, Bitzer M, Roberts IS, Kopp JB, ten Dijke P, Mundel P, et al. Apoptosis in podocytes induced by TGF-β and Smad7. J Clin Invest 2001;108:807-16.

95. Schiffer M, Schiffer LE, Gupta A, Shaw AS, Roberts IS, Mundel P, et al. Inhibitory smads and TGF-β signaling in glomerular cells. J Am Soc Nephrol 2002;13:2657-66.

96. Schiffer M, Mundel P, Shaw AS, Bottinger EP. A novel role for the adaptor molecule CD2-associated protein in transforming growth factor-β-induced apoptosis. J Biol Chem 2004;279:37004-12.

97. Schwarz K, Simons M, Reiser J, Saleem MA, Faul C, Kriz W, et al. Podocin, a raft-associated component of the glomerular slit diaphragm, interacts with CD2AP and nephrin. J Clin Invest 2001;108:1621-9.

98. Sedeek M, Callera G, Montezano A, Gutsol A, Heitz F, Szyndralewiez C, et al. Critical role of Nox4-based NADPH oxidase in glucose-induced oxidative stress in the kidney: implications in type 2 diabetic nephropathy. Am J Physiol Renal Physiol 2010;299:F1348-58.

99. Shankland SJ, Al'Douahji M. Cell cycle regulatory proteins in glomerular disease. Exp Nephrol 1999;7:207-11.

100. Shankland SJ. The podocyte's response to injury: role in proteinuria and glomerulosclerosis. Kidney Int 2006;69:2131-47.

101. Shankland SJ, Pippin JW, Reiser J, Mundel P. Podocytes in culture: past, present, and future. Kidney Int 2007;72:26-36.

102. Shi Y, Massague J. Mechanisms of TGF-β signaling from cell membrane to the nucleus. Cell 2003;113:685-700.

103. Shibata S, Nagase M, Yoshida S, Kawachi H, Fujita T. Podocyte as the target for aldosterone: roles of oxidative stress and Sgk1. Hypertension 2007;49:355-64.

104. Shih NY, Li J, Cotran R, Mundel P, Miner JH, Shaw AS. CD2AP localizes to the slit diaphragm and binds to nephrin via a novel C-terminal domain. Am J Pathol 2001;159:2303-8.

105. Smoyer WE, Mundel P, Gupta A, Welsh MJ. Podocyte α-actinin induction precedes foot process effacement in experimental nephrotic syndrome. Am J Physiol 1997;273:F150-7.

106. Stieger N, Worthmann K, Teng B, Engeli S, Das AM, Haller H, et al. Impact of high glucose and transforming growth factor-β on bioenergetic profiles in podocytes. Metabolism 2012;61:1073-86.

107. Susztak K, Raff AC, Schiffer M, Bottinger EP. Glucose-induced reactive oxygen species cause apoptosis of podocytes and podocyte depletion at the onset of

diabetic nephropathy. Diabetes 2006;55:225-33.

108. Takano Y, Yamauchi K, Hiramatsu N, Kasai A, Hayakawa K, Yokouchi M, et al. Recovery and maintenance of nephrin expression in cultured podocytes and identification of HGF as a repressor of nephrin. Am J Physiol Renal Physiol 2007;292:F1573-82.

109. Tao JL, Wen YB, Shi BY, Zhang H, Ruan XZ, Li H, et al. Endoplasmic reticulum stress is involved in podocyte apoptosis induced by saturated fatty acid palmitate. Chin Med J (Engl) 2012;125:3137-42.

110. Tossidou I, Starker G, Kruger J, Meier M, Leitges M, Haller H, et al. PKC-α modulates TGF-β signaling and impairs podocyte survival. Cell Physiol Biochem 2009;24:627-34.

111. Tossidou I, Schiffer M. TGF-β/BMP pathways and the podocyte. Semin Nephrol 2012;32:368-76.

112. Tryggvason K. Unraveling the mechanisms of glomerular ultrafiltration: nephrin, a key component of the slit diaphragm. J Am Soc Nephrol 1999;10:2440-5.

113. Tryggvason K, Ruotsalainen V, Wartiovaara J. Discovery of the congenital nephrotic syndrome gene discloses the structure of the mysterious molecular sieve of the kidney. Int J Dev Biol 1999;43:445-51.

114. Velez JC, Bland AM, Arthur JM, Raymond JR, Janech MG. Characterization of renin-angiotensin system enzyme activities in cultured mouse podocytes. Am J Physiol Renal Physiol 2007;293:F398-407.

115. Vogelmann SU, Nelson WJ, Myers BD, Lemley KV. Urinary excretion of viable podocytes in health and renal disease. Am J Physiol Renal Physiol 2003;285:F40-8.

116. Wang D, Dai C, Li Y, Liu Y. Canonical Wnt/β-catenin signaling mediates transforming growth factor-β1-driven podocyte injury and proteinuria. Kidney Int 2011;80:1159-69.

117. Whaley-Connell A, Habibi J, Johnson M, Tilmon R, Rehmer N, Rehmer J, et al.

Nebivolol reduces proteinuria and renal NADPH oxidase-generated reactive oxygen species in the transgenic Ren2 rat. Am J Nephrol 2009;30:354-60.

118. Whaley-Connell A, Habibi J, Wei Y, Gutweiler A, Jellison J, Wiedmeyer CE, et al. Mineralocorticoid receptor antagonism attenuates glomerular filtration barrier remodeling in the transgenic Ren2 rat. Am J Physiol Renal Physiol 2009;296:F1013-22.

119. Whaley-Connell A, Nistala R, Habibi J, Hayden MR, Schneider RI, Johnson MS, et al. Comparative effect of direct renin inhibition and AT1R blockade on glomerular filtration barrier injury in the transgenic Ren2 rat. Am J Physiol Renal Physiol 2010;298:F655-61.

120. Whaley-Connell AT, Chowdhury NA, Hayden MR, Stump CS, Habibi J, Wiedmeyer CE, et al. Oxidative stress and glomerular filtration barrier injury: role of the renin-angiotensin system in the Ren2 transgenic rat. Am J Physiol Renal Physiol 2006;291:F1308-14.

121. Winn MP, Conlon PJ, Lynn KL, Farrington MK, Creazzo T, Hawkins AF, et al. A mutation in the TRPC6 cation channel causes familial focal segmental glomerulosclerosis. Science 2005;308:1801-4.

122. Wu DT, Bitzer M, Ju W, Mundel P, Bottinger EP. TGF-β concentration specifies differential signaling profiles of growth arrest/differentiation and apoptosis in podocytes. J Am Soc Nephrol 2005;16:3211-21.

123. Wu RF, Ma Z, Liu Z, Terada LS. Nox4-derived H2O2 mediates endoplasmic reticulum signaling through local Ras activation. Mol Cell Biol 2010;30:3553-68.

124. Wyatt CM, Meliambro K, Klotman PE. Recent progress in HIV-associated nephropathy. Annu Rev Med 2012;63:147-59.

125. Xavier S, Niranjan T, Krick S, Zhang T, Ju W, Shaw AS, et al. TβRI independently activates Smad- and CD2AP-dependent pathways in podocytes. J Am Soc Nephrol 2009;20:2127-37.

126. Xia L, Wang H, Goldberg HJ, Munk S, Fantus IG, Whiteside CI. Mesangial cell

NADPH oxidase upregulation in high glucose is protein kinase C dependent and required for collagen IV expression. Am J Physiol Renal Physiol 2006;290:F345-56.

127. Xu ZG, Yoo TH, Ryu DR, Cheon Park H, Ha SK, Han DS, et al. Angiotensin II receptor blocker inhibits p27Kip1 expression in glucose-stimulated podocytes and in diabetic glomeruli. Kidney Int 2005;67:944-52.

128. Yamamoto T, Nakamura T, Noble NA, Ruoslahti E, Border WA. Expression of transforming growth factor β is elevated in human and experimental diabetic nephropathy. Proc Natl Acad Sci U S A 1993;90:1814-8.

129. Yu L, Lin Q, Liao H, Feng J, Dong X, Ye J. TGF-β1 induces podocyte injury through Smad3-ERK-NF-kappaB pathway and Fyn-dependent TRPC6 phosphorylation. Cell Physiol Biochem 2010;26:869-78.

130. Yue J, Mulder KM. Activation of the mitogen-activated protein kinase pathway by transforming growth factor-β. Methods Mol Biol 2000;142:125-31.

131. Zhang C, Xia M, Boini KM, Li CX, Abais JM, Li XX, et al. Epithelial-to-mesenchymal transition in podocytes mediated by activation of NADPH oxidase in hyperhomocysteinemia. Pflugers Arch 2011;462:455-67.

132. Zhang YE. Non-Smad pathways in TGF-β signaling. Cell Res 2009;19:128-39.

133. Ziyadeh FN. Mediators of diabetic renal disease: the case for TGF-β as the major mediator. J Am Soc Nephrol 2004;15 Suppl 1:S55-7.

134. Zorov DB, Filburn CR, Klotz LO, Zweier JL, Sollott SJ. Reactive oxygen species (ROS)-induced ROS release: a new phenomenon accompanying induction of the mitochondrial permeability transition in cardiac myocytes. J Exp Med 2000;192:1001-14.

VIII. ABSTRACT IN KOREAN

마우스 신장 족세포에서 TGF-β에 의한 병적 변화

족세포의 손상은 단백뇨를 특징으로 하는 만성 신장 질환을 초래한다. 한편 신장조직에서의 TGF-β 농도 증가는 족세포 손상으로 인한 세포 사멸 및 탈락과 관련 있음이 알려져 있다. 본 연구에서는 불멸화된 마우스 신장 족세포에서 TGF-β에 의한 세포사멸 기전을 밝히고자 하였다. 외부에서 투여된 TGF-β1 은 선택적으로 Nox4 의 발현을 증가시켜 세포 내 활성산소 수준을 높히고, 이로 인해 caspase-3 를 활성화시켜 세포사멸을 초래하였다. 마우스 족세포의 Nox4 는 주로 미토콘드리아에 분포하였으며, TGF-β1 에 의한 Nox4 발현 증가는 미토콘드리아의 막전압을 현저히 탈분극시켰다. TGF-β1 투여로 인한 활성산소 생성 및 caspase 활성화는 항산화제, Nox 억제제인 DPI, 그리고 Nox4 에 대한 siRNA 전처치에 의해 억제되었다. 또한 TGF-β1 에 의한 모든 병적 변화들은 TGF-β 제 1 형 수용체 차단제인 SB431542 에 의해 완전히 소실되었다. Smad2 와 Smad3 발현을 억제시킨 경우 TGF-β1 투여로 인한 Nox4 발현양 증가, 활성산소 생성, 미토콘드리아 탈분극 및 caspase 활성화가 모두 감소하였다. 이러한 변화와 더불어 TGF-β1 투여는 mTOR 및 그 하부 신호전달 타깃인 p70S6K 를 인산화시켰다. mTOR 제 1 형 복합체 억제제인 rapamycin 을 투여한 경우 TGF-β1 에 의한 활성산소 생성, 총 Nox 활성도 증가, 미토콘드리아

탈분극, 그리고 caspase 활성화 등을 차단하였는데, 이는 TGF-β에 의한 신장 족세포의 사멸효과에 mTOR 가 역할을 담당하고 있음을 의미한다. 이와 관련된 ERK1/2 의 인산화가 TGF-β1 투여 후 빠른 시간 내에 나타나며, ERK1/2 활성화 억제제를 투여하면 TGF-β1 에 의한 mTOR 및 p70S6K 인산화, Nox 활성도 증가, 미토콘드리아 탈분극, 및 caspase-3 활성화가 모두 방지되었다. 이상의 결과들을 종합하여 고려할 때 TGF-β에 의한 산화 스트레스 및 족세포의 사멸은 TGF-β 수용체-Smad2/3-미토콘드리아 Nox4 축을 매개로 나타나며 ERK 및 mTOR 의 활성화 역시 Nox 활성도 증가를 통해 함께 기여한다고 제시할 수 있으며, 이러한 기전들은 당뇨병성 신증과 같은 단백뇨 관련 사구체 질환의 발생 및 진행에 관여하고 있을 것으로 사료된다.

핵심 되는 말: 신장 족세포, Transforming growth factor-β, 세포사멸, NADPH oxidase 4, 미토콘드리아, mTOR, ERK1/2.